An Observational Study of the Chemical Composition in Massive Star-Forming Regions

Miho IKEDA

Doctor of Science

Department of Astronomical Science
School of Mathematical and Physical Science
The Graduate University for Advanced Studies

1998

Contents

Abstract 1

1 General Introduction 4

1 Interstellar Molecules 5

2 Formation Mechanism of Interstellar Molecules 5

2.1 Gas-phase Reactions 6

2.2 Grain-surface Reactions 7

3 Chemistry of Massive Star-Forming Regions 8

4 The Motivation and Contents of the Thesis 9

2 Mapping Observations of the O-bearing Organic Molecules toward Sagittarius B2 11

1 Introduction 12

2 Observations 13

3 Results 14

3.1 CH_3OH 14

3.2 $(CH_3)_2O$ 15

3.3 C_2H_5OH & $HCOOCH_3$ 15

3.4 Column Densities 16

4 Discussion 18

4.1 Abundances of the O-bearing Molecules 18
4.2 Comparison of Spatial Distribution with those of Other Molecules and the Spatial Relation to H II Regions 19
4.3 Extended Component of the O-bearing Molecules 20
5 Conclusions 22

3 Mapping Observations of the NH- & NH_2-bearing Large Organic Molecules toward Sagittarius B2 32

1 Introduction 34
2 Observations 35
3 Results 36
3.1 CH_3NH_2 and CH_2NH 36
3.2 NH_2CHO 37
3.3 NH_2CN 38
3.4 Column Densities and Fractional Abundances 38
4 Discussion 40
4.1 Comparison of Spatial Distribution with those of Other Molecules and Dust Continuum 40
4.2 Formation Mechanism of the NH- and NH_2-bearing Molecule 41
5 Conclusions 43

4 Detection of a New Cyclic Molecule c-C_2H_4O, and Survey Observations of c-C_2H_4O and CH_3CHO toward Massive Star-Forming Regions 50

1 Introduction 52
2 Observations 53
2.1 Detection Observations of c-C_2H_4O at Haystack, NRO, and SEST . 53
2.2 Survey Observations of c-C_2H_4O and CH_3CHO toward Southern Sources 54

2.3 Survey Observations of c-C_2H_4O and CH_3CHO toward Northern Sources 55

3 Results 56

3.1 Detection of c-C_2H_4O 56

3.2 Survey of c-C_2H_4O and CH_3CHO 56

4 Discussion 58

4.1 Chemistry of the C_2H_4O group 58

4.2 Comparisons of Observed Molecular Abundances with Chemical Models 60

4.3 Comparison of Observed Abundances of Molecules with Gas Kinetic Temperatures and Dust Temperatures 62

4.4 Excitation of Molecules 62

4.5 Star Formation Rate vs Molecular Abundances 63

5 Conclusions 64

5 Summary **85**

1 Formation Mechanism of Large Organic Molecules 86

2 Chemical Evolution and Star-Formation 88

Acknowledgements **92**

References **93**

Abstract

In order to understand the formation mechanism of interstellar molecules and clarify the relation between the chemical composition and the physical condition in massive star-forming regions, I have conducted mapping observations of O-, NH-, and NH_2-bearing organic molecules toward SgrB2 and survey observations of cyclic-C_2H_4O and CH_3CHO toward several massive star-forming regions.

First, we have conducted the mapping observations of the O-bearing large organic molecules (CH_3OH, C_2H_5OH, $HCOOCH_3$ and $(CH_3)_2O$) toward the SgrB2 molecular cloud and investigated the relation between the distribution of the O-bearing molecules and H II regions. Mapping observations were carried out in the range of RA $\times$ DEC $\sim$ $2' \times 3'$ including submillimeter continuum sources SgrB2(N) and (M) associated with H II regions. We found that all molecules have emission peak within 10″-15″ of SgrB2(N) and all molecular abundances are enhanced toward emission peak compared to the gas-phase reaction models. Especially, both of CH_3OH and $(CH_3)_2O$ emission peaks are located within 10″ from SgrB2(N) and theses peaks are also coincident with the position of the centimeter continuum sources. Their distributions are compact. It is believed that SgrB2(N) is younger than SgrB2(M) and star-formation is active. This indicates that production mechanisms of CH_3OH and $(CH_3)_2O$ are closely related with star-formation. From compact distribution around H II regions and enhancement of the abundance, it is likely that CH_3OH is produced on the grain surface and evaporated from grain mantle by UV radiation from young O,B-type stars embedded in SgrB2(N). $(CH_3)_2O$ is believed to be produced from CH_3OH in the gas-phase. Therefore, $(CH_3)_2O$ around H II regions would be produced from dust-evaporated CH_3OH. C_2H_5OH and $HCOOCH_3$ have also peaks within $\sim$ 20″ from SgrB2(N) and are more extended than CH_3OH and $(CH_3)_2O$. $HCOOCH_3$ is produced in the gas-phase from H_2CO which can be also produced in gas-phase reactions. On the other hand, the extended distribution of C_2H_5OH cannot be explained by gas-phase chemistry. In SgrB2, it is known that SiO is extended and SiO is

thought to be produced in the gas-phase from Si released from grain through sputtering. Sputtering is induced by active motions in a molecular cloud. C_2H_5OH may be produced on the grain and evaporated through such sputtering. For production mechanism of the O-bearing molecules, it is likely that grain-surface chemistry plays an important role.

Next, in order to investigate the spatial relation between the distributions of the NH- and NH_2-bearing molecules and H II regions or dust continuum we performed mapping observations of CH_3NH_2, CH_2NH, NH_2CHO and NH_2CN toward SgrB2. We obtained the results different from the O-bearing molecules. The CH_3NH_2, CH_2NH and NH_2CHO distributions have peaks at the west of SgrB2(N) and (M) and they are elongated from the north to the south. The NH_2CN distribution shows a strong peak at $\sim 50''$ northeast of SgrB2(N). In this peak methanol maser emission also has a peak, and intensity peaks of HNCO and HCO_2^+ are located near this position. In HNCO peak it is believed that there may be an infrared source which is younger than SgrB2(N). NH_2CN may also be excited by FIR from this very young source. We compared our mapping results with 1.3 mm dust continuum which has strong peaks at SgrB2(N) and (M) and has an envelope elongated from the north to the south. This envelope shape is similar to the distributions of the NH- and NH_2-bearing molecules. The distribution of HC_3N which traces high density ($\sim 10^6$ cm $^{-3}$) gas, is also close to the envelope shapes of the NH- and NH_2-bearing molecules. This indicates that the NH- and NH_2-bearing molecules reflect the high density gas rather than H II regions. Moreover, the fractional abundances of these molecules are not enhanced from those predicted by gas-phase reaction models. On the other hand it is suggested that the NH- and NH_2-bearing molecules are produced from NH_3 and NH_2 in gas-phase. NH_3 is believed to be produced on dust grain, and NH_2 is produced from NH_3. Therefore the formation mechanism of the NH- and NH_2-bearing molecules may be related to NH_3.

Lastly, we expand the observations of large organic molecules to several massive star-forming regions. Since we recently detected a new interstellar cyclic molecule cyclic-C_2H_4O which is an isomer of CH_3CHO in SgrB2(N), we searched for cyclic-C_2H_4O and CH_3CHO in several massive star-forming regions. We detected these molecule in more than 20 massive star-forming regions and several other organic molecules (CH_3OH, C_2H_5OH, $HCOOCH_3$, $(CH_3)_2O$, HCOOH, C_2H_3CN, and C_2H_5CN etc) were also detected in these star-forming regions. We estimated the fractional abundances and the excitation temperatures of these molecules, and found that most of the fractional abundances are enhanced by a few orders of magnitude in all of the sources comparing to those predicted from pure gas-phase reaction models. This indicates that the observed abundances of

large organic molecules cannot be explained by gas-phase reactions.

When we compared our results with the models including grain surface reactions, a part of abundances can be explained by these reaction models. However there are no models which can explain all abundances of observed molecules. We found that all molecular abundances, except for cyclic-C_2H_4O and CH_3CHO, increase with the increase in either of gas kinetic temperature and dust temperature. This indicates that these large organic molecules are formed on the grain and are released back to the gas-phase with the increase in the dust temperature. Although the abundances of cyclic-C_2H_4O and CH_3CHO increase with the gas kinetic temperature, it seems that there is no correlation between the abundances and the dust temperature. This indicates that contribution of gas-phase reactions would be larger than that of grain-surface reactions. We also found positive correlation between the column densities of C_2H_4O group (cyclic-C_2H_4O and CH_3CHO) and that of C_2H_5OH. These results support an assumption that C_2H_4O group is produced from dust evaporated C_2H_5OH in the gas-phase. On the other hand, the excitation temperatures are different from species to species: low excitation temperature were derived (10-40 K) for cyclic-C_2H_4O, CH_3CHO, and HCOOH whereas high temperature (70-250 K) for CH_3OH, $(CH_3)_2O$, C_2H_3CN and C_2H_5CN. Temperatures of C_2H_5OH and $HCOOCH_3$ were intermediate. Variety of excitation temperatures seems to indicate the molecular line emission arises in regions with different physical conditions. However we cannot exclude a possibility of subthermal excitation condition, and high spatial resolution mapping observations of these molecules in several massive star-forming regions may be necessary.

Chapter 1

General Introduction

1. Interstellar Molecules

More than one hundred molecules have been detected in interstellar space up to the present (Table. 1). Most of these molecules are found in a few standard sources, and each source has its own characteristics; carbon chain molecules are found mainly in dark clouds such as Taurus Molecular Cloud-1 (TMC-1), large organic molecules in massive star-forming regions such as Orion Molecular Cloud-1 (OMC-1) and Sagittarius B2 (SgrB2), and metal-containing molecules in circumstellar envelops of late-type stars such as IRC+10216. Although the carbon chain molecules are short-lived, such molecules can exist in the dark clouds because kinetic temperatures of dark clouds are very low ($\sim$ 10 K). These molecules have double or triple bonds and contain few hydrogen atoms. Since hydrogen is the most abundant atom in the universe, this is the most prominent feature of chemistry in the dark clouds. On the other hand, in regions where many massive stars are formed, many kinds of molecules are detected. In this way, chemical composition changes from source to source, and varies along with the evolution of a molecular cloud.

Of these observed molecules, some molecules are used as probes of physical conditions in a molecular cloud. Symmetric-top molecules such as NH_3, CH_3CCH, and CH_3CN are used to derive gas kinetic temperatures of a cloud because the transitions between different K components occur only by collision. Since the most abundant species, H_2, does not have a permanent electric dipole moment, it is not observed by radio wave. Then second abundant species, CO, is used to estimate the H_2 column density using an empirical conversion factor with respect to H_2. Since the electric dipole moment of CO is small (0.11 Debye), the excitation temperature of CO is nearly equal to gas kinetic temperature. Therefore, CO is also used to derive gas kinetic temperature. HCN has high critical density ($\sim 10^4$ cm^{-3}), so that the HCN transitions are used as high density tracers.

2. Formation Mechanism of Interstellar Molecules

Since the density and the temperature in interstellar space are much lower than those in the terrestrial conditions, it is very difficult to produce the molecules by reactions which normally occur in terrestrial conditions : ternary association in which a third species receives excess reaction energy. Then two-body ion-molecule reactions with no activation energy barriers are considered. All of the interstellar species cannot

be explained by this ion-molecule reaction scheme. It is hard to explain the formation of saturated organic molecules only by the gas-phase reactions. Because reaction rates of ion-molecule reactions to form saturated organic molecules are very small and the abundances of observed saturated molecules cannot be explained. For example, for methanol, following reactions have been proposed (Herbst & Leung 1989):

$$CH_3^+ + H_2O \rightarrow CH_3OH_2^+ + h\nu \quad (1.1)$$

$$CH_3OH_2^+ + e \rightarrow CH_3OH + H. \quad (1.2)$$

Since the rate coefficient of reaction (1.1) is small ($\sim 10^{-12}$ cm^{3}s^{-1} $T = 300$ K)(Millar et al. 1991), observational results in hot core cannot be reproduced by such reactions. In the same way, ethanol is believed to be produced as follows (Herbst & Leung 1989):

$$H_3O^+ + C_2H_4 \rightarrow C_2H_5OH_2^+ + h\nu \quad (1.3)$$

$$C_2H_5^+ + H_2O \rightarrow C_2H_5OH_2^+ + h\nu \quad (1.4)$$

$$C_2H_5OH_2^+ + e \rightarrow C_2H_5OH + H. \quad (1.5)$$

The abundances relative to the H_2 abundance are predicted to be $X(CH_2H_5OH) \sim 10^{-13}$ ($T = 50$ K)(Lee et al. 1996). This value is about four orders of magnitude lower than that of observational results. Then grain-surface reactions in which grain plays a role of a catalyst are proposed. Hydrogen molecules which are the most abundant molecule in the interstellar space are also believed to be formed on the grain-surface. Some solid molecules have also been detected in the grain-mantles by infrared observations.

2.1. Gas-phase Reactions

In gas-phase, molecular bonds can be created through radiative association:

$$A + B \dashrightarrow AB + h\nu$$

in which the excess bond energy is released through the emission of a photon. In principle, the reaction product could also relax through a collision with the third species, but due to the low densities in the interstellar space, this is highly unlikely. Reactions between two neutral species are predicted to be very slow at low temperatures due to their weak long-range interaction and high activation barriers.

On the other hand, ion-molecule reactions are fast ($\sim 10^{-9}$ cm^3s^{-1}) due to small activation energy barriers, and this type of reaction is assumed to be the dominant creation process for molecules in interstellar clouds. Practically, there are many molecular ion in interstellar space, indicating a lot of interstellar molecules are produced by ion-molecule reactions. Moreover, many ion-molecule reaction models have been developed (Suzuki et al. 1979; Herbst & Leung 1989; Millar et al. 1991; Lee et al. 1996), and abundances of simple molecules are well explained by these ion-molecule reactions.

2.2. Grain-surface Reactions

The major problem in the gas-phase chemistry is that it does not explain how molecular hydrogen, H_2, is formed since the simple radiative association $H + H \rightarrow H_2 + h\nu$ is very improbable. Due to the low densities in the interstellar space, there is not the third species which receive the excess bond energy of this reaction. In the interstellar space, only dust grain can receive this excess energy. It is commonly accepted today that H_2 is formed through recombination of two adsorbed H atoms on a grain surface and the H_2 molecule is subsequently evaporated to the gas phase (the sublimation temperature is ~ 4 K). In contrast to cold dark clouds, there are several species whose abundances cannot be explained by ion-molecule reactions in massive star-forming regions. Observed abundances of large organic molecules are higher than the predicted abundances from chemical models of gas-phase reactions by a few orders of magnitude. In order to explain the observed abundances of large organic molecules, grain-surface reactions have been incorporated. Molecules formed on dust grain are believed to be evaporated to the gas-phase from grain mantles which are heated by UV radiation from young O,B-stars.

Charnley et al. (1992) developed a model for two cores in Orion-KL: the Compact Ridge and the Hot Core. They calculated the abundances of large organic molecules which were evaporated from grain mantle or formed from dust-evaporated precursor species in gas-phase. They considered that the difference in chemical compositions between two cores was caused by the difference between initial mantle composition. Their results explain a part of the observational results in Orion-KL. Moreover, Caselli et al. (1993) considered the last 10^5 yr of the accretion phase of a protostellar object embedded in a dense and massive cloud with density and temperature gradients. They include N-bearing molecules (CH_3NH_2, C_2H_3CN and C_2H_5CN), and explain the observational result of C_2H_3CN in Hot Core. A chemical model for G34.3+0.2 were developed by Millar et al. (1997), by considering three component: ultracompact core, compact core,

and Halo.

Thus several chemical models including grain-surface reactions are developed, and succeeded to explain a part of observed abundances of large organic molecules. However, there are no chemical models which can explain all of molecular abundances.

3. Chemistry of Massive Star-Forming Regions

With respect to chemical composition, most studied massive star-forming regions are SgrB2 and OMC-1. In SgrB2, many species were detected for the first time. OMC-1 has two well-known regions : the Hot Core which is active star-forming region and the Compact Ridge which does not show sign of star-formation. It is known that the chemical composition of these regions are different; The Hot Core is rich in N-bearing molecules, C_2H_3CN and C_2H_5CN and the Compact Ridge is rich in O-bearing molecules, C_2H_5OH, $HCOOCH_3$ and $(CH_3)_2O$. Such large organic molecules have high abundances in these regions, which are a few orders of magnitude higher than gas-phase reaction model predictions. Therefore it is believed that such large organic molecules are formed on the dust grain. In order to observe these organic molecules in radio wave, they must evaporate from grain mantles. Then a heating source is needed. In a massive star-forming region, UV radiation from young O,B-stars embedded in a H II region is considered as a heating source. However the past observations of large organic molecules were limited toward one or a few points in a central region of a molecular cloud so that a spatial relation between the distributions of large organic molecules and H II regions is still unknown. If large organic molecules are evaporated from a grain-mantle which is heated by UV photon from O,B-stars, such molecules can only be found around H II regions. And it is unknown if there is any difference between the distributions of large organic molecules and simple species which are formed by gas-phase reactions. It is necessary to investigate the distributions of large organic molecules.

Simple species are used as probes which trace a physical condition of a molecular cloud. It is clear that large organic molecules are closely related with star formation because most of the large organic molecules are detected only toward massive star-forming regions. However there are many evolutional stage in the massive star-forming regions and it is unknown what a condition of star-formation large organic molecules reflect. It is important to compare abundaces of several large organic molecules with the physical conditions (temperature, density and dust temperature, etc) in several massive

star-forming regions.

4. The Motivation and Contents of the Thesis

In order to study the relation between the chemical composition and the physical condition in massive star-forming regions, I discuss the following issues:

1. Production mechanism of large organic molecules which are abundant in massive star-forming regions,
2. The spatial relation between the distribution of large organic molecules and the H II regions or the dust continuum,
3. The relation between the abundances of large organic molecules and the physical conditions in several massive star-forming regions.

The outline of this thesis is as follows; In Chapter 2, mapping observations of the O-bearing large organic molecules (CH_3OH, C_2H_5OH, $HCOOCH_3$, and $(CH_3)_2O$) toward massive star-forming region SgrB2 are described. I discuss the production mechanism of the O-bearing molecules and the spatial relation between the distribution of these molecules and the H II regions. The same mapping observations of the NH and NH_2-bearing molecules (CH_3NH_2, CH_2NH, NH_2CHO, and NH_2CN) toward SgrB2 are described in Chapter 3. Moreover, I compare the distributions of the NH- and NH_2-bearing molecules with dust continuum distributions in this chapter. In Chapter 4, I report detection of a new cyclic interstellar molecule, cyclic-C_2H_4O, toward SgrB2, and survey observations of cyclic-C_2H_4O and its isomeric molecule, CH_3CHO, in several massive star-forming regions. These two molecules were detected in more than 20 star-forming regions and other large organic molecules (CH_3OH, C_2H_5OH, $HCOOCH_3$, $(CH_3)_2O$, HCOOH, C_2H_3CN and C_2H_5CN, etc) were also detected in these sources. I discuss the relation between molecular abundances of the large organic species and the physical conditions in each source. Finally, I summarize the results of this thesis, and present the conclusions.

Table 1. Interstellar molecules detected as of December 1998

Simple hydrides, oxides, sulfides, and related molecules				
H_2(IR)	CO	NH_3	CS	NaCl*
HCl	SiO	SiH_4^*(IR)	SiS	AlCl*
H_2O	SO_2	C_2(IR)	H_2S	KCl*
N_2O	OCS	CH_4^*(IR)	PN	AlF*
	CO_2			
Nitriles, acetylene, derivatives, and related molecules				
C_3^*(IR)	HCN	CH_3CN	HNC	$C_2H_4^*$(IR)
C_5^*(IR)	HC_3N	CH_3C_3N	HNCO	$C_2H_2^*$(IR)
C_3O	HC_5N	CH_3C_5N?	HNCS	
C_3S	HC_7N	CH_3C_2H	HNCCC	
C_4Si*	HC_9N	CH_3C_4H	CH_3NC	
	$HC_{11}N$	CH_3CH_2CN	HCCNC	
	CH_2CHO	CH_2CHCN		
Aldehydes, alcohols, ethers, ketones, amides, and related molecules				
H_2CO	CH_3OH	HCOOH	CH_2NH	H_2C_3
H_2CS	CH_3CH_2OH	$HCOOCH_3$	CH_3NH_2	H_2C_4
CH_3CHO	CH_3SH	CH_3COOH	NH_2CN	H_2C_6
NH_2CHO	$(CH_3)_2O$			
H_2CCO	$(CH_3)_2CO$			
Cyclic molecules				
$c-C_3H_2$	SiC_2	$c-C_3H$	$c-C_2H_4O$	
Molecular ions				
CH^+(OPT)	HCO^+	$HCNH^+$	H_3O^+	HN_2^+
HCS^+	$HOCO^+$	HC_3NH^+	HOC^+	H_3^+
CO^+	H_2COH^+	SO^+		
Radicals				
OH	C_2H	CN	C_2O	C_2S
CH	C_3H	C_3N	NO	NS
CH_2	C_4H	C_5N	SO	SiC*
NH(UV)	C_5H	HCCN*	HCO	SiN*
NH_2	C_6H	CH_2CN	MgNC	CP*
HNO	C_7H	CH_2N	MgCN	
	C_8H	NaCN		

With respect to molecules detected in the range of infrared, optical, and ultraviolet, the wave length range are indicated as IR, OPT, and UV, respectively in parenthesis.

*Detected only in the circumstellar envelope of late-type star IRC+10216.

?Claimed but not yet confirmed.

Chapter 2

Mapping Observations of the O-bearing Organic Molecules toward Sagittarius B2

ABSTRACT

Mapping observations of the O-bearing large organic molecules, methanol (CH_3OH), ethanol (C_2H_5OH), methyl formate ($HCOOCH_3$) and dimethyl ether ($(CH_3)_2O$), were carried out toward SgrB2, using the 45-m radio telescope of the Nobeyama Radio Observatory. Emissions of CH_3OH and $(CH_3)_2O$ peak at $\sim 10''$ northeast of the continuum source, SgrB2(N), and FWHM of their distributions are comparable to or smaller than the beam size, $17''$. Emissions of C_2H_5OH and $HCOOCH_3$ also peak toward SgrB2(N), with diameter $\leq 14''$, and are extended to the whole mapping region. This is different from CH_3OH and $(CH_3)_2O$ results. Since the upper energy levels of observed C_2H_5OH and $HCOOCH_3$ lines are lower (13-18 K) than those of CH_3OH and $(CH_3)_2O$ (31-328 K), the transitions of C_2H_5OH and $HCOOCH_3$ can be excited even in low temperature region. It is likely that extended distribution of $HCOOCH_3$ is due to those of precursor H_2CO which produced in gas-phase reactions. Extended C_2H_5OH emission may be due to sputtering which release Si or Si-bearing material from grains to gas-phase.

The fractional abundances of these molecules are obtained to be $X(CH_3OH) = 3 \times 10^{-8}$, $X(C_2H_5OH) = 4 \times 10^{-9}$, $X(HCOOCH_3) = 2 \times 10^{-9}$, and $X((CH_3)_2O) = 2 \times 10^{-9}$, respectively. Comparing these values with predicted values by pure gas-phase models, we found that the observational results are higher than the predictions by 2–4 orders of magnitude. This indicates that the abundances of the O-bearing large organic molecules are hard to be explained by pure gas-phase reactions, whereas grain-surface reactions seem to play more important roles. Since emission peaks are near SgrB2(N), it is likely that dust grains are heated by UV radiation from young O,B-stars in H II regions, then the O-bearing molecules produced on dust grains are evaporated into the gas-phase.

1. Introduction

In massive star-forming regions many saturated molecules are detected. Especially, it is known that SgrB2 which is located in the Galactic center region is rich in large organic molecules, and many molecules were detected in this molecular cloud for the first time. Although simple molecules can be formed by the ion-molecule reactions in the gas-phase, the large organic molecules cannot be explained by such reaction scheme. The

abundances of large organic molecules derived from observations are much higher than those predicted by gas-phase chemical models by a few orders of magnitude. Therefore, it is believed that the grain-surface reactions play important roles in producing large organic molecules in massive star-forming regions. If organic molecules are produced on dust grains, heating source is needed in order for the molecules to be observed in the gas-phase. Some 50 compact H II regions, maintained by the ionizing UV radiation from young massive stars, have been resolved by interferometric observations in the centimeter continuum emission and the radio recombination lines toward SgrB2 (Gaume et al. 1995; De Pree et al. 1995, 1996). The majority of these compact H II regions are concentrated to two compact cores, SgrB2(M) and SgrB2(N), where submillimeter continuum is strong. It is believed that many young O,B-stars are embedded in these cores, and they heat dust grains, making molecules evaporated.

There are some line survey observations toward SgrB2(M) and (N) (Sutton et al. 1991; Nummelin et al. 1998), and many large organic molecules have been detected. However, these observations are limited toward one point or a few points. Therefore spatial relation between large organic molecules and H II region is still unknown very well. We also need to investigate whether the distributions of molecules which are believed to be formed from dust-evaporated molecule are correlated with their parent molecules. In order to clarify this relation, we carried out mapping observations of the O-bearing large organic molecules, CH_3OH, C_2H_5OH, $HCOOCH_3$, and $(CH_3)_2O$, toward SgrB2.

2. Observations

Observations were performed from 1993 November to 1994 January. We used the 3 mm and 4 mm receivers simultaneously. The system temperatures of the receivers were $\sim$ 350 K and $\sim$ 300 K, respectively. For the backend, we used two sets of acousto-optical spectrometers (AOS), one with a bank of eight high-resolution AOS with the frequency resolution of 37 kHz and 40 MHz bandwidth, and the other with a bank of eight wide-band AOS with the frequency resolution of 250 kHz and 250 MHz bandwidth. Pointing was checked every two hours by observing the SiO maser in VX Sgr. The estimated pointing accuracy was $\sim$ 5″ rms. The observations were made in position-switching mode. The line parameters, beam sizes, receiver and main-beam efficiencies are summarized in Table 1. All molecules were observed with the 15″ grid

spacing in a range of 2′ × 3′ (RA × DEC). Moreover, transitions of C_2H_5OH and the $7_{2,6}$ - $7_{1,7}$ transition of $(CH_3)_2O$ at 104.7 GHz were observed with the 10″ grid spacing in a range of 40″ × 40″ toward SgrB2(N). The on-source integration time was 2–10 minutes.

3. Results

3.1. CH_3OH

We show profiles of CH_3OH toward its emission peak in Figures 1(a) and 1(b). We observed two transitions at 88940.047 MHz and 88594.843 MHz. Since both of transitions are the K-type doubling transitions of 15_3 - 14_4 A, their line strengths and the upper level energies are almost equal. Therefore these two lines reflect the same physical condition. The profiles of these transitions are very similar. CH_3OH lines have two velocity components ($\sim$ 64 km s^{-1} and $\sim$ 73 km s^{-1}) at the emission peak, and the intensity of the 73 km s^{-1} component is weaker than that of the 64 km s^{-1} component by a factor of 2 - 3. 64 km s^{-1} is consistent with the typical radial velocity for large organic molecules toward SgrB2. Gaussian fitting was applied to the profiles, and the line width were obtained to be $\sim$ 9 km s^{-1} for the 64 km s^{-1} component and $\sim$ 6 km s^{-1} for the 73 km s^{-1} component. respectively. Other organic molecules also have two velocity components. According to Miao et al. (1995), spectra of the $10_{1,10}$ - $9_{1,9}$ transition of C_2H_5CN toward SgrB2(N) show velocity components at 63 and 75 km s^{-1}. In a similar way, spectra of the 10_8 - 9_8 transition of C_2H_3CN and the $8_{6,2}$ - $7_{6,1}$ E transition of $HCOOCH_3$ also have two velocity components at 63 and 74 km s^{-1} for C_2H_3CN, and at 64 and 75 km s^{-1} for $HCOOCH_3$, respectively. Near SgrB2(N), the high velocity components of these molecules have narrow line width ($\sim$ 3 - 6 km s^{-1}), and the low velocity components are broader ($\sim$ 9 - 12 km s^{-1}) and stronger ($\sim$ factor 2) than the high velocity components. This indicates that these molecules and CH_3OH exist in the same volume.

Integrated intensity map of the 88594.843 MHz line is shown in Figure 2(a). Emission peak is located about 10″ northeast of SgrB2(N), and there is little emission toward SgrB2(M). Above mentioned organic molecules also peak at a region with diameter < 0.1 pc toward SgrB2(N), while almost no emission is detected toward SgrB2(M) (Miao et al. 1995). The emission distribution around SgrB2(N) is compact and its FWHM is comparable to or smaller than the beam size (FWHM) at this

frequency of 17″, which corresponds to 0.7 pc if the distance to SgrB2 is assumed to be 8.5 kpc.

3.2. $(CH_3)_2O$

We observed two different energy level transitions of $(CH_3)_2O$: the $7_{2,6}$ - $7_{1,7}$ lines at 104.7 GHz (E_u=31 K) and the $15_{2,13}$ - $15_{1,14}$ lines at 88.7 GHz (E_u=117 K). $(CH_3)_2O$ has four torsional substates, AA,EE,AE, and EA, due to internal rotation of two CH_3 groups. The frequency separation between components of the $7_{2,6}$ - $7_{1,7}$ lines are about 2.6 MHz, and these are separated enough (Figure 1(c)). On the other hand the $15_{2,13}$ - $15_{1,14}$ lines are separated by 1.4 MHz, and all substates lines are completely blended (Figure 1(d)). V_{LSR} is 62 - 65 km s^{-1}. Line width of the $15_{2,13}$ - $15_{1,14}$ line is 15 - 20 km s^{-1} and those of each component of the $7_{2,6}$ - $7_{1,7}$ line are 4 - 6 km s^{-1}. The integrated intensity maps of both lines, integrated over all components are shown in Figures 2(b) and 2(c). The distributions of both lines are similar. Both lines peak about 10″ northeast of SgrB2(N), and this peak coincides with that of CH_3OH. The $15_{2,13}$ - $15_{1,14}$ line also distributes compactly around the peak like CH_3OH, and the $7_{2,6}$ - $7_{1,7}$ line slightly extended toward the west of SgrB2(M). Such a similarity of the distribution between CH_3OH and $(CH_3)_2O$ is also seen in OMC-1. According to Minh et al. (1993), both of emission of CH_3OH and $(CH_3)_2O$ peak at the southern condensation that has formed by the interaction of the outflow from IRc2 with the quiescent material (Blake et al. 1986). Integrated intensity of the $15_{2,13}$ - $15_{1,14}$ lines is lower than that of the $7_{2,6}$ - $7_{1,7}$ lines. This may be due to the energy level difference of the observed transition (117 K and 31 K).

3.3. C_2H_5OH & $HCOOCH_3$

We observed two C_2H_5OH transitions, the $7_{0,7}$ - $6_{1,6}$ line at 104487.22 MHz and the $5_{1,5}$ - $4_{0,4}$ line at 104808.62 MHz. The $7_{0,7}$ - $6_{1,6}$ line is blended with the $11_{9,2}$-$10_{9,1}$ and the $11_{9,3}$-$10_{9,2}$ lines of C_2H_3CN at 104490.364 MHz. The profile of the $5_{1,5}$ - $4_{0,4}$ line which is not blended with other lines as shown in Figure 1(e). The emission of these lines appeared in almost of our observing points. V_{LSR} is 60 - 73 km s^{-1} and line width of the $5_{1,5}$ - $4_{0,4}$ line is 12 - 24 km s^{-1}.

Since the $7_{0,7}$ - $6_{1,6}$ line is blended with C_2H_3CN, we show only the integrated

intensity map of the $5_{1,5}$ - $4_{0,4}$ line (Figure 2(d)). The distribution is extended in our mapping area. This is different from our CH_3OH result. The upper level energy of the $5_{1,5}$ - $4_{0,4}$ line is low (13 K), so that this transition can be excited even in low temperature region. Emission peak of the $5_{1,5}$-$4_{0,4}$ transition is located at SgrB2(N) and the second peak is located about 40″ west of SgrB2(M).

For $HCOOCH_3$, we observed the $7_{1,6}$ - $6_{1,5}$ E and A lines. They are separable as shown in Figure 1(f). V_{LSR} and line width are 61 - 70 km s^{-1} and 5 - 12 km s^{-1}, respectively. Integrated intensity maps of two transitions are shown in Figures 2(e) and 2(f), respectively. Both maps have emission peak located about 14″ east of SgrB2(N). The A-species line has other peaks at $\sim$ 30″ south of SgrB2(N) and at $\sim$ 35″ west of SgrB2(M), and the E line has a sub peak at $\sim$ 25″ southwest of SgrB2(M). These transitions also have low upper level energy (18 K) so that this is the reason for extended distribution to be excited. The reason why the O-bearing organic molecules have extended distributions will be discussed in section 4.3.

3.4. Column Densities

For molecules we observed two different energy transitions ($(CH_3)_2O$ and C_2H_5OH), we made the column density and the rotation temperature maps. For the other molecules (CH_3OH and $HCOOCH_3$), at each emission peak, we assumed the rotation temperatures, T_{rot}, by using the line survey data of this region taken by the NRO 45-m radio telescope (Ohishi et al. 1998) and the SEST 15-m radio telescope (Nummelin et al. 1998), and derived the column densities. The column densities were derived by assuming that all lines are optically thin under the LTE condition. This analysis is called the rotation diagram analysis, and is commonly adopted for the analysis of molecular lines observed in interstellar medium (See Appendix). Obtained rotation temperatures and column densities are listed in Table 2.

We found the rotation temperature of CH_3OH to be 148 K toward SgrB2(N) from the NRO survey data using the rotation diagram analysis. On the other hand, Nummelin et al. (1998) estimated the temperature toward SgrB2(N) by introducing two components: core and halo. They found high rotation temperature of 238 K and very small beam filling factor, $\eta_{bf} = 0.008$, for core. For halo, they found low temperature of 45 K. Since our mapping result of CH_3OH shows compact distribution, we adopted a temperature of 200 K. We obtained the column density of CH_3OH to be 1.5×10^{17}

cm^{-2}, which is smaller than the value, 5×10^{18} cm^{-2}, obtained by Nummelin et al. (1998) for core. This may be because of very small beam filling factor they estimated.

For $(CH_3)_2O$, the rotation temperature was estimated using the $15_{2,13}$ - $15_{1,14}$ and the $7_{2,6}$ - $7_{1,7}$ lines. The rotation temperature were obtained to be $\sim$ 60 K toward the column density peak which coincides with the emission peak (10″ northeast of SgrB2(N)) and $\sim$ 70 K toward SgrB2(N). These temperatures are lower than the value, 194 K, obtained by Nummelin et al. (1998). This discrepancy may arise from the difference of transitions in the analyses. However, the column density we obtained toward the column density peak, 7.6×10^{15} cm^{-2}, is close to the value 7.9×10^{15} cm^{-2} obtained by Nummelin et al. (1998) toward SgrB2(N). We show the column density and the rotation temperature maps in Figure 4. The range of the column density is (3 - 8) $\times$ 10^{15} cm^{-2} excluding the data less than 2 σ level, and those of the rotation temperature is 20 - 70 K. The distribution of the column density also concentrates toward the emission peak. This indicates $(CH_3)_2O$ abundance is enhanced greatly toward this position.

For C_2H_5OH, we performed the analysis like for $(CH_3)_2O$. However, the $7_{0,7}$ - $6_{1,6}$ line is blended with the $11_{9,3}$ - $10_{9,2}$ and the $11_{9,2}$ - $10_{9,1}$ lines of C_2H_3CN. Therefore we tried to estimate the contribution of C_2H_3CN lines to the $7_{0,7}$ - $6_{1,6}$ line of C_2H_5OH and to remove the contribution. When we observed the $7_{0,7}$ - $6_{1,6}$ line of C_2H_5OH, we found other lines of C_2H_3CN in the same spectrometer. These lines have rotation quantum number, J, equal to the $11_{9,2}$-$10_{9,1}$ and the $11_{9,3}$-$10_{9,2}$ lines of C_2H_3CN and different projected quantum number, k, (k = 3-8 and 10). Then we estimated the contribution of the $11_{9,2}$-$10_{9,1}$ and the $11_{9,3}$ - $10_{9,2}$ lines of C_2H_3CN from the other C_2H_3CN lines using the rotation diagram analysis. However we could not express the population distribution of C_2H_3CN by a single rotation temperature and could not estimate the contribution of C_2H_3CN at 104.5 GHz line.

Since the other C_2H_3CN line emissions are only detected toward SgrB2(N), the contribution of the $11_{9,2}$-$10_{9,1}$ and the $11_{9,3}$ - $10_{9,2}$ lines of C_2H_3CN to the $7_{0,7}$ - $6_{1,6}$ line of C_2H_5OH would be limited toward SgrB2(N). Therefore toward SgrB2(N), the column density of C_2H_5OH was derived with the method like for CH_3OH. The rotation temperature toward SgrB2(N) were obtained using the *trans* and the *gauche* transitions observed by the line survey. We obtained the rotation temperature of 72 K toward SgrB2(N) from NRO data. Nummelin et al. (1998) also obtained 73 K toward the same position. Then we assumed rotation temperature toward the emission peak of the $5_{1,5}$-$4_{0,4}$ line to be 70 K. The column density toward the emission peak, 1.9×10^{16}

cm^{-2}, is higher than 4.2×10^{15} cm^{-2} obtained by Nummelin et al. (1998). We showed the column density and the rotation temperature maps in Figure 5 together with the integrated intensity of the $11_{6,6}$ - $10_{6,5}$ and the $11_{6,5}$ - $10_{6,4}$ (these lines are blended) lines of C_2H_3CN. Toward SgrB2(N), the column density was calculated assuming a rotation temperature of 70 K. The range of the column density is (1-20) $\times 10^{15}$ cm^{-2}.

The second peak appears about 45″ northwest of the strongest peak in both of the column density and the rotation temperature maps. Neither of the $5_{0,5}$ - $4_{1,4}$ nor the $7_{1,7}$ - $6_{0,6}$ lines show peak in this position in their integrated intensity maps, and no continuum source has been detected toward this position. In this second peak, the column density is higher ($\sim 5 \times 10^{16}$ cm $^{-2}$) than the surrounding region by about an order of magnitude, and the rotation temperature is $\sim$ 150 K. Moreover, we found the third peak at $\sim$ 40″ west of SgrB2(M) in both of the column density map and the rotation temperature map. This position nearly coincides with the peak of integrated intensity. The column density and the rotation temperature in this position are $N \sim 8 \times 10^{15}$ cm $^{-2}$ and $T_{\rm rot} \sim 50$ K, respectively. The third peak is close to the sub emission peak of the $7_{1,6}$ - $6_{1,5}$ A line of $HCOOCH_3$.

For $HCOOCH_3$, we found the rotation temperature of 55 K toward SgrB2(N) using the a-type transitions of NRO data. On the other hand Nummelin et al. (1998) assumed the rotation temperature of 200 K and obtained the column density of 1.1×10^{16} cm^{-2} which is higher than our result. This discrepancy would also be due to difference in transitions in analyses. We assumed the rotation temperature of 60 K and obtained the column density of 7.7×10^{15} cm^{-2}.

4. Discussion

4.1. Abundances of the O-bearing Molecules

We derived the fractional abundances of O-bearing molecules relative to hydrogen molecule in their emission peaks. Since all of emission peaks are located near SgrB2(N) we assumed the column density to be $N(H_2) = 5 \times 10^{24}$ cm^{-2} (Martín-Pintad et al. 1990). Derived abundances of molecules are shown in Table 2. Compared with values from a pure gas-phase model (Lee et al. 1996), observed abundances are higher than the calculated results by 2-4 orders of magnitude (Table 2). This indicates that abundances of the O-bearing large organic molecules cannot be explained by pure gas-phase reactions,

and other reaction scheme such as grain-surface reactions may be necessary.

Then we compared our results with models including grain-surface reactions (Caselli et al. 1993, hereafter CHH; Charnley et al. 1992, hereafter CTM). Our results of CH_3OH, $HCOOCH_3$ and $(CH_3)_2O$ are similar to the predicted abundances in the Compact Ridge model of CTM. However, observed C_2H_5OH abundance is higher than the Compact Ridge model values of CTM and CHH by 3-4 orders of magnitude, and higher than the Hot Core model predictions of both of CTM and CHH by 5-6 orders of magnitude.

It is believed that important elements which are initially included on the dust mantle are CO, H_2O, NH_3, CH_4, H_2CO, and CH_3OH, and so on. Such composition of dust mantle cannot explain present observational results of C_2H_5OH. Charnley et al. (1995) investigated the gas-phase chemistry in dense cores where ice mantles containing ethanol and other alcohols have been evaporated. Their calculations showed that methanol, ethanol, propanol, and butanol drive a chemistry leading to the formation of several large ethers and esthers. Evaporated ethanol reacts with molecular ions, HCO^+ and H_3O^+, and protonated ethanol is produced. This protonated ethanol reacts with methanol or ethanol, and recombines with an electron, and finally, $CH_3OC_2H_5$ and $(C_2H_5)_2O$ are formed. According to their calculation, these molecules attain high abundances and should be present in detectable quantities within cores rich in ethanol and methanol. If such molecules were detected, it would be a strong evidence that ethanol is one of the important elements of dust mantle, and present observational results would be explained by this model.

4.2. Comparison of Spatial Distribution with those of Other Molecules and the Spatial Relation to H II Regions

The emission peaks of all observed molecules coincide with the continuum source SgrB2(N) within 15″. In this region the 5 GHz continuum emission peaks (See Figure 1 of Martín-Pintado et al. 1990; Benson & Johnston 1984). Such distribution is very different from emission of several simple molecules ; HC_3N $J = 11$ - 10 peaks in the west of SgrB2(M) and elongated from the north to the south (de Vicente et al. 1997), SO 2_3-1_2 peaks near SgrB2(M) and (N) (Figure 3), and $C^{18}O$ $J = 1$ - 0 peaks toward SgrB2(M) and elongated widely (Lis & Goldsmith 1991). These simple molecules are believed to be produced by ion-molecule reactions or neutral-neutral reactions in the gas-phase. Then the difference between the distributions of the O-bearing large organic molecules

and those of simple molecules indicates that the O-bearing large organic molecules are produced under localized conditions different from those for simple molecules.

Many observational facts suggest that SgrB2(N) is younger than SgrB2(M). High velocity H_2O masers (Reid et al. 1988) show that this region is young, because these masers appear to last for only $\sim 7 \times 10^4$ yr after the formation of an ultra compact H II region (Genzel & Downes 1979). Based on the HC_3N observations (Lis et al. 1993), the outflow age of SgrB2(N) is calculated to be 5,000 years and that of SgrB2(M) is 10,000 years. Lis et al. (1991) derived a relation between the luminosity-to-mass ratio and star formation rate per unit. Based on their hypothesis, Miao & Snyder (1997) estimated the luminosity-to-mass ratio of ~ 30 $L_\odot M_\odot^{-1}$ for SgrB2(N) and ~ 450 $L_\odot M_\odot^{-1}$ for SgrB2(M). In fact, the presence of only 3 UC H II regions in SgrB2(N) indicates that only a few massive stars have recently formed. The core mass of SgrB2(N) is estimated to be $\sim 10^4$ $M_\odot$ (see, Goldsmith et al. 1990; Lis et al. 1993); there appears to be plenty of material from which more stars are formed. In contrast, there are 30 O and early B-type stars presently located in SgrB2(M) (Gaume & Claussen 1995). With so many massive stars in this region, the strong UV radiation field would dissociate all but the most tightly bound molecules.

Therefore it is likely that the O-bearing large organic molecules are closely related with ongoing massive star-formation, and exist in early phase of evolution of molecular cloud. Caselli et al. (1993) have calculated abundances of several large organic molecules in Orion Compact Ridge and Hot Core. In this model, during the collapse phase of the molecular cloud, molecules are liberated from grains into the gas-phase and also formed in the gas-phase, which dramatically increases their abundances. The authors found that after 10^5 yr, due to the higher gas density and the transitory nature of large abundances of organic molecules in ion-molecule chemistry, many molecules tend to decrease sharply in abundance. If SgrB2(N) is younger than SgrB2(M) our observational result that the O-bearing large organic molecules are concentrated toward SgrB2(N) is consistent with this scenario. Although no model calculations have been made for SgrB2, such scenario proposed for Orion might be applied to SgrB2.

4.3. Extended Component of the O-bearing Molecules

For C_2H_5OH and $HCOOCH_3$, the extended distributions are also seen. The upper level energies of these transitions are lower (13-18 K) than those of CH_3OH and $(CH_3)_2O$

(31-328 K). Therefore, although these transitions of CH_3OH and $(CH_3)_2O$ can be excited toward only high temperature region (for example SgrB2(N)), those of C_2H_5OH and $HCOOCH_3$ can be excited even in low temperature region. 36 GHz emission of CH_3OH is also extended from the northeast of the SgrB2(N) to the west of SgrB2(N) and (M) (Liechti and Wilson 1996). This indicates that CH_3OH exists even in the extended region. Since CH_3OH can be produced even in gas-phase reaction, CH_3OH which exist far from H II regions may be produced in gas-phase reaction. On the other hand, $HCOOCH_3$ is believed to be produced from dust-evaporated H_2CO in the gas-phase reactions as follows:

$$\begin{aligned} CH_3OH_2^+ + H_2CO &\rightarrow H_2COOCH_3^+ + H_2 \\ H_2COOCH_3^+ + e &\rightarrow HCOOCH_3 + H \end{aligned} \qquad (2.1)$$

The sublimation temperature of H_2CO is lower ($\sim$ 45 K for $n(H_2) \sim 10^5$) than that of CH_3OH ($\sim$ 70 K for $n(H_2) \sim 10^5$) (Nakagawa 1980). This indicates that H_2CO can evaporate in lower dust temperature region. Therefore, distribution of H_2CO may be extended than those of CH_3OH. Since H_2CO can also be produced even in the gas-phase reactions, if reaction 2.1 is correct, the extended distribution of $HCOOCH_3$ may trace that of H_2CO which is evaporated from low temperature dust grains or produced in gas-phase reactions.

For $(CH_3)_2O$, the $15_{2,13}$ - $15_{1,14}$ line shows compact distribution, however, the $7_{2,6}$ - $7_{1,7}$ line shows slightly extended distribution. $(CH_3)_2O$ is believed to be produced from dust-evaporated CH_3OH in gas-phase reactions like $HCOOCH_3$ as follows:

$$\begin{aligned} CH_3OH_2^+ + CH_3OH &\rightarrow (CH_3)_2OH^+ + H_2O \\ (CH_3)_2OH^+ + e &\rightarrow (CH_3)_2O + H \end{aligned} \qquad (2.2)$$

Therefore the slightly extended distribution of $(CH_3)_2O$ would reflect the extended distribution of low energy CH_3OH emission. However, the reactants of this reaction are related with only CH_3OH, so that this distribution would be more compact compared to $HCOOCH_3$.

Sublimation temperature of C_2H_5OH is similar ($\sim$ 67 K for $n(H_2) \sim 10^5$) with that of CH_3OH. Therefore if CH_3OH which exist far from H II regions were evaporated from dust grains, C_2H_5OH could also be evaporated from dust grains. However, dust temperature of the SgrB2 molecular cloud is low ($\sim$ 34 K) (Gordon et al. 1988). Therefore we need to consider some candidates which heat dust grains except for SgrB2(N).

The subpeak of the $5_{0,5}$ - $4_{1,4}$ line of C_2H_5OH which is located in the west of SgrB2(N) is close to the sub peak of $HCOOCH_3$. In this position, C_2H_5OH shows slightly higher rotation temperature ($\sim$ 50K) than the surrounding region. This indicates that very young IR sources which cannot be observed by radio continuum may be embedded. If such young sources existed, they would heat dust grains.

According to Schilke et al. (1997), SiO is produced in the gas-phase of molecular outflows, through the sputtering of Si-bearing material in grains. The sputtering is driven by neutral particle impact on charged grains in C-type shocks. And it is known that SiO lines are broadened and shifted relative to the emission from the ambient gas (Martín-Pintado et al. 1992). It is likely that dynamical effects are responsible for the release of Si, or Si-bearing material, from the grains into the gas-phase. In the SgrB2 molecular cloud, SiO is detected and it is well known that the distribution is extended widely (Martín-Pintado et al. 1997). This indicates that there are some turbulence which may occur sputtering of the Si-bearing material in grains in a wide region of the SgrB2 molecular cloud. C_2H_5OH may also be released during such sputtering process as well.

5. Conclusions

We carried out mapping observations of the O-bearing large organic molecules toward the SgrB2 molecular cloud. All emission peaks are located within 10″-15″ of SgrB2(N) which is associated with H II regions and in which there are young O,B-type stars. Especially, CH_3OH and $(CH_3)_2O$ distributions are compact and close to each other. $(CH_3)_2O$ is believed to be formed in the gas-phase from CH_3OH that has been evaporated from dust mantle. Since CH_3OH has high abundance in the emission peak, $(CH_3)_2O$ would be formed from abundant and highly excited CH_3OH in this region. And the distributions of the O-bearing molecules associated H II regions indicate that the production of these organic molecules are closely related with active star-formation.

C_2H_5OH and $HCOOCH_3$ show extended distributions. The low energy transition of $(CH_3)_2O$ also show slightly extended distribution. This trend is seen in the case of low energy 36GHz emission of CH_3OH. This indicates that these molecules exist in a region far from H II regions. It is believed that $HCOOCH_3$ is produced from $CH_3OH_2^+$ and H_2CO, and $(CH_3)_2O$ is produced from $CH_3OH_2^+$ and CH_3OH. Therefore the extended distributions of $HCOOCH_3$ and $(CH_3)_2O$ would reflects those of low energy CH_3OH. Since production mechanism of $(CH_3)_2O$ is related to only CH_3OH, the distribution

would more reflect that of CH_3OH rather than $HCOOCH_3$, and be compact. The extended distribution of C_2H_5OH cannot be interpreted by gas-phase reactions. Since in SgrB2, SiO which is produced in gas-phase through the sputtering shows extended distribution, C_2H_5OH may be also evaporated from dust grains by such sputtering.

We obtained the column densities of the O-bearing molecules to be $N(CH_3OH) = 1.5 \times 10^{17}$, $N(C_2H_5OH) = 1.9 \times 10^{16}$, $N(HCOOCH_3) = 7.7 \times 10^{15}$, and $N((CH_3)_2O) = 7.6 \times 10^{15}$, respectively, in the emission peak. The fractional abundances of $X(CH_3OH) = 3 \times 10^{-8}$, $X(C_2H_5OH) = 4 \times 10^{-9}$, $X(HCOOCH_3) = 2 \times 10^{-9}$, and $X((CH_3)_2O) = 2 \times 10^{-9}$, respectively. This observational results cannot be explained by pure gas-phase reaction models, however, the model calculations which include grain-surface reactions for two hot cores in Orion-KL, Compact Ridge and Hot Core, can nearly explain observational results except for C_2H_5OH. If C_2H_5OH were one of the element which is initially included on the dust grains, observational results could be reproduced.

Appendix

Rotation Diagram Analysis

The rotational temperature and the column density were determined from the observed line intensities using the rotational diagram method, which is commonly adopted for the analysis of molecular lines observed in interstellar medium (e.g. Turner 1991). This method is based on the assumption that the lines are optically thin and that the rotation temperature between the upper and lower levels of the transition is much higher than that of the 2.7 K continuum background. The observed line intensity $\int T_{\rm b} dv$ is proportional to the column density N as follows :

$$\int T_{\rm b} dv = \frac{8\pi^3 \nu \mu^2 S N}{3kQ} \exp\left(-\frac{E_{\rm u}}{kT_{\rm rot}}\right)$$

where ν is the transition frequency, S the line strength, μ the dipole moment, Q the partition function at temperature $T_{\rm rot}$, and $E_{\rm u}$ is the energy of the upper level. From this we can obtain the following relation :

$$\ln\left(\frac{3k}{8\pi^3 \nu \mu^2 S} \int T_{\rm b} dv\right) = \ln\left(\frac{N}{Q}\right) - \frac{E_{\rm u}}{kT_{\rm rot}}$$

In this method, a plot of the natural logarithm of the line intensities versus the energy of the upper level should produce a straight line whose intercept at $E_{\rm u} = 0$ is proportional to the molecular column density and whose slope gives $T_{\rm rot}$.

Table 1. Line parameters and characteristics of the NRO 45-m telescope

Molecule	Transition	Frequency [MHz]	E_u[a] [K]	θ_{mb}[b] ["]	η_{mb}[c] [%]
CH_3OH	$15_{3,13}$-$14_{4,10}$ A^+	88594.843	328	17	50
CH_3OH	$15_{3,12}$-$14_{4,11}$ A^-	88940.047	328	17	50
$(CH_3)_2O$	$15_{2,13}$-$15_{1,14}$ AA	88709.072	117	17	50
$(CH_3)_2O$	$15_{2,13}$-$15_{1,14}$ EE	88707.644	117	17	50
$(CH_3)_2O$	$15_{2,13}$-$15_{1,14}$ EA	88706.216	117	17	50
$(CH_3)_2O$	$15_{2,13}$-$15_{1,14}$ AE	88706.216	117	17	50
$HCOOCH_3$	$7_{1,6}$-$6_{1,5}$ E	88843.176	18	17	50
$HCOOCH_3$	$7_{1,6}$-$6_{1,5}$ A	88851.620	18	17	50
C_2H_5OH	$7_{0,7}$-$6_{1,6}$	104487.22	16	15	49
C_2H_5OH	$5_{1,5}$-$4_{0,4}$	104808.62	13	15	49
$(CH_3)_2O$	$7_{2,6}$-$7_{1,7}$ AA	104705.93	31	15	49
$(CH_3)_2O$	$7_{2,6}$-$7_{1,7}$ EE	104703.30	31	15	49
$(CH_3)_2O$	$7_{2,6}$-$7_{1,7}$ EA	104700.62	31	15	49
$(CH_3)_2O$	$7_{2,6}$-$7_{1,7}$ AE	104700.62	31	15	49

[a] E_u is the upper level energy above the ground state

[b] θ_{mb} is the beam size

[c] η_{mb} is the main beam efficiency

Table 2. Fractional abundances of the observed molecules at the emission peak and predicted abundances from chemical model

Molecule	T_{rot} [K]	N [cm^{-2}]	X	model calculations				
				Lee et al.[a]	Caselli et al.[b]		Charnley et al.[c]	
					C.R[d]	H.C[e]	C.R[f]	H.C[g]
CH_3OH	200[h]	1.5(17)	3(-8)	6.5(-10)	2.0(-5)	1.0(-10)	7.2(-7)	1.7(-10)
C_2H_5OH	70[h]	1.9(16)	4(-9)	2.4(-13)	8.5(-12)	4.4(-13)	9.2(-12)	4.2(-14)
$HCOOCH_3$	60[h]	7.7(15)	2(-9)	5.6(-12)	3.7(-8)	1.3(-13)	7.7(-9)	4.4(-12)
$(CH_3)_2O$	60	7.6(15)	2(-9)	1.7(-13)	3.2(-8)	1.0(-13)	1.5(-8)	1.3(-15)

[a]Gas-phase model; T_k = 50 K, $n_H = 10^5$ cm^{-3}, 10^5 yr (Lee et al. 1996)

[b]Model for Orion-KL (Caselli et al. 1993)

[c]Model for Orion-KL (Charnley et al. 1992)

[d]Compact Ridge; T_k = 100 K, $n_H = 10^6$ cm^{-3}, 3.2×10^4 yr

[e]Hot Core; T_k = 200 K, $n_H = 1.3 \times 10^7$ cm^{-3}, 3.2×10^4 yr

[f]Compact Ridge; T_k = 100 K, $n_H = 2 \times 10^6$ cm^{-3}, 4×10^4 yr

[g]Hot Core; T_k = 200 K, $n_H = 2 \times 10^7$ cm^{-3}, 6.3×10^4 yr

[h]T_{rot} is assumed

a(b) means a $\times 10^b$.

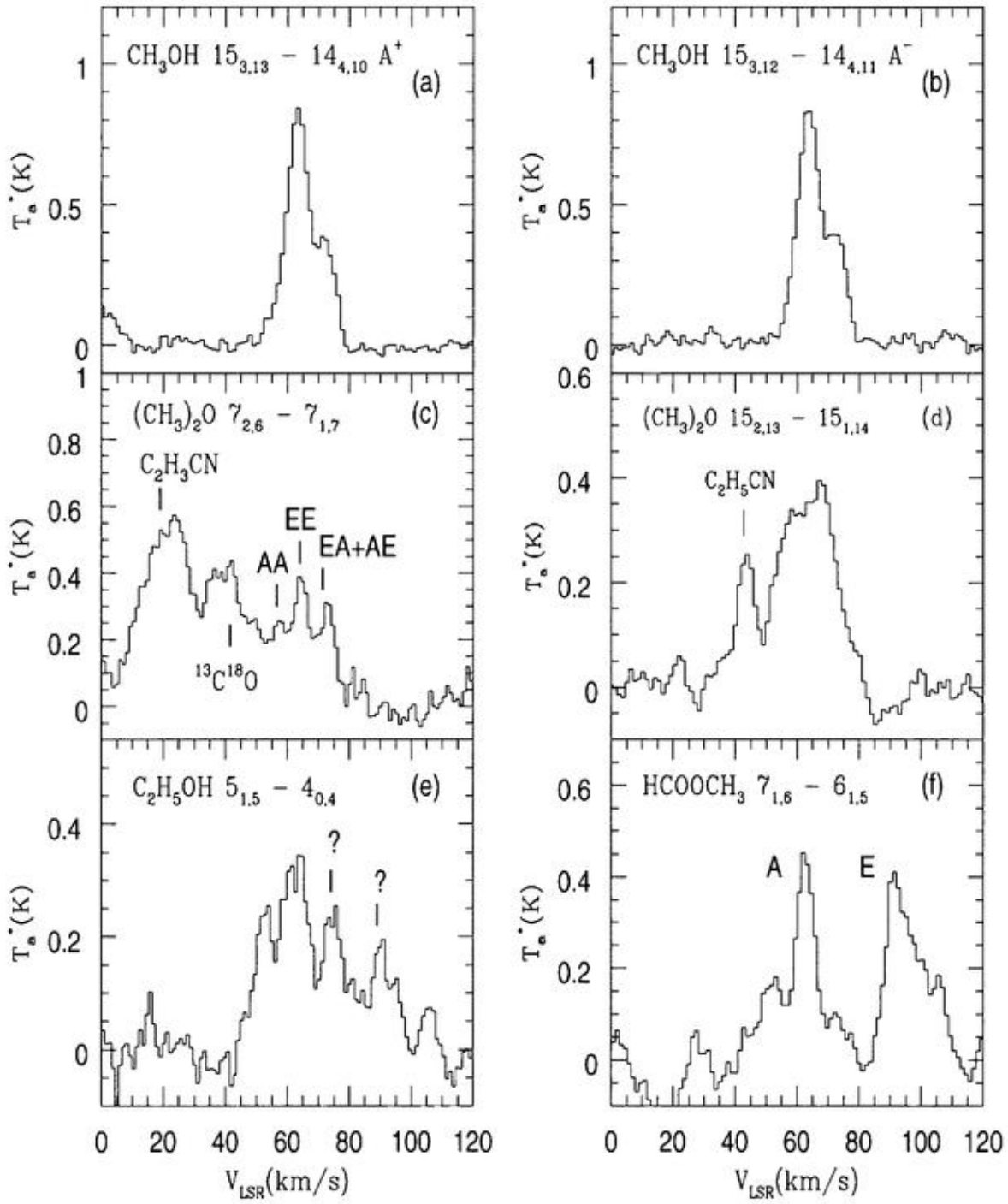

Fig. 1.— Spectra of (a) CH_3OH $15_{3,13}$-$14_{4,10}$ A^+ transition at 88594.843 MHz; (b) CH_3OH $15_{3,12}$-$14_{4,11}$ A^- transition at 88940.047 MHz; (c) $(CH_3)_2O$ $7_{2,6}$-$7_{1,7}$ transition at 104700.62 MHz (EA, AE), 104703.30 MHz (EE), and 104705.93 MHz (AA); (d) $(CH_3)_2O$ $15_{2,13}$-$15_{1,14}$ transition at 88706.216 MHz (EA, AE), 88707.644 MHz (EE), and 88709.072 MHz (AA); (e) C_2H_5OH $5_{1,5}$-$4_{0,4}$ transition at 104808.62 MHz. Question mark indicate unidentified line; (f) $HCOOCH_3$ $7_{1,6}$-$6_{1,5}$ transition at 88843.176 MHz (E) and 88851.620 MHz (A).

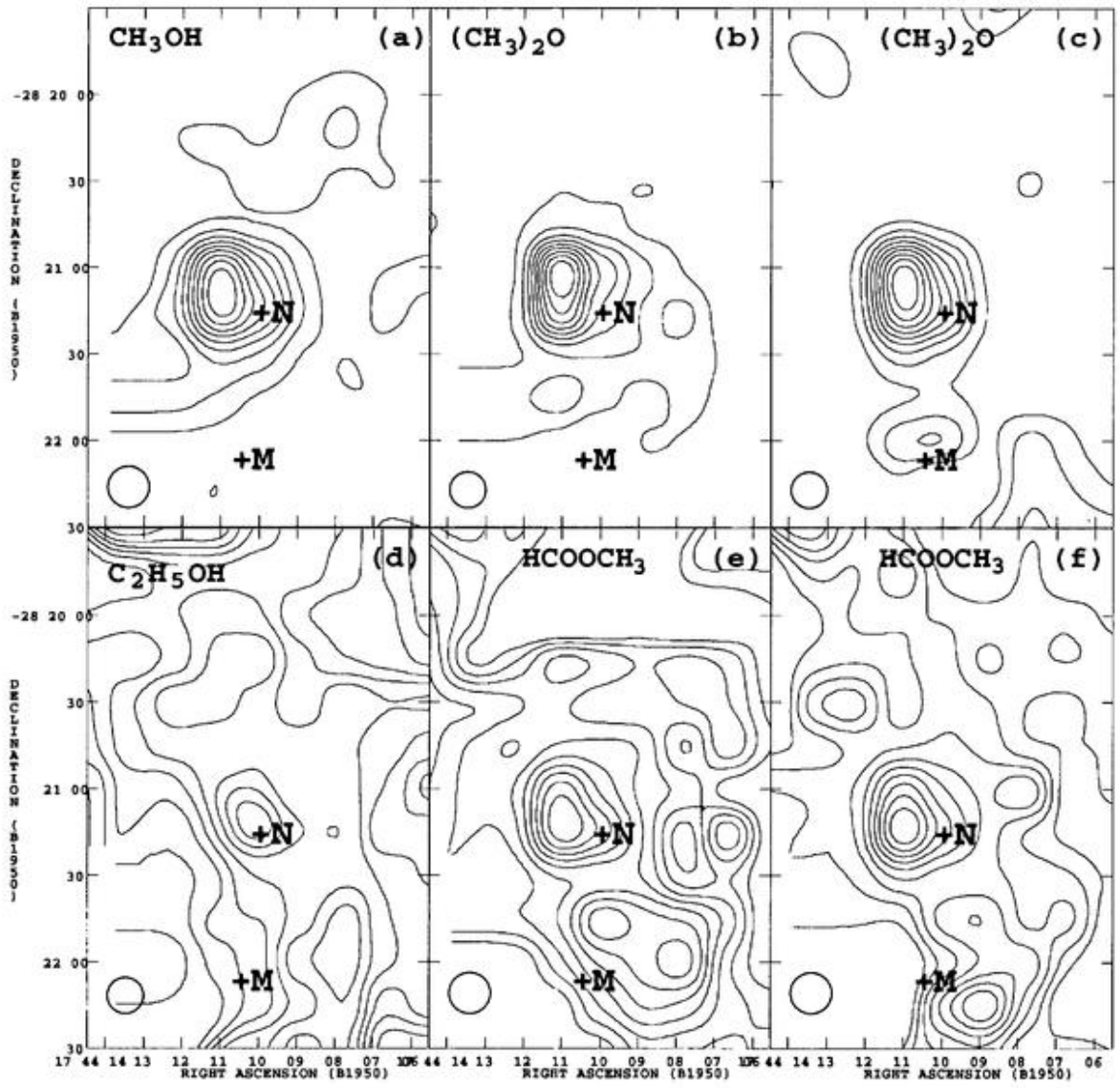

Fig. 2.— Integrated intensity distribution of (a) the $15_{3,13}$-$14_{4,10}$ A^+ transition of CH_3OH; (b) the $7_{2,6}$-$7_{1,7}$ transition of $(CH_3)_2O$; (c) the $15_{2,13}$-$15_{1,14}$ transition of $(CH_3)_2O$; (d) the $5_{1,5}$-$4_{0,4}$ transition of C_2H_5OH; (e) the $7_{1,6}$-$6_{1,5}$ A transition of $HCOOCH_3$; (f) the $7_{1,6}$-$6_{1,5}$ E transition of $HCOOCH_3$. Two crosses represent the position of SgrB2(M) and SgrB2(N). The contours are 10 to 90 % in steps of 10 % of the maximum value. The circle in the lower left-hand corner indicates the beam size, θ_{mb}.

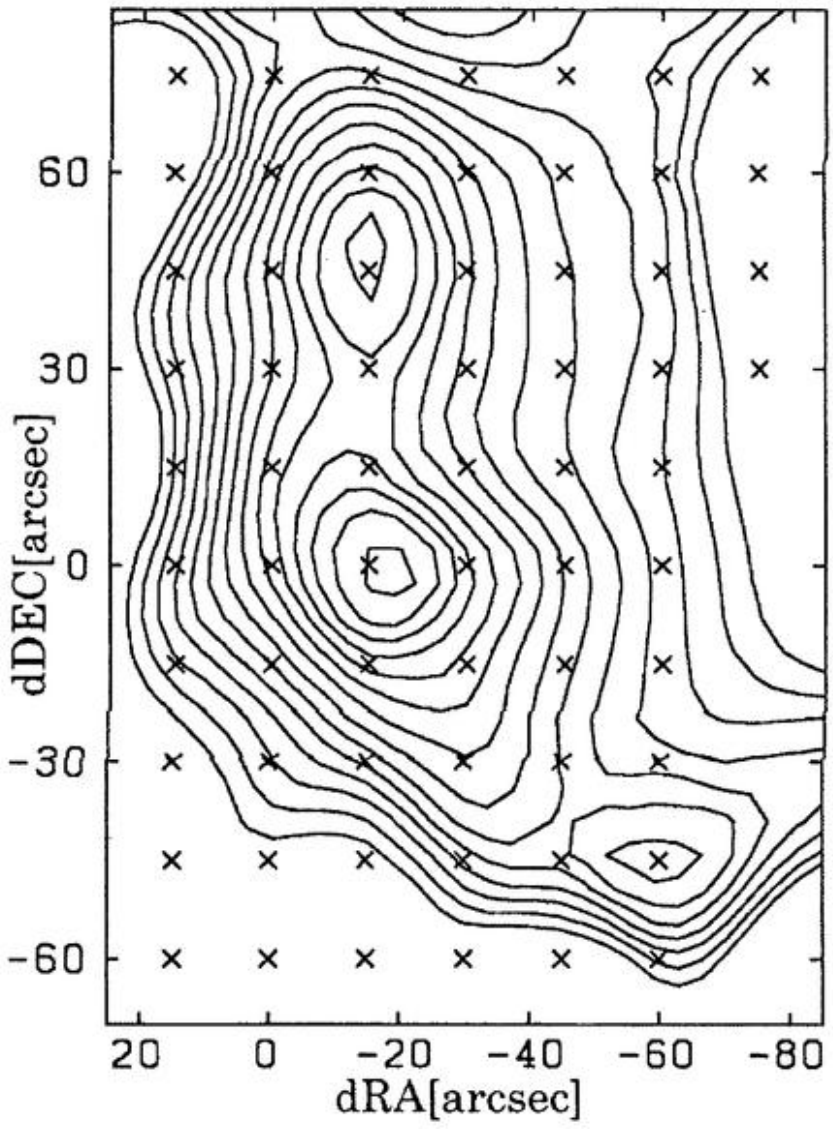

Fig. 3.— Integrated intensity distribution of 2_3 - 1_2 SO. The contours are 2 to 60 K*km s^{-1} in steps of 2 K*km s^{-1}. The (0,0) position is RA(1950.0)= $17^h44^m10.^s6$, Dec(1950.0)=-28°22′05″ (SgrB2(M)).

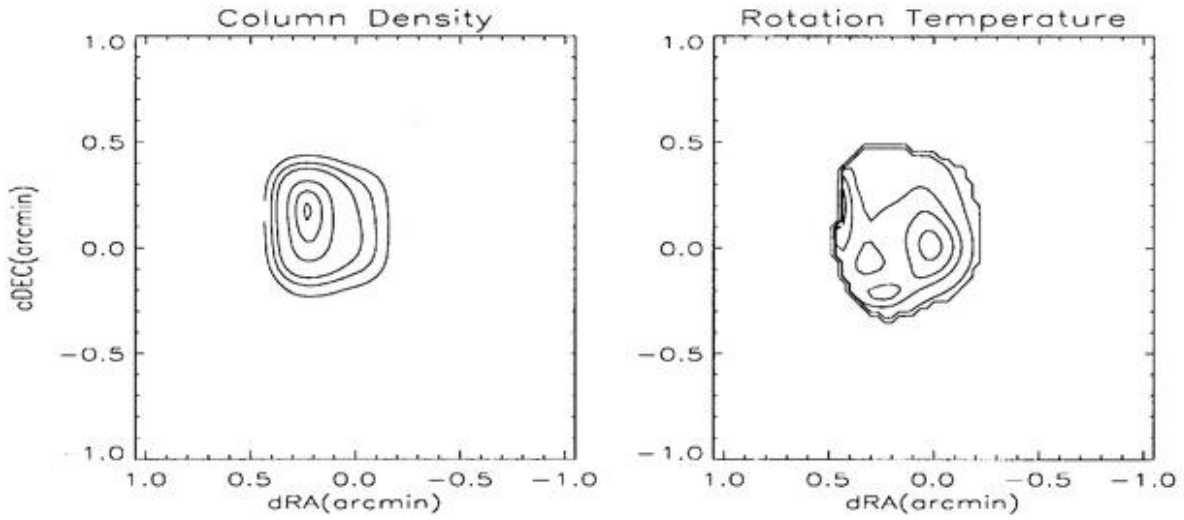

Fig. 4.— The column density and the rotation temperature maps of $(CH_3)_2O$. *left* : The contours are 3, 4, 5, 6, 7 and 7.5 × 10^{15} cm^{-2}. *right* : The contours are 20, 50, 60, 65 and 70 K. The (0,0) position is RA(1950.0)=$17^h44^m10.^s0$, Dec(1950.0)=-28°21′15″(SgrB2(N)).

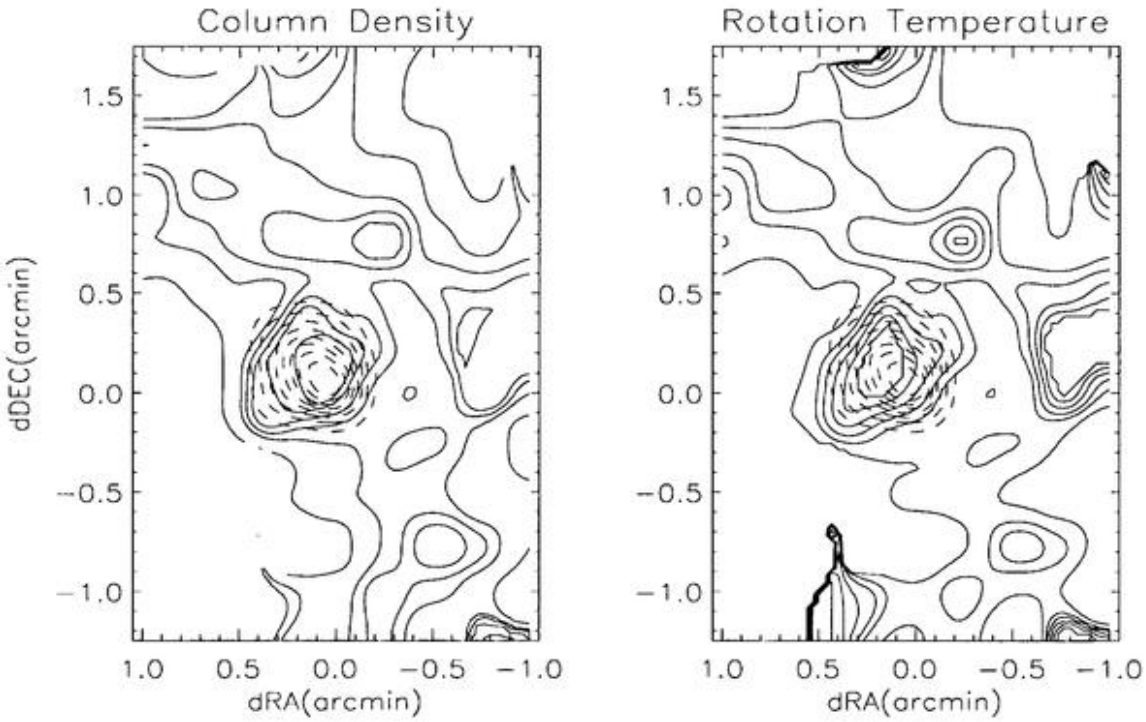

Fig. 5.— The column density and the rotation temperature maps of C_2H_5OH (solid line) and the integrated intensity of the 11_6-10_6 lines at 104429.311 MHz of C_2H_3CN. *left* : The contours are 1, 2, 3, 4, 7, 10, 50, 100 and 500 $\times 10^{15}$ cm $^{-2}$. *right* : The contours are 10, 20, 30, 40, 60, 80, 100, 150 and 200 K. the contours of integrated intensity of C_2H_3CN are 20 to 90 % in steps of 10 % of the maximum value 9.2 K*km s^{-1}. The (0,0) position is RA(1950.0)=$17^h44^m10.^s0$, DEC(1950.0)=-28°21′15″.

Chapter 3

Mapping Observations of the NH- & NH_2-bearing Large Organic Molecules toward Sagittarius B2

ABSTRACT

Mapping observations of methylamine (CH_3NH_2), methylenimine (CH_2NH), formamide (NH_2CHO) and cyanamide (NH_2CN) were carried out toward SgrB2, using the 45-m radio telescope of the Nobeyama Radio Observatory. The mapping observations of CH_3NH_2 and CH_2NH were carried out for the first time.

CH_3NH_2 has the strongest emission peak at $\sim$ 17″ southwest of SgrB2(N) and the second peak at $\sim$ 38″ south of SgrB2(M). The second peak position coincides with SgrB2(S) where OH maser has been detected. The emission distribution is elongated from the north to the south in the west of SgrB2(M) and (N), and the FWHM of the distribution is about 1.2′ × 2′.

The emission peak of CH_2NH is located south of the CH_3NH_2 peak and $\sim$ 19″ northwest of SgrB2(M). The distribution of CH_2NH is also extended from the north to the south. The FWHM of the distribution is slightly wider, $\sim$ 2′ × 3′ because of larger beam size (49″) than that of CH_3NH_2 (21″).

In the case of NH_2CHO, we observed two transitions, $5_{1,5}$ - $4_{1,4}$ at 102.1 GHz and $5_{2,4}$ - $4_{2,3}$ at 105.9 GHz. The distribution of these two lines are different. The $5_{1,5}$ - $4_{1,4}$ line peak is located $\sim$ 42″ west of SgrB2(M) and the second peak is located $\sim$ 58″ northeast of SgrB2(N). Emission peak of the $5_{2,4}$ - $4_{2,3}$ line is $\sim$ 17″ southwest of SgrB2(N). The FWHM of the distribution of the $5_{1,5}$ - $4_{1,4}$ line is about 2′ × 3.5′, and that of $5_{2,4}$ - $4_{2,3}$ line is smaller than that of the $5_{1,5}$ - $4_{1,4}$ line, about 1′ × 1.5′.

The distribution of NH_2CN is different from those of the other NH- and NH_2-bearing molecules; emission peak is located at $\sim$ 54″ northeast of SgrB2(N). The distribution shows a L-like structure which is extended from the north of the SgrB2(N) to the west of SgrB2(M) and (N). The size is about 2.3′ × 2.5′.

We compared our results with previous observations and found that the elongated distribution of the NH- and NH_2-bearing molecules are very similar to the envelope of the 1.3 mm dust continuum (Gordon et al. 1993) and the HC_3N J = 1 - 0 line (de Vicente et al. 1997). The distribution of NH_2CN is similar to those of HNCO (Minh et al. 1998; Wilson et al. 1996) and CH_3OH maser at 36 GHz (Liechti et al. 1996). Emission peaks of these molecules are also located near the emission peak of NH_2CN.

From the mapping observations of the NH- and NH_2-bearing molecules, we found that the production mechanism of these molecules may be different from the O-bearing

and/or CN-bearing organic molecules, which are believed to be produced on dust grains and are evaporate from dust mantle by UV radiation from O,B-stars in II II regions. It is likely that the NH- and NH_2-bearing molecules reflect the distribution of the high density gas. This indicates that production mechanism of the NH- and NH_2-bearing molecules may be the gas-phase reactions like HC_3N.

1. Introduction

The NH- and NH_2-bearing organic molecules (CH_3NH_2, CH_2NH, NH_2CHO and NH_2CN) were discovered toward SgrB2 for the first time, and have not been detected in other objects for many years. Existence of methylamine (CH_3NH_2) was originally suggested in SgrB2 by Fourikis et al. (1974) on the basis of a marginal detection of the 2_{02} - 1_{10} Aa-state transition at 8.78 GHz, and Kaifu et al. (1974) claimed its detection by observing the 5_{15} - 5_{05} Aa-state and the 4_{14} - 4_{04} As-state transitions at 73 and 86 GHz, respectively. Methylenimine (CH_2NH) was originally observed by Godfrey et al. (1973) on the basis of the 1_{10} - 1_{11} transition at 5.3 GHz. Recently, Dickens et al. (1996) carried out a survey of CH_2NH in several molecular clouds with various temperatures, and detected it toward some molecular clouds. They found that the abundance ratio, CH_2NH/HCN, in cold, dense regions with no sign of star formation could be explained by pure gas-phase reactions, however in hot regions, the CH_2NH abundance was enhanced. Bernstein et al. (1995) noted that CH_2NH is a product of UV irradiation of model interstellar icy grain mantles. Formamide (NH_2CHO) was first detected at 6 cm (Rubin et al. 1971). Kuan and Snyder (1996) mapped this molecule toward SgrB2(N) using the three-element millimeter array of the Berkeley-Illinois-Maryland Association (BIMA) at Hat Creek Radio Observatory. They found NH_2CHO was detected only toward SgrB2(N). Cyanamide (NH_2CN) was first detected at 8.5GHz and 100.6GHz by Turner et al. (1975) toward SgrB2. Then Turner (1991) detected several transitions of this molecule toward SgrB2 and Orion-KL.

Since these molecules are large organic molecules and the saturation degrees are high, it is believed that their formation on the dust grain is important like other O-bearing large organic molecules (CH_3OH, C_2H_5OH, $HCOOCH_3$, $(CH_3)_2O$ etc). However, there have been few observations of the NH- and NH_2-bearing large organic molecules, so that the formation mechanism of these molecules are still unknown. In order to study the chemical role of dust grains on production of organic species in massive star forming

regions, it is important to compare the distributions of these molecules with H II regions and/or dust continuum distributions. Then we carried out mapping observations toward SgrB2 in the NH- and NH_2-bearing molecular species.

We performed mapping observations of the O-bearing large organic molecules (see Chap. 2). Since nitrogen is one of the basic element in the universe as oxygen, it is important to investigate molecules which include nitrogen, and to analyze the results together with the observational results of the O-bearing molecules.

2. Observations

The initial observations in the CH_3NH_2 lines were made in 1996 September, using the 12-m radio telescope of the National Radio Astronomy Observatory at Kitt Peak, Arizona. We used the 3 mm SIS receiver, with system temperature was $\sim$ 300 K. In the observations, we simultaneously used the hybrid autocorrelator with the 600 MHz total bandwidth with the frequency resolution of 781 kHz, and the filter banks with the frequency resolution of 1 MHz. The pointing was checked by observing planets(Jupiter, Saturn and Venus), and focus was checked at the same time. The beam size at the frequency of CH_3NH_2 was about 70". The on-source integration time was about 30 minutes per point.

Higher spatial resolution observations in the CH_3NH_2 and CH_2NH lines were made in 1997 April and May, and those in the NH_2CHO and NH_2CN lines were made in 1998 April using the 45m radio telescope of the Nobeyama Radio Observatory. We used three SIS receivers covering the 7 mm, 4 mm and 3 mm regions. Typical system temperatures of the three receivers were $\sim$ 200 ,$\sim$ 300 and $\sim$ 350 K, respectively. The backend was consisted of two sets of acousto-optical radio spectrometers (AOSs), one with a bank of eight high-resolution AOSs with the frequency resolution of 37 kHz and 40 MHz bandwidth, the other with a bank of eight wide-band AOSs with the frequency resolution of 250 kHz and 250 MHz bandwidth. The pointing was checked every two hours by observing the SiO maser of VX Sgr. The estimated pointing accuracy was $\sim$ 5″ rms. The observations were made in position-switching mode. The line parameter, beam sizes and main-beam efficiencies are summarized in Table 1. The on-source integration time was 60 - 320 seconds per position.

3. Results

3.1. CH_3NH_2 and CH_2NH

At Kitt Peak, we observed six lines of CH_3NH_2: the Aa $1_{1,1}$ - $0_{0,0}$ line at 79009.6 MHz, the Aa $3_{1,3}$ - $3_{0,3}$ line at 76839.7 MHz, the Aa $5_{1,5}$ - $5_{0,5}$ line at 73044.9 MHz, the Ea 1_{-1} - 0_0 line at 79209.4 MHz, the Ea 2_{-1} - 2_0 line at 78928.1 MHz, the Ea 4_{-1} - 4_0 line at 76782.5 MHz. The Ea 1_{-1} - 0_0 line was observed as absorption and the other lines were observed as emission. We mapped the Aa $3_{1,3}$ - $3_{0,3}$ and the Aa $5_{1,5}$ - $5_{0,5}$ line and the intensity of the Aa $3_{1,3}$ - $3_{0,3}$ line was slightly stronger than the Aa $5_{1,5}$ - $5_{0,5}$ line. Their emission peaks were found near both of SgrB2(M) and SgrB2(N). However, since the beam size was larger ($\sim 70''$) than the separation between SgrB2(N) and (M) ($\sim 50''$), we could not see which source corresponded to the CH_3NH_2 emission peak.

Therefore we carried out higher spatial resolution (beam size = $49''$ and $15''$-$21''$) mapping observations using the 45-m radio telescope. We observed the Aa $4_{1,4}$ - $4_{0,4}$ line at 75135.452 MHz of CH_3NH_2, because this transition was expected to have the highest intensity from Kitt Peak observations. We also observed the $4_{0,4}$ - $3_{1,3}$ line at 105794.118 MHz and the $3_{0,3}$ - $2_{1,2}$ line at 35065.723 MHz of CH_2NH. In Figures 1(a) $\sim$ 1(c), we show profiles of these transitions. The mapping area is about $3'20'' \times 4'40''$ which includes SgrB2(M) and SgrB2(N), with a grid spacing of $20''$. The $3_{0,3}$ - $2_{1,2}$ transition of CH_2NH has the V_{LSR} of 53 $\sim$ 68 km s^{-1} and linewidth of 13 $\sim$ 30 km s^{-1}. There exists a small peak velocity gradient from the north ($\sim$ 68 km s^{-1}) to the south ($\sim$ 53 km s^{-1}). The $4_{0,4}$ - $3_{1,3}$ line of CH_2NH is blended with the $H^{13}CCCN$ J = 12 - 11 line at 105799.093 MHz, separated from CH_2NH about 14 km s^{-1}. The detected lines have linewidth between 22 $\sim$ 32 km s^{-1}, and it was hard to separate two lines. The Aa $4_{1,4}$ - $4_{0,4}$ line of CH_3NH_2 has the V_{LSR} of 58 $\sim$ 67 km s^{-1} and linewidth between 10 $\sim$ 18 km s^{-1}. These V_{LSR} and linewidth are typical for large organic molecules in SgrB2.

We show integrated intensity maps of these molecules in Figures 2(a) and 2(b). For CH_2NH, only the map of the $3_{0,3}$ - $2_{1,2}$ line is shown. The emissions of both molecules are elongated from the north to the south in the west of SgrB2(M) and (N), and there is little emission in the eastern side. This is consistent with that the emission of many molecular species suddenly weaken in the east. For instance, in the west of SgrB2(M) and (N), it is known that HC_3N has peak and is elongated from the north to the south (de Vicente et al. 1997).

The FWHM of the distribution of CH_3NH_2 is (RA $\times$ DEC) = $1.2' \times 2'$. The peak

position of CH_3NH_2 is located about 19" southwest of SgrB2(N). This is displaced from those of other O-bearing and CN-bearing organic molecules (CH_3OH, C_2H_5OH, $HCOOCH_3$, $(CH_3)_2O$, C_2H_3CN and C_2H_5CN, etc) which are concentrated toward SgrB2(N) and the 5 GHz continuum source. (See Chap. 2; Miao & Snyder 1997). And the second peak is $\sim$ 38" south of SgrB2(M), which coincides with SgrB2(S) where OH maser has been detected. The brightness temperatures of CH_2NH are higher than those of CH_3NH_2 in the whole mapping region. The distribution is also extended from the north to the south like CH_3NH_2, but because the beam size at 35 GHz ($\sim$ 49") is larger than that at 75 GHz ($\sim$ 21"), CH_2NH emission looks slightly more extended (2' $\times$ 3'). The peak position of CH_2NH is $\sim$ 30" south of the strongest peak of CH_3NH_2 and $\sim$ 19" northwest of SgrB2(M).

3.2. NH_2CHO

We observed the $5_{1,5}$ - $4_{1,4}$ line at 102064.353 MHz and the $5_{2,4}$ - $4_{2,3}$ line at 105972.601 MHz. The profiles of these transitions are shown in Figures 1(d) and 1(e). The $5_{1,5}$ - $4_{1,4}$ transition has the V_{LSR} of 50 $\sim$ 73 km s^{-1} and the linewidth of 11 $\sim$ 24 km s^{-1}. There exists a small peak velocity gradient from the northwest ($\sim$ 73 km s^{-1}) to the southeast ($\sim$ 50 km s^{-1}). In the $5_{2,4}$ - $4_{2,3}$ line, the V_{LSR} is 58 $\sim$ 70 km s^{-1} and the linewidth is 10 $\sim$ 20 km s^{-1}. Peak velocity has a small gradient from the north ($\sim$ 70 km s^{-1}) to the south ($\sim$ 58 km s^{-1}).

The mapping area of NH_2CHO is about 2'40" $\times$ 4'40", with a grid spacing of 20". This area includes SgrB2(M) and (N), but is slightly smaller than those of CH_3NH_2 and CH_2NH. Integrated intensity maps of NH_2CHO are shown in Figures 2(c) and 2(d). In the $5_{1,5}$-$4_{1,4}$ transition, the distribution is elongated from the north to the south in the west of SgrB2(M) and (N), like CH_3NH_2 and CH_2NH. The FWHM width of the emitting region is about 2' $\times$ 3.5'. The peak position of this line is located about 42" west of SgrB2(M) and a weak peak is located $\sim$ 58" northeast of SgrB2(N). In the $5_{2,4}$ - $4_{2,3}$ line, the emitting region is elongated from the north to the south like $5_{1,5}$ -$4_{1,4}$ line, however, is more compact than that of the $5_{1,5}$ -$4_{1,4}$ line. The FWHM of the emitting region of the $5_{2,4}$ - $4_{2,3}$ line is about 1' $\times$ 1.5'. The peak position of the emitting region is about 17" southwest of SgrB2(N). This peak position is displaced from that of the $5_{1,5}$ - $4_{1,4}$ line about 44" and nearer to SgrB2(N) than the peak position of the $5_{1,5}$ - $4_{1,4}$ line.

Since the kinetic temperature of SgrB2(N) is higher ($\sim$ 400 K) than that of

SgrB2(M) ($\sim$ 300 K) (de Vicente et al. 1997) and the energy of the $5_{2,4}$ - $4_{2,3}$ line is higher (27 K) than that of $5_{1,5}$ - $4_{1,4}$ line (18 K), it is considered that near SgrB2(N), NH_2CHO is highly excited than SgrB2(M). Previous interferometric observations of NH_2CHO were made in the $4_{3,2}$ - $3_{3,1}$ and the $4_{3,1}$ - $3_{3,0}$ line (Kuan and Snyder 1996) using the BIMA array with the spatial resolution of 10.″8 × 4.″6. They found a compact emission peak toward SgrB2(N). The difference between our single dish map and the interferometric map is probably because of the different beam sizes between the two observations. Furthermore interferometric observations are not sensitive to extended emissions.

3.3. NH_2CN

The V_{LSR} of the $5_{1,4}$ - $4_{1,3}$ line of NH_2CN is 50 $\sim$ 73 km s^{-1} and the linewidth is 10 $\sim$ 25 km s^{-1}. The mapping area in this line is about 3′20″ × 4′40″. The distribution of NH_2CN is quite different from those of three other molecules(Figure 2(e)). The strongest emission peak is located about 54″ northeast of SgrB2(N). The emission is elongated from the north of SgrB2(N) to the west of SgrB2(M) and (N). The second peak of the $5_{1,5}$ - $4_{1,4}$ line of NH_2CHO coincides with this emission peak of NH_2CN, and the shape of emission region of NH_2CN in the west of SgrB2(M) and (N) is similar to that of the $5_{1,5}$ - $4_{1,4}$ line of NH_2CHO. In this strongest emission peak, some other observations show similar results; 36 GHz methanol emission peaks (Liechti and Wilson 1996), and the elongated shape of methanol distribution is similar with that of NH_2CN. Wilson et al. (1996) found the peak of the $1_{0,1}$ - $0_{0,0}$ line of HNCO located $\sim$ 45″ north of SgrB2(N). This HNCO peak is about 23″ west of NH_2CN peak. Moreover, Minh et al. (1998) found that HCO_2^+ and HNCO exist mainly at 2′ north of SgrB2(M). This peak position is $\sim$ 35″ northwest of NH_2CN peak. We show these molecular emission peaks in the integrated intensity map of NH_2CN.

3.4. Column Densities and Fractional Abundances

The column densities of these molecules were derived from the observed intensities toward their emission peaks using the rotation diagram analysis (See Chap. 2 Appendix). We assumed the excitation temperatures of CH_3NH_2 and CH_2NH derived using the line survey data at NRO (Ohishi et al. 1998) and at SEST (Nummelin et al. 1998) like

O-bearing molecules.

For NH_2CHO, since we observed the $5_{1,5}$ - $4_{1,4}$ line and the $5_{2,4}$ - $4_{2,3}$ line, we estimated the rotational excitation temperature and the column density simultaneously. The column density map and the rotational excitation temperature map are shown in Figure 4. We found that the rotational excitation temperature toward the emission peak of the $5_{2,4}$ - $4_{2,3}$ line was negative and could not obtain the column density. Then we needed to assume the excitation temperature to estimate the column density. Since the rotational excitation temperatures of a region surrounding the emission peak of the $5_{2,4}$ - $4_{2,3}$ line are about 100 K (Figure 4), we assumed the temperature higher than 100 K. Practically, from the SEST data, Nummelin et al. (1998) obtained 176 K toward SgrB2(N) and we obtained 149 K toward the same position from the NRO data. Therefore we assumed 150 K. The column density of NH_2CHO toward the emission peak of the $5_{2,4}$ - $4_{2,3}$ line was obtained to be 2.5×10^{15} cm^{-2}. Toward the emission peak of the $5_{1,5}$ - $4_{1,4}$ line, the column density and the rotational excitation temperature were obtained to be $N = 2.5 \times 10^{14}$ cm^{-2} and $T_{\rm rot} = 23$ K, respectively.

In contrast, Kuan and Snyder (1996) found N(NH_2CHO)=$4.9 \times 10^{15} \sim 2.7 \times 10^{16}$ cm^{-2} with the spatial resolution of $10''.8 \times 4''.6$, Sutton et al. (1991) found 2.6×10^{15} cm^{-2} using a $14''$ beam toward SgrB2(N), and Turner (1991) found 1.2×10^{14} cm^{-2} using a $75''$ beam toward SgrB2(OH). The differences between our result and other observational results are probably due to the different beam sizes, the different excitation and the different observing position.

From NRO data, we obtained the rotation temperature of NH_2CN of 49 K for SgrB2(NW) which is located about $1'$ west of SgrB2(N) and not associated H II regions. Then we assumed 50 K for the emission peak of NH_2CN. The column density was 4.0×10^{14} cm^{-2}.

At the emission peak, we derived the fractional abundance N(molecule)/N(H_2) to be (3-13) $\times 10^{-10}$, (4-18) $\times 10^{-10}$, (5-25) $\times 10^{-10}$, and (8-40) $\times 10^{-11}$, for CH_3NH_2, CH_2NH, NH_2CHO, and NH_2CN, respectively. The column densities of H_2 used here were 1.0×10^{24} cm^{-2} toward SgrB2(M) and 5.0×10^{24} cm^{-2} toward SgrB2(N) from Martín-Pintado (1990).

4. Discussion

4.1. Comparison of Spatial Distribution with those of Other Molecules and Dust Continuum

The distributions of the NH- and NH_2-bearing molecules are different from those of the O-bearing molecules (See Chap. 2). However, there are some species whose distributions are similar with those of the NH- and NH_2-bearing molecules.

de Vicente et al. (1997) performed the observations of the HC_3N J = 1-0 line. The emission peak of HC_3N is about 20″ west of SgrB2(M) and the distribution is elongated from the north to the south in the west side of SgrB2(M) and (N). This elongated distribution is similar to those of the NH- and NH_2-bearing molecules. Furthermore all molecules we observed except for NH_2CN have peak in the west of SgrB2(M) and (N). Toward the north, this elongated distribution of HC_3N bends to the east. This trend is also seen in the case of the NH- and NH_2-bearing molecules. The $5_{1,5}$ - $4_{1,4}$ line of NH_2CHO shows the second peak which is located $\sim$ 58″ northeast of SgrB2(N), and the emission distribution slightly bends toward this position from the west of SgrB2(N). CH_2NH shows the distribution structure which is slightly elongated toward the northeast of SgrB2(N). Since HC_3N is a high density tracer, the distributions of the NH- and NH_2-bearing molecules may reflect high density gas.

The map of the HC_3N line is almost identical to those of the CH_3CN J = 5-4 line (de Vicente et al. 1997), which is a gas kinetic temperature tracer, and the 1.3 mm dust emission (Gordon et al. 1993). The emission of the 1.3 mm continuum has prominent peaks toward SgrB2(M) and (N). However, its extended envelope shape is similar to those of HC_3N and the NH- and NH_2-bearing molecules. We reproduced the 1.3mm continuum map in Figure 3. This suggests that the distributions of the NH- and NH_2-bearing molecules trace the dust distribution. The similarity among the distributions of the NH- and NH_2-bearing molecules, those of HC_3N and dust continuum suggests that the NH- and NH_2-bearing molecules exist in the entire region where gas column density is high. This is very different from the behaviors of the O-bearing molecules whose distributions shows strong peaks toward H II regions.

Furthermore, NH_2CN shows emission peak toward the north of SgrB2(N). The emission of NH_2CN is extended from the west to the east in the north of SgrB2(N) and from the north to the south in the west of SgrB2(M) and (N). This distribution is connected with each other and the shape is like a character L. Toward the north of

SgrB2(N), some other species peak here. The $4_{0,4}$ - $3_{0,3}$ and the $5_{0,5}$ - $4_{0,4}$ lines of HNCO and the $4_{0,4}$ - $3_{0,3}$ and the $5_{0,5}$ - $4_{0,4}$ lines of HCO_2^+ have emission peak which is located 35″ northwest of NH_2CN emission peak (Minh et al. 1998). They identified redshifted and blueshifted high-velocity components which are located symmetrically around the emission peak, along the Galactic plane. The flow energies are enough to initiate new star formation in this position. Therefore the authors concluded that large-scale collapsing motion may cause a strong shock in this position and result in enhancement of HCO_2^+ and HNCO. Wilson et al. (1996) found that the peak of the $1_{0,1}$ - $0_{0,0}$ line of HNCO is located about 23″ west of our NH_2CN peak. They concluded that HNCO could be excited by absorbing far and mid-infrared photons. However, no continuum source has been detected toward this position by submillimeter observations. Therefore there may be an infrared source which is much younger than SgrB2(N) in this position. Since NH_2CN has comparatively low vibrational excited energy level, this molecule may also be excited by far and mid-infrared photons. 36 GHz methanol maser has a peak which coincides with the NH_2CN peak (Liechti et al. 1996).

4.2. Formation Mechanism of the NH- and NH_2-bearing Molecule

Now we compare our results with several chemical models: for instance, the gas-phase model of Lee et al. (1996), the grain-surface model of Allen and Robinson (1977) and the three-phase (gas, mantle and grain) model of Hasegawa et al. (1993)(Table 2). The model abundances which include only the grain-surface reactions are much higher than our observational results by 2-3 orders of magnitude. The abundances of CH_3NH_2 and CH_2NH obtained from the observations are similar to both of the pure gas-phase model and the three-phase model. The abundance of NH_2CHO has not been calculated in neither of the grain-surface model nor the three-phase model, and the abundance of NH_2CN has not been calculated in the three-phase model. Therefore we could not conclude which model can explain our observational results for NH_2CHO and NH_2CN.

Dickens et al. (1997) found CH_2NH in several molecular clouds, and that relative abundances, CH_2NH/HCN, in region where gas kinetic temperature is high is higher than those in region where gas kinetic temperature is low. On the other hand, since CH_3NH_2, NH_2CHO and NH_2CN include nitrogen as the NH_2-group, these molecules may be related to NH_3. The linewidths, V_{LSR}, velocity structures and the spatial distributions of these NH_2-bearing molecules and those of CH_2NH are similar, so that we considered that observed NH- and NH_2-bearing molecules exist in the same physical environment

and the formation mechanism are similar. In the gas-phase, formation mechanism of all of these molecules are thought to be related with NH_3. According to Herbst (1998), these NH- and NH_2-bearing molecules are formed from NH_3 or NH_2 radical as follows:

$$\begin{aligned} &CH_3^+ + NH_2 \rightarrow CH_2NH_2^+ + H + h\nu \\ &CH_2NH_2^+ + e \rightarrow CH_2NH + H \end{aligned} \tag{3.1}$$

$$\begin{aligned} &CH_3^+ + NH_3 \rightarrow CH_3NH_3^+ + h\nu \\ &CH_3NH_3^+ + e \rightarrow CH_3NH_2 + H \end{aligned} \tag{3.2}$$

$$NH_3 + H_2CO \rightarrow NH_2CHO + H \tag{3.3}$$

$$NH_3 + CN \rightarrow NH_2CN + H \tag{3.4}$$

According to van Dishoeck (1993), NH_2 is formed from ion-molecule reactions and photolysis of NH_3, and NH_3 is formed on dust grain. Flower et al. (1995) suggest that NH_2 is formed from NH_3 which is formed on dust grain. In short, it is considered that reaction (3.1) is also related with NH_3, and we considered formation mechanism of CH_2NH may be related to NH_3 rather than HCN. On the other hand, NH_3 is believed to be produced on dust grains. Since the distribution of the 1.3 mm dust continuum is similar with those of the NH- and NH_2-bearing molecules, these molecules may be produced from NH_3 which was produced on dust grains and was evaporated from them. However, in order to clarify the relation of the NH_2, NH_3 and NH-, NH_2-bearing molecules, higher spatial resolution map of NH_2 and NH_3 are necessary. Although there are some NH_3 maps toward SgrB2 (Hüttemeister et al. 1993 ; 1995), they observed with low spatial resolution ($\sim 40''$). Peng et al. (1993) found that NH_2D and $^{15}NH_3$ concentrate toward SgrB2(N) using the BIMA millimeter-wave interferometer, however, interferometric observations do not have sensitivity for extended distribution. In order to compare the extended envelope shape of the NH- and NH_2-bearing molecules with NH_3 distribution, high spatial resolution single dish mapping observations in higher frequency transitions, such as NH_2D are essential.

5. Conclusions

We have mapped CH_3NH_2, CH_2NH, NH_2CHO and NH_2CN toward SgrB2 molecular cloud. The emission of all molecules are elongated from the north to the south, and the peak positions are shifted from H II regions, SgrB2(M) and (N). This is very different from the results of the O-bearing and the CN-bearing organic molecules which show prominent peak toward SgrB2(N). These results may suggest that the formation mechanism of the NH- and NH_2-bearing molecules are different from the O-bearing and the CN-bearing molecules.

We obtained the column densities, 1.3×10^{15} cm^{-2}, 1.8×10^{15} cm^{-2}, 2.5×10^{15} cm^{-2}, 8.4×10^{14} cm^{-2}, for CH_3NH_2, CH_2NH, NH_2CHO, and NH_2CN toward the emission peak, corresponding to the fractional abundances of (3-13) $\times 10^{-10}$, (4-18) $\times 10^{-10}$, (5-25) $\times 10^{-10}$, (2-8) $\times 10^{-10}$, respectively. We compared these results with several model calculations ; the pure gas-phase model (Lee et al. 1996), the grain-surface model (Allen & Robinson 1977), and the three-phase model (Hasegawa et al. 1993). The calculated abundances of the grain-surface model are higher than our observational results by 2-3 orders of magnitude. Other models do not include all of observed molecules and difference between the pure gas-phase and the three-phase model are small.

The similarity of the linewidths, V_{LSR}, the velocity structures and the spatial distribution of the NH- and NH_2-bearing molecules implies that these molecules are produced in the gas-phase under the same physical condition via NH_2/NH_3.

However, we need to compare distributions of the NH- and NH_2-bearing molecules with higher spatial resolution NH_2 and NH_3 maps in order to clarify the production mechanisms of CH_3NH_2, CH_2NH, NH_2CHO and NH_2CN.

Table 1. Line parameters and beam sizes of the NRO 45-m telescope

Molecule	Transition	Frequency [MHz]	E_u[a] [K]	θ_{mb}[b] [″]	η_{mb}[c] [%]
CH_3NH_2	$4_{1,4}$-$4_{0,4}$ Aa	75135.452	24	21	50
CH_2NH	$3_{0,3}$-$2_{1,2}$	35065.723	18	49	90
	$4_{0,4}$-$3_{1,3}$	105794.118	30	15	49
NH_2CHO	$5_{1,5}$-$4_{1,4}$	102064.353	18	16	49
	$5_{2,4}$-$4_{2,3}$	105972.601	27	15	49
NH_2CN	$5_{1,4}$-$4_{1,3}$	100629.500	29	16	49

[a] E_u is the upper level energy above the ground state

[b] θ_{mb} is the beam size

[c] η_{mb} is the main beam efficiency

Table 2. Comparison of column densities (N) and fractional abundances (X) with theoretical interstellar chemical models

Molecule	T_{rot}[a]	N	X	model calculations		
	[K]	[cm^{-2}]		gas-phase[b]	grain-surface[c]	three-phase[d]
CH_3NH_2	50	1.3(15)	3(-10)−1(-9)	1.6(-10)	1.1(-8)	6.5(-10)
CH_2NH	80	1.8(15)	4(-10)−2(-9)	1.6(-10)	8.9(-7)	8.9(-10)
NH_2CHO	150	2.5(15)	5(-10)−3(-9)	-	1.6(-7)	-
NH_2CN	50	4.0(14)	8(-11)−4(-10)	2.7(-10)	4.0(-8)	-

[a] T_{rot} are assumed.

[b] T_k = 50 K, $n_H = 10^5$ cm^{-3}, 10^5 yr (Lee et al. 1996)

[c] T_d = 10 K, T_k = 70 K, $n_H = 10^6$ cm^{-3}, 10^5 yr (Allen & Robinson 1977)

[d] $T_d = T_k$ = 10 K, $n_H = 2 \times 10^4$ cm^{-3}, 10^5 yr (Hasegawa et al. 1993)

a(b) means a $\times$ 10^b.

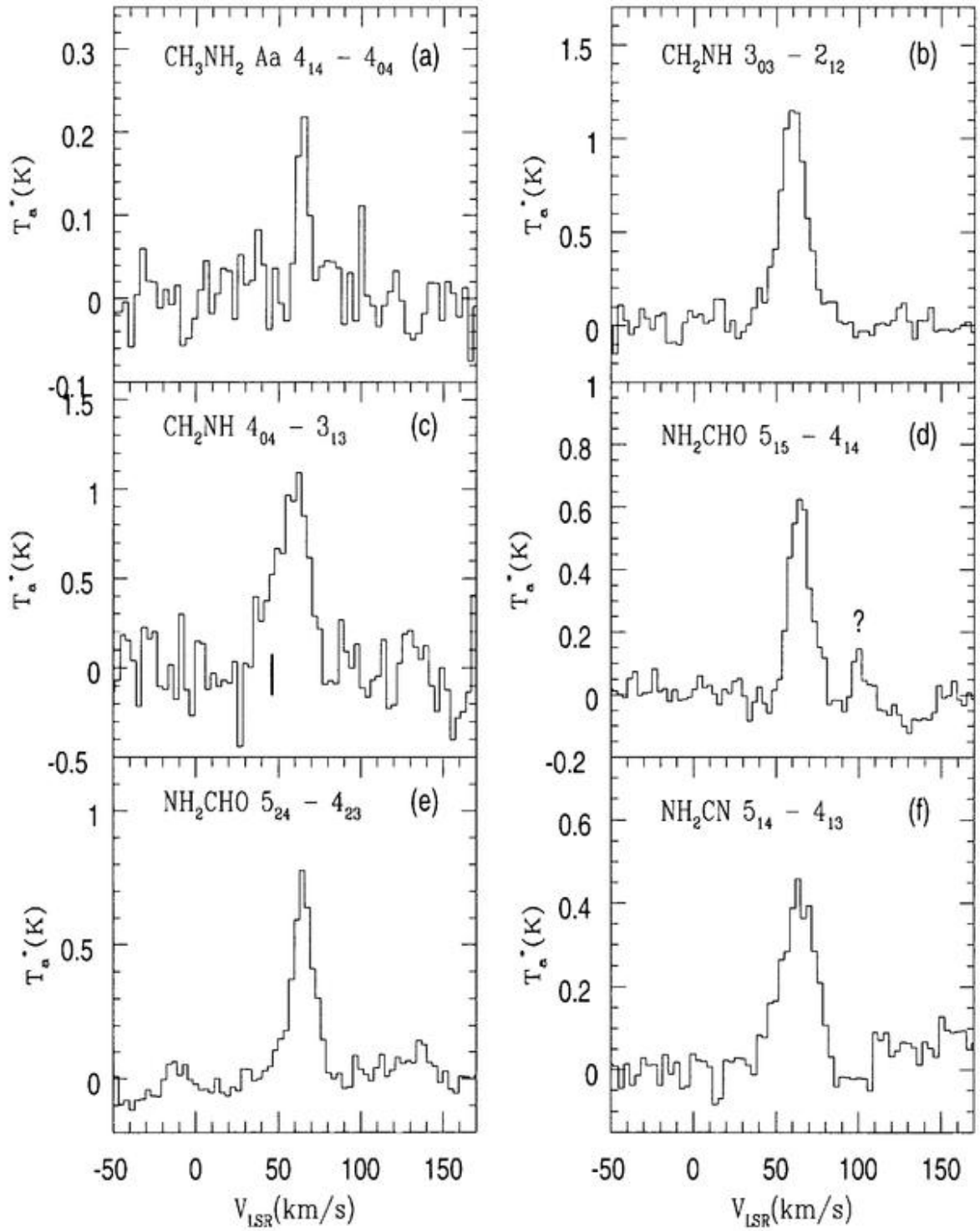

Fig. 1.— Spectra of (a) CH_3NH_2 $4_{1,4}$-$4_{0,4}$ transitions at 75135.452 MHz; (b) CH_2NH $3_{0,3}$-$2_{1,2}$ transition at 35065.723 MHz; (c) CH_2NH $4_{0,4}$-$3_{1,3}$ transition at 105794.118 MHz. The 105974.118 MHz line is blended with $H^{13}CCCN$ J = 12-11 transition at 105799.093 MHz. Vertical line under the spectrum indicates velocity of $H^{13}CCCN$ line. (d) NH_2CHO $5_{1,5}$-$4_{1,4}$ transition at 102064.353 MHz; (e) NH_2CHO $5_{2,4}$-$4_{2,3}$ transition at 105972.601 MHz; (f) NH_2CN $5_{1,4}$-$4_{1,3}$ transition at 100629.500 MHz

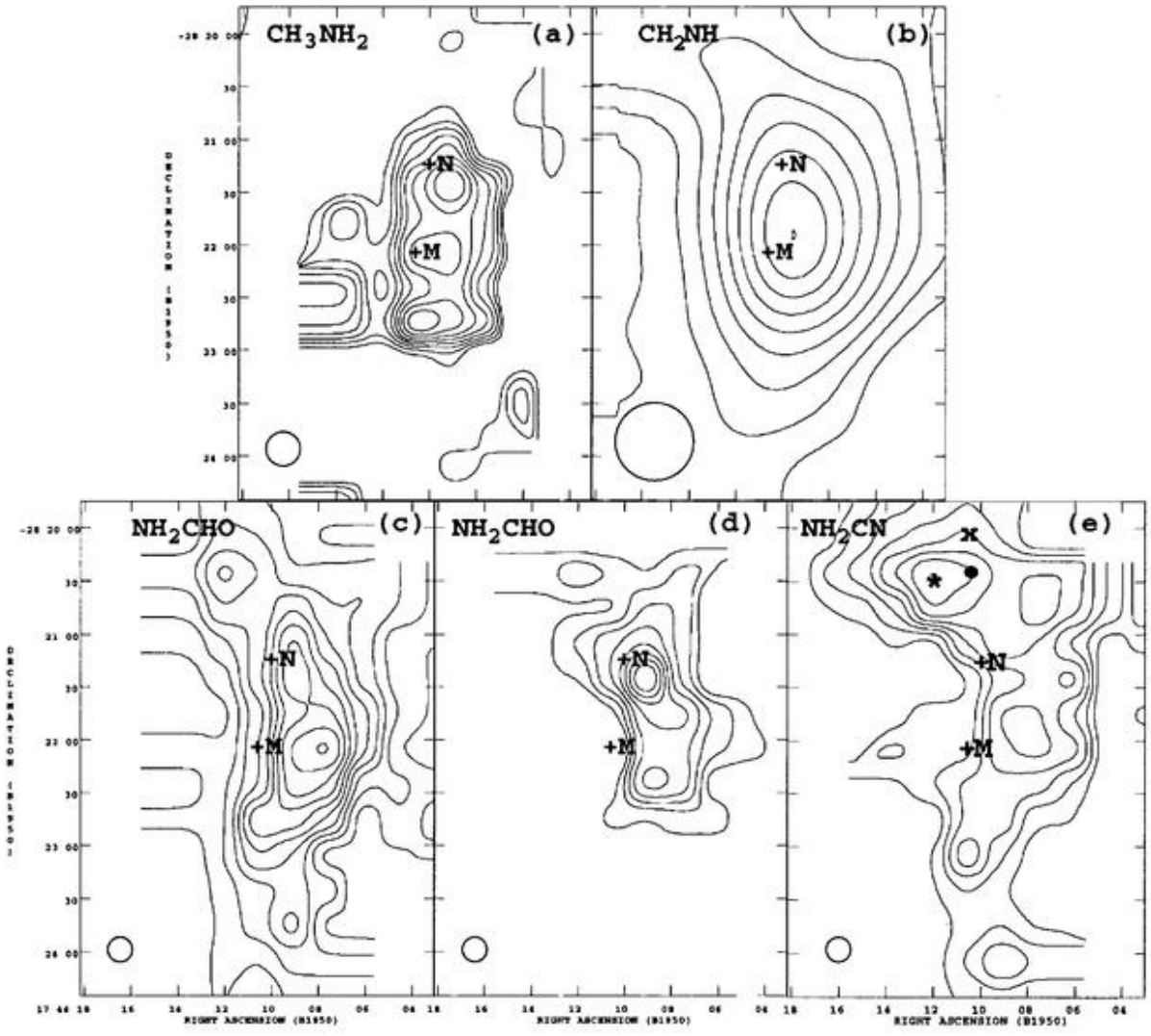

Fig. 2.— Integrated intensity distribution of (a) the $4_{1,4}$-$4_{0,4}$ transition of CH_3NH_2; (b) the $3_{0,3}$-$2_{1,2}$ transition of CH_2NH; (c) the $5_{1,5}$-$4_{1,4}$ transition of NH_2CHO; (d) the $5_{2,4}$-$4_{2,3}$ transition of NH_2CHO; (e) the $5_{1,4}$-$4_{1,3}$ transition of NH_2CN. The contours are 20 to 90 % in steps of 10 % of maximum of integrated intensity. Cross marks represent the position of H II regions SgrB2(M) and (N). Dot mark in Fig.(e) indicates the emission peak of the $1_{0,1}$ - $0_{0,0}$ line of HNCO (Wilson et al. 1996). X in Fig.(e) indicates the emission peak of the $4_{0,4}$ - $3_{0,3}$ line and the $5_{0,5}$ - $4_{0,4}$ line of HNCO and HCO_2^+ (Minh et al. 1998). Asterisk marks in Fig.(e) indicates the emission peak of the 4_{-1} - 3_0 maser line at 36 GHz of methanol (Liechti et al. 1996). The circle in the lower left-hand corner indicates the beam size, θ_{mb}.

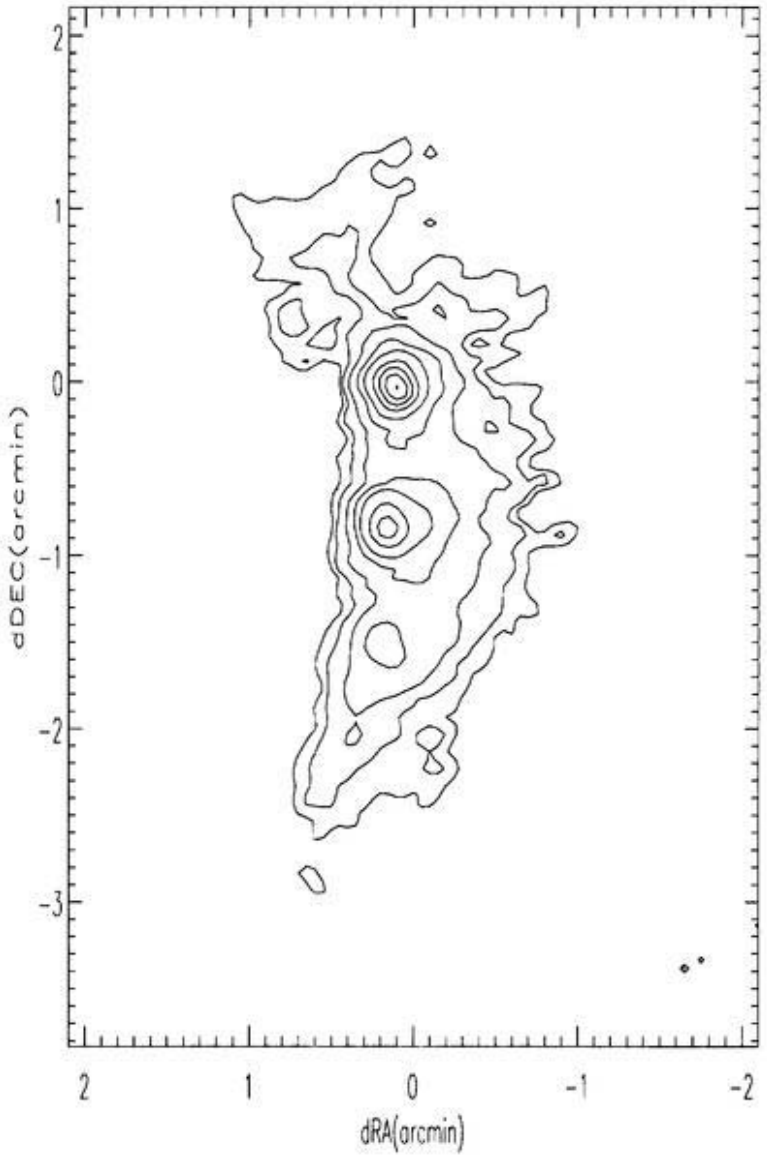

Fig. 3.— Contour map of at $\lambda 1300\mu$m with the MRT (Gordon et al. 1993). The contours are 1.5, 2.5, 5, 10 and 18 to 98% in steps of 20% of the maximum emission of 55Jy/beam. Center position is SgrB2(N) : RA(1950.0)=$17^h44^m10^s.0$, DEC(1950.0)=-28°21′15″.

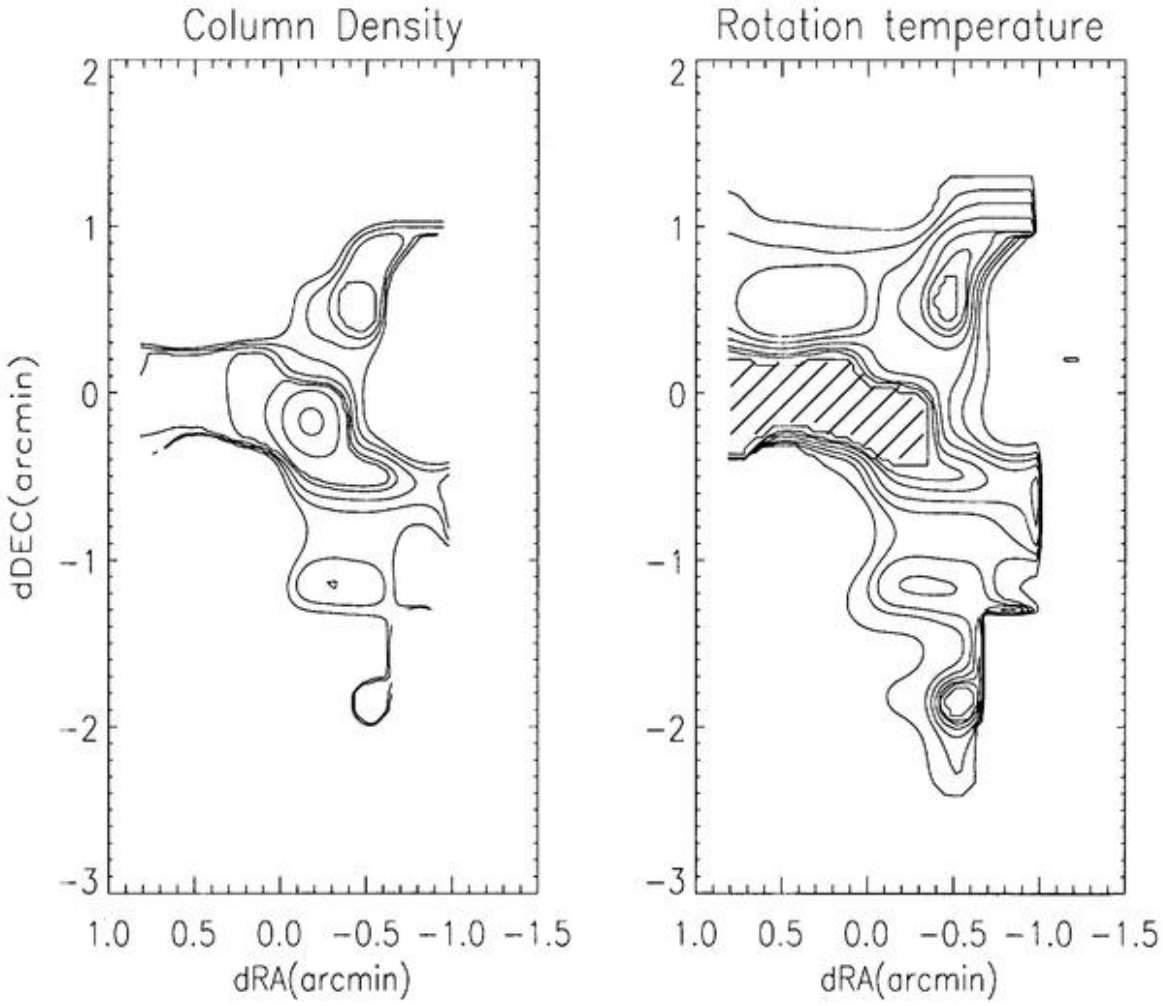

Fig. 4.— The column density and the rotational excitation temperature maps of NH_2CHO. *left* : The contours are 2, 3, 5, 10, 15, 20 and 25 $\times 10^{14}$ cm^{-2}. *right* : The contours are 10, 20, 30, 50, 100, 200 and 500 K. Center position is SgrB2(N) : RA(1950.0)=$17^h44^m10^s.0$, DEC(1950.0)=-28°21′15″. The slanted lines of right panel indicate negative temperature.

Chapter 4

Detection of a New Cyclic Molecule c-C_2H_4O, and Survey Observations of c-C_2H_4O and CH_3CHO toward Massive Star-Forming Regions

ABSTRACT

We detected a new interstellar cyclic molecule, ethylene oxide (cyclic-C_2H_4O hereafter c-C_2H_4O), toward SgrB2(N). Our results indicate the rotation temperature, T_{rot} = 18 K, and the column density, N(c-C_2H_4O) = 3 × 10^{14} cm^{-2}, corresponding to the fractional abundance relative to molecular hydrogen of 6 × 10^{-11}. This is at least a factor of 200 higher than the abundance for this molecule calculated by a gas-phase model by Lee et al. (1996). This indicates that the grain chemistry might play an important role in the production of c-C_2H_4O.

In order to investigate the relation between the grain chemistry and the production of c-C_2H_4O, we carried out survey observations of c-C_2H_4O and its structural isomer acetaldehyde (CH_3CHO) toward 20 massive star-forming regions and two dark clouds. c-C_2H_4O and CH_3CHO were detected in 10 massive star-forming regions, and CH_3CHO was also detected in five other massive star-forming regions. Column densities and rotational temperatures were derived using the rotation diagram method. The resulting rotational temperatures of c-C_2H_4O and CH_3CHO are in a range of 8-36 K. Since kinetic temperature of regions where c-C_2H_4O and CH_3CHO were detected are in a range of 40-400 K, low rotational temperatures of both molecules indicate that these species are excited in the outer, cooler parts around the hot core regions or that the excitation is significantly subthermal. Column densities of these molecules were derived to be (0.1-2.1) × 10^{13} cm^{-2} for c-C_2H_4O and (0.2-5.0) × 10^{14} cm^{-2} for CH_3CHO , respectively. The fractional abundances with respect to H_2 are X(c-C_2H_4O) = 1 × 10^{-11} - 6 × 10^{-10}, and X(CH_3CHO) = 7 × 10^{-12} - 3 × 10^{-9}.

We also detected multiple transitions of CH_3OH, C_2H_5OH, $(CH_3)_2O$, $HCOOCH_3$, HCOOH, C_2H_3CN, and C_2H_5CN. Comparing the abundances of c-C_2H_4O and CH_3CHO in each source with those of other large organic molecules, we found that although the abundances of other organic molecules increase with increasing the dust temperature of each cloud, abundances of c-C_2H_4O and CH_3CHO show little correlation with dust temperatures. And the rotation temperatures of other organic molecules are higher than those of c-C_2H_4O and CH_3CHO. This may indicate that the molecular line emission arises in regions with different physical conditions: c-C_2H_4O, CH_3CHO and HCOOH which show low rotation temperatures exist in cooler outer region around the hot core region; CH_3OH, $(CH_3)_2O$, C_2H_3CN and C_2H_5CN which show high rotation temperature exist in a hot region near the central stars; and C_2H_5OH and $HCOOCH_3$ which show intermediate rotation temperature exist in a region between the hot and cooler part.

We investigated the relation between the column density of C_2H_5OH and that of C_2H_4O group (c-C_2H_4O + CH_3CHO). Because C_2H_5OH is believed to be precursor of the formation reaction of c-C_2H_4O and CH_3CHO in the gas-phase. We found positive correlation between them. Since the fractional abundances of C_2H_5OH are enhanced toward all sources in which C_2H_5OH is detected, it seems that C_2H_5OH is produced on the grain-surface. And the fractional abundances of C_2H_4O group are also 1-3 orders of magnitude larger than the predicted value from pure gas-phase reaction model toward all sources except for Orion-S. This indicates that since c-C_2H_4O and CH_3CHO are produced from C_2H_5OH which is evaporated from grain-mantle, the fractional abundances of c-C_2H_4O and CH_3CHO are enhanced.

1. Introduction

Ethylene oxide (c-C_2H_4O) is a three-membered C-O-C ring, with each carbon fully hydrogenated. It is a higher energy isomer of molecules, acetaldehyde (CH_3CHO) and vinyl alcohol (CH_2CHOH). Only CH_3CHO has been detected thus far in the ISM, although searches for CH_2CHOH have been attempted (Irvine et al. 1989). Although CH_3CHO has been detected toward both giant molecular clouds (e.g. Gilmore et al. 1976) and dark clouds (Matthews et al. 1985), the production mechanism is still unknown. It is believed that the production and destruction pathways of c-C_2H_4O is close to that of CH_3CHO. Therefore, the detection of c-C_2H_4O would provide information about production mechanism of these C_2H_4O group. Then, firstly, we searched for c-C_2H_4O toward SgrB2 molecular cloud where a number of large organic molecules have been detected.

Because of the unusual structure of ethylene oxide relative to most known interstellar molecules, it is also interesting to investigate the distribution and abundance of such a molecule and compare them with other organic molecules, CH_3OH, C_2H_5OH, C_2H_3CN, and C_2H_5CN, etc. Since structural isomers typically share some production and destruction pathways, the relative abundance of two such isomers may be able to provide important constraints on astrochemical models. Therefore, we surveyed c-C_2H_4O and CH_3CHO in a number of molecular clouds. The majority of the targeted sources are warm/hot ($T_k \sim$ 40-400 K) and dense ($n_{H_2} \sim 10^5$-10^6 cm $^{-3}$) molecular clouds. On the other hand, other large O-bearing molecules (CH_3OH, C_2H_5OH, $HCOOCH_3$ and $(CH_3)_2O$ have been detected toward regions where methanol maser was detected in the

past. Therefore, we picked up some methanol maser sources as our survey targets.

In section 2 we describe the details of the observations. In section 3 we present the results of the detection of c-C_2H_4O toward SgrB2, and the survey observations of c-C_2H_4O and CH_3CHO in massive star-forming regions. In section 4 we compare the abundances of c-C_2H_4O and CH_3CHO with chemical models, abundances of other organic molecules, and physical conditions of each source. Finally, in section 5, we summarize our main conclusions.

2. Observations

2.1. Detection Observations of c-C_2H_4O at Haystack, NRO, and SEST

The search observations of c-C_2H_4O were carried out using three radio telescopes; Haystack[1], NRO[2], and SEST[3].

The observations at Haystack to search for the lowest energy transition of c-C_2H_4O, 1_{11}-0_{00} at 39581.6 MHz, were performed during 1995 November. We used the 7 mm HEMT receiver which resulted in a typical system temperature of 150-250 K. The backend consists of an autocorrelator spectrometer with 53.3 MHz bandwidth and the frequency resolution of 52 kHz. The observations were made in dual beamswitch mode. Pointing was checked every two hours by observing Mars and Jupiter. The pointing accuracy was estimated to be 5″ rms. Follow-up observations of other 7 mm transitions of c-C_2H_4O in SgrB2(N) were performed from 1996 December to 1997 March, using the same experimental procedure described above.

After the possible detection of the 1_{11}-0_{00} transition toward SgrB2(N), we checked data obtained from two spectral line surveys toward three positions (M [RA(1950.0) = $17^h44^m10.^s4$, DEC(1950.0) = -28°22′03″], NW [RA(1950.0) = $17^h44^m06.^s6$, DEC(1950.0) = -28°21′20″], and N [RA(1950.0) = $17^h44^m10.^s1$, DEC(1950.0) = -28°21′17″]) in the

---

[1]Radio astronomy at the Haystack Observatory of the Northeast Radio Observatory Corporation is supported by the National Science Foundation.

[2]Nobeyama Radio Observatory is a branch of the National Astronomical Observatory of Japan, an interuniversity research institute operated by the Ministry of Education, Science and Culture of Japan.

[3]The Swedish ESO-submillimeter Telescope is operated jointly by ESO and the Swedish National Facility for Radio Astronomy, Onsala Space Observatory, at Chalmers University of Technology.

SgrB2 molecular cloud. Spectra in the frequency ranges of 30-50 and 79-116 GHz were taken with the 45-m telescope of Nobeyama Radio Observatory (NRO) (Ohishi et al. 1998), and in the frequency ranges of 218-263 GHz with the 15-m Swedish ESO-Submillimeter Telescope (SEST) (Nummelin et al. 1998).

The Nobeyama spectral survey was performed from 1988 December to 1996 May. We used a HEMT receiver for the 30-35 GHz observations, and SIS receivers for the 35-50 GHz and the 79-116 GHz observations. The typical system temperatures of the HEMT receiver were 150 K, and those of SIS receivers ranged from 300 to 600 K. For the backend, we used a bank of acousto-optical spectrometers (AOS) with the frequency resolution of 250 kHz and the bandwidth of 250 MHz each. Pointing was checked every two hours by using the SiO maser from VX Sgr, and the pointing accuracy was estimated to be better than 5″ rms. The data were taken in position-switching mode.

The SEST spectral survey was carried out from 1990 August to 1994 November. The Schottky receiver used in 1990-1991, which had the system temperatures around 1300 K, was replaced in 1991 with an SIS-equipped receiver with the system temperatures of typically 600 K. The SEST wideband AOSs used for the survey have channel separations of 0.7 MHz, resulting in the frequency resolution of 1.4 MHz. Pointing accuracy was estimated to be less than 5″ rms. The observation was carried out in dual beam-switching mode. Transition data and characteristics of telescopes are listed in Table 1.

2.2. Survey Observations of c-C_2H_4O and CH_3CHO toward Southern Sources

Survey observations toward southern sources were performed using the 15-m radio telescope of SEST in October 1997. The 1.3 mm and 3 mm data were obtained simultaneously using the IRAM-built 230/115 GHz SIS receiver, with both channels tuned to single-sideband (SSB) operation. The system temperatures were 200-600 K in the 1.3 mm band and 180-250 K in the 3 mm band. The main-beam efficiency is 60 % for the 230 GHz band and 75 % for the 115 GHz band. The telescope pointing and subreflector focusing were checked regularly by the SiO masers in VX Sgr and AH Sco. We estimate the uncertainty in antenna temperature due to pointing and calibration errors to be 20%. The 3 mm receiver channel was connected to a narrow-band (86 MHz) acousto-optical spectrometer (AOS) with a nominal channel separation of 43 kHz, and in the 1.3 mm band a wide-band (1 GHz) AOS with a channel spacing of 700 kHz per

channel was used. All data were obtained in dual beam-switching mode. Transition data of c-C_2H_4O and characteristic of telescopes are listed in Table 2.

2.3. Survey Observations of c-C_2H_4O and CH_3CHO toward Northern Sources

Survey observations toward northern sources were carried out using two radio telescopes; the 12-m radio telescope of NRAO[4], and the 45-m radio telescope of NRO.

In the observations at NRAO, transitions of c-C_2H_4O and CH_3CHO in the frequency ranges of 220-250 GHz were observed in 1998 April. We used the 1 mm SIS receiver with the system temperature of 600-1000 K. The backend consisted of the hybrid autocorrelator spectrometer with 300 MHz bandwidth (two receivers hooked up to 300 MHz total bandwidth each) and two filter banks with the channel separations of 250 kHz and 500 kHz. The observations were carried out using the position switching mode with an offset of 5′ in azimuth. Pointing was checked every four hours through continuum measurements of both Jupiter and DR21, and pointing accuracy was estimated to be 5″ rms.

The Nobeyama observations were performed in 1998 May. We used two SIS receivers covering the 4 mm and 3 mm regions. Both receivers were used simultaneously. The system temperatures of these receivers were 300-350 K. The backend consists of two sets of acousto-optical radio spectrometers (AOSs), one with a bank of eight high-resolution AOSs with the frequency resolution of 37 kHz and 40 MHz bandwidth, the other with a bank of eight wide-band AOSs with the frequency resolution of 250 kHz and 250 MHz bandwidth. Pointing was checked every two hours by observing nearby SiO masers. The estimated pointing accuracy was $\sim$ 5″ rms. The observations were made in position-switching mode. The line parameters and beam sizes are summarized in Table 3.

We searched for c-C_2H_4O and CH_3CHO in 11 southern sources and 12 northern sources. These sources are listed in Table 4. In these sources, G34.3+0.2 were observed at SEST, NRAO, and NRO.

[4]National Radio Astronomy Observatory at Kitt Peak, Arizona

3. Results

3.1. Detection of c-C_2H_4O

We detected 10 transitions of c-C_2H_4O toward SgrB2(N). The lines which were identified as c-C_2H_4O have V_{LSR} of 60 $\sim$ 64 km s^{-1}, with one transition at 69 km s^{-1}. The last line is emitted from an energy level which is only 2 K above the ground state, and may suffer from self absorption. The former velocities are typical for large organic molecules toward the SgrB2 molecular cloud. Linewidths of observed lines are in a range of 10-30 km s^{-1}, and are consistent with those of other large organic molecules. Of these ten lines, seven lines which were clearly identified as c-C_2H_4O were included in the rotation diagram analyses, and the rotation temperature and the column density were derived to be T_{rot} = 18 K and N(c-C_2H_4O) = 3 $\times$ 10^{14} cm^{-2}. We showed spectra of c-C_2H_4O in Figure 1, and the rotation diagram of c-C_2H_4O in Figure 2.

3.2. Survey of c-C_2H_4O and CH_3CHO

c-C_2H_4O and CH_3CHO were detected toward 10 sources (NGC 6334F, G327.3−0.6, G31.41+0.31, G34.3+0.2, DR21(OH), NGC 7538, W3(H_2O), W51e1/e2, Orion Hot Core and Orion Compact Ridge). Moreover CH_3CHO was detected toward G322.2+0.6, Orion 3'N, G75.78+0.34, G10.47+0.03 and Orion-S. Spectra of c-C_2H_4O and CH_3CHO are shown in Figure 3.

The radial velocities of the c-C_2H_4O and CH_3CHO lines are consistent within 2-3 km s^{-1} and agree well with velocities measured for lines from other molecules towards all of the sources.

In order to estimate the fractional abundances of c-C_2H_4O and CH_3CHO relative to H_2, we have calculated the beam averaged H_2 column density from the integrated intensity of the C^{17}O (J = 1-0) line at 112359 MHz, with respect to southern sources, which was located within the wide-band AOS spectrum centered on the CH_3CHO (6_{16}-5_{15} A, E) line of the SEST observations. On the assumption that X[^{18}O]/X[^{17}O] = 3.65 (Penzias 1981), X[C^{18}O] $\equiv$ N(C^{18}O)/N(H_2) = 2 $\times$ 10^{-7} (Frerking et al. 1982), and C^{17}O is optically thin, we have estimated H_2 column densities using an equation $N(H_2) \equiv X[^{18}O]/X[^{17}O]X[C^{18}O] \times N(C^{17}O)$. For northern sources, we referred to the H_2 column densities in literatures.

In order to compare intensities of lines in the 1.3 mm and 3 mm bands of southern source observations, we applied a correction for the beam-filling factor to the intensity of each observed line. Assuming that both of the source brightness distribution and the antenna response are Gaussian, this correction factor, η_s, can be written as

$$\eta_s = \frac{\theta_s^2}{\theta_{mb}^2 + \theta_s^2}$$

where θ_s is the source size and θ_{mb} is the (frequency dependent) beam-size of the antenna. In our analysis we have adopted a source size equal to the size of the smallest beam, 20″ (at 254 GHz). The corrected main-beam brightness temperature was subsequently calculated as T_{mb}/η_s, and if the spectral-line emission arises in a source having a Gaussian brightness distribution with a FWHM of 20″, this quantity will be equal to the peak brightness temperature of the source. The adopted source size is in agreement with size estimates for G327 (Bergman 1992), G31 (Cesaroni et al. 1991), and G34 (Mehringer & Snyder 1996). After this correction we derived the rotation temperatures and the column densities for c-C_2H_4O and CH_3CHO using the rotation diagram method. The difference between the beam size of 3 mm data of NRO and those of 1 mm data of NRAO are small, so that we did not apply the correction for the beam-filling factor for northern source observations.

The rotation temperatures of c-C_2H_4O and CH_3CHO are in the range of 8 - 36 K, and the differences among sources are small. The column densities are (1.2-30) $\times$ 10^{13} cm^{-2} for c-C_2H_4O and (0.2-50) $\times$ 10^{14} cm^{-2} for CH_3CHO, respectively. The fractional abundances relative to H_2 are X(c-C_2H_4O) = 1 $\times$ 10^{-11} - 6 $\times$ 10^{-10}, and X(CH_3CHO) = 7 $\times$ 10^{-12} - 3 $\times$ 10^{-9}. Abundances of CH_3CHO are always higher than those of c-C_2H_4O. The ratio, $N(CH_3CHO)/N$(c-C_2H_4O), varies between 1.2 (SgrB2(N)) and 13.2 (W51e1/e2). The resulting rotation temperatures, molecular column densities, and fractional abundances relative to H_2 for each source can be found in Table 5

In the regions where c-C_2H_4O and CH_3CHO were detected we coincidentally detected several other large asymmetric molecules, e.g., CH_3OH, C_2H_5OH, HCOOH, $HCOOCH_3$, $(CH_3)_2O$, C_2H_3CN, C_2H_5CN, and hydrogen recombination line H40α. These molecules, except for the recombination line, were also analyzed using the rotation diagram analysis. Fractional abundances of these molecules are $X(CH_3OH)$ = 4 $\times$ 10^{-9} - 1 $\times$ 10^{-6}, $X(C_2H_5OH)$ = 2 $\times$ 10^{-9} - 2 $\times$ 10^{-8}, $X((CH_3)_2O)$ = 7 $\times$ 10^{-10} - 4 $\times$ 10^{-8}, $X(HCOOCH_3)$ = 5 $\times$ 10^{-10} - 9 $\times$ 10^{-8}, $X(C_2H_3CN)$ = 1 $\times$ 10^{-10} - 2 $\times$ 10^{-9}, $X(C_2H_5CN)$ = 2 $\times$ 10^{-9} - 3 $\times$ 10^{-8}, and X(HCOOH) = 1 $\times$ 10^{-11} - 1 $\times$ 10^{-9}. Thus the fractional abundances are different in different sources. The rotation temperatures

are also varied in different sources and could be divided into three groups : high $T_{\rm rot}$ (70-250 K) for CH_3OH, C_2H_3CN, C_2H_5CN and $(CH_3)_2O$, low $T_{\rm rot}$ (10-40 K) for HCOOH, and intermediate $T_{\rm rot}$ (35-80 K) for C_2H_5OH and $HCOOCH_3$. This indicates that the emission of these molecules may arise in regions with different physical conditions. The column densities, and the fractional abundances are also listed in Table 5.

4. Discussion

We found c-C_2H_4O and CH_3CHO toward dense ($n_{\rm H_2} \sim 10^5$-10^6 cm^{-3}), warm/hot ($T_{\rm k} \sim$ 40-400 K) molecular clouds with ongoing O,B star-formation. This indicates that the production of c-C_2H_4O and CH_3CHO may be related with massive star-formation. In this section we discuss formation mechanism of both molecules and relation between the abundances of c-C_2H_4O and CH_3CHO and physical condition of each source.

The beam sizes of northern source observations are larger (16″-27″) than separation of Orion Hot Core and Compact Ridge ($\sim$ 10″), so that the data of them include the other contributions. And during the Orion observations at NRO, we could not obtain above-mentioned pointing accuracy ($\sim$ 5″) because of strong wind. Therefore we averaged the data of Hot Core and Compact Ridge, and call them "Orion" data hereafter.

4.1. Chemistry of the C_2H_4O group

Laboratory experiment of production of c-C_2H_4O and CH_3CHO has been made (Hawkins & Andrews 1983). In liquid argon the reaction between ethylene and ozone produces primarily c-C_2H_4O, CH_3CHO, and H_2CCO. CH_2CHOH is also produced via this reaction, however, is maybe converted into H_2CCO by H_2 elimination. CH_2CHOH is thermodynamically less stable than CH_3CHO, and the barrier to isomerization via intermolecular rearrangement is predicted to be high($\sim$ 4,300 K) (Hawkins & Andrews 1983). Non detection of CH_2CHOH might be caused by the high energy barrier.

In "hot core" sources, such as SgrB2(N), the formation of complex molecules is thought to involve gas-phase reactions of simple saturated species which have been liberated from grain surfaces due to energetic processes associated with star formation. According to Herbst (1997), two possible pathways to the formation of C_2H_4O, where

C_2H_4O indicate c-C_2H_4O, CH_3CHO, and CH_2CHOH, involve C_2H_5 and C_2H_5OH, both of which are suggested to be either totally formed on grains or via grain synthesis of precursors. The first route to C_2H_4O is the following neutral-neutral reaction,

$$O + C_2H_5 \rightarrow C_2H_4O + H \tag{4.1}$$

which has been studied in the laboratory and is rapid. The laboratory experiment has been performed by mass spectroscopy, so that branching ratio to each isomeric form is unknown. Another production pathway might be the following chain of reactions:

$$\begin{aligned} &CH_3^+ + C_2H_5OH \rightarrow C_2H_5O^+ + CH_4, \\ &C_2H_5O^+ + e \rightarrow C_2H_4O + H. \end{aligned} \tag{4.2}$$

The new standard chemical model of Lee et al. (1996) predicts a fractional abundance of 5×10^{-12} for the isomeric group of molecules, c-C_2H_4O, CH_3CHO, and CH_2CHOH combined. From our data of the detection of c-C_2H_4O toward SgrB2(N) and the survey observations of c-C_2H_4O and CH_3CHO, fractional abundances, X(c-C_2H_4O + CH_3CHO), are in the range from 7×10^{-12} (Orion-S) to 3×10^{-9} (G327.3−0.6). Observed fractional abundances, except for Orion-S, are 1-3 order of magnitude higher than the predicted value from the chemical model. On the other hand, an enhancement of C_2H_5OH abundance ($\sim 10^{-9}$) has been reported in Orion-KL (Ohishi et al. 1995) and suggested its formation on dust grain. Therefore c-C_2H_4O and CH_3CHO may be produced via reaction (4.2), and because of enhancement of C_2H_5OH, which is formed on dust grain, the enhancement of c-C_2H_4O and CH_3CHO was introduced.

On the other hand, CH_3CHO has also been detected in dark cloud (Matthews et al. 1985), however, C_2H_5OH has not been detected in dark cloud. Because dust temperature is very low ($\sim$ 10 K) in dark clouds, therefore molecules produced on dust grains cannot be evaporated from them. Herbst & Leung (1989) proposed following reaction to form CH_3CHO for dark cloud;

$$H_3O^+ + C_2H_2 \rightarrow C_2H_5O^+ + h\nu \tag{4.3}$$

The rate coefficient of reaction (4.3) is $k = 4 \times 10^{-12}$ $(T/300)^{-1.6}$ cm^3s^{-1}. Therefore, reaction (4.3) effectively proceeds in low temperature rather than in high temperature. $C_2H_5O^+$ recombines with an electron, and CH_3CHO is produced. According to their calculation for temperature $\leq$ 10 K, predicted abundance of CH_3CHO is 1.1×10^{-10} in the steady state. This value is consistent with observed value 6×10^{-10} in TMC-1

(Irvine et al. 1987). Therefore CH_3CHO in dark cloud is produced by the reaction different from that in hot core.

It is important to compare the abundances of c-C_2H_4O and CH_3CHO with that of C_2H_5OH which is thought to be a precursor of the C_2H_4O group molecules. If c-C_2H_4O and CH_3CHO are produced by reaction (4.2), there must be positive correlation between the column densities of C_2H_4O group and C_2H_5OH. The relation between the column densities N(c-C_2H_4O+CH_3CHO)and N(C_2H_5OH) is shown in Figure 4. N(c-C_2H_4O+CH_3CHO) increases with the increase of N(C_2H_5OH). Therefore it is concluded that the formation scheme in hot cores to c-C_2H_4O and CH_3CHO is consistent with the reaction (4.2).

4.2. Comparisons of Observed Molecular Abundances with Chemical Models

We compared the fractional abundances of molecules with the pure gas-phase model (Lee et al. 1996). We show in Figure 5 a plot of ratios of observed fractional abundances relative to calculated fractional abundances from the pure gas-phase model. Since c-C_2H_4O is not distinguished from CH_3CHO in the model calculations, the sum of abundances of c-C_2H_4O and CH_3CHO are plotted. All of observed molecular abundances, except for C_2H_3CN and HCOOH, are enhanced by 1-4 orders of magnitude. C_2H_3CN has been detected toward G34.3+0.2 using the BIMA array with 13.″3 × 8.″3 angular resolution (Mehringer & Snyder 1996), and they found $N(C_2H_3CN)$ = (4.3-7.1) × 10^{14} cm^{-2}. This value is an order of magnitude larger than our single dish result. This difference is due to compact distribution of C_2H_3CN smaller than our single dish beam size. Qualitatively, this compact distribution of C_2H_3CN is probably valid for the other hot-core sources as well. Therefore, we might underestimate the C_2H_3CN abundances toward such hot-core sources. Figure 5 indicates that the abundances of almost of large organic molecules in hot molecular clouds cannot be explained by only pure gas-phase reaction scheme, and other reactions, e.g., the grain-surface reactions, may be more important. However, we should note that in this gas-phase model the gas kinetic temperature and the density of H_2 are assumed to be T_k = 50 K and 10^5 cm^{-3}, respectively, and these are intermediate values in observed molecular clouds.

The model including the grain-surface reactions have been developed for the hot cores in Orion (Charnley, Tielens, & Millar 1992, hereafter CTM; Caselli, Hasegawa, &

Herbst 1993, hereafter CHH) and G34.3+0.2 (Millar, Macdonald, & Gibb 1997, hereafter MMG). We show the abundances of the observed molecules and predicted abundances from these models in Table 6. In Figures 6 $\sim$ 8, we plot ratios of observed fractional abundances relative to calculated abundances from these models. In Orion two hot-core sources (Compact Ridge and Hot Core) are considered. The physical conditions are (Blake et al. 1987): T_k = 100 K, $n_H = 2 \times 10^6$ cm^{-3} for the Compact Ridge, T_k = 200 K, $n_H = 2 \times 10^7$ cm^{-3} for the Hot Core. Comparing our observed molecular abundances with the model values by CHH, we found that the calculated abundances of $(CH_3)_2O$ in Compact Ridge and HCOOH in Hot Core are close to the observed values.

However, the abundances of C_2H_4O (c-C_2H_4 + CH_3CHO) and CH_3OH predicted by the Compact Ridge model are 1-4 orders of magnitude higher than observed values whereas the Hot Core model underestimates all of molecules by 1-7 orders of magnitude except for HCOOH, C_2H_3CN and C_2H_5CN. Comparing with the model by CTM, observed $(CH_3)_2O$ abundance is close to that of the Compact Ridge model, and observed C_2H_4O and CH_3OH abundances are also similar. The sources where C_2H_4O abundance is low are similar to the Hot Core rather than the Compact Ridge. The other way, in both of CHH and CTM, the Compact Ridge model underestimates the abundance of C_2H_5OH by 2-3 orders of magnitude, and the Hot Core model also underestimates it by 4-5 orders of magnitude. And both the Hot Core model by CHH and by CTM underestimates the abundance of $(CH_3)_2O$ by 5-7 orders of magnitude.

In the G34.3 model, three components are considered: an Ultra Compact Core (T_k = 300 K, $n_{H_2} = 2 \times 10^7$ cm^{-3}), a Compact Core (T_k = 75-190 K, $n_{H_2} = 10^6$ cm^{-3}), and a Halo (T_k = 18-75 K, n_{H_2} = 800-10^6 cm^{-3}). In sources where C_2H_4O abundance is high observed abundances of C_2H_4O are close to this model value, and those of $(CH_3)_2O$ and CH_3OH agree well with the model. However, in sources where their abundances are low C_2H_4O and CH_3OH abundances are lower than this model by 1-2 orders of magnitude, and all observed C_2H_5OH abundances are higher than this model by 4-6 orders of magnitude.

In chemical models which considers hot molecular cloud conditions, the abundances of these organic molecules increase from the onset of dust evaporation to abundance peak (10^4- 10^5 yr). The variation of abundances of our observed molecules might indicate a chemical evolution of observed molecular cloud.

We note that these chemical models have assumed equal temperatures of gas and dust. In the observed molecular cloud, gas temperatures and dust temperature are

different. Further development of chemical model considering several physical conditions are necessary.

4.3. Comparison of Observed Abundances of Molecules with Gas Kinetic Temperatures and Dust Temperatures

Now we investigate a relation between the fractional abundances of molecules and physical condition of each source. We compare the fractional abundances with kinetic temperatures of each source (Figure 9). The abundances of molecules increase with increasing kinetic temperature, except for SgrB2(N). On the other hand, when we compared the abundances with the dust temperatures of each source (Figure 10), the abundances of molecules, except for c-C_2H_4O and CH_3CHO, increase with increasing dust temperature. Since the data points for $(CH_3)_2O$ and HCOOH are few, it is unclear whether there are correlations between the dust temperatures and the abundances of $(CH_3)_2O$ and HCOOH. Our observational results are consistent with the scenario that large organic molecules are formed on dust grains and are released back to the gas-phase by evaporation from grain mantle, or are formed from dust-evaporated molecules.

On the other hand, although there are sufficient data with respect to c-C_2H_4O and CH_3CHO, it seems that there are no correlations between the dust temperature and the molecular abundances. Therefore grain-surface reaction may not play an important role in the production of c-C_2H_4O and CH_3CHO.

4.4. Excitation of Molecules

The deduced rotation temperatures of observed molecules can be grouped as follows: T_{rot} for c-C_2H_4O, CH_3CHO, and HCOOH are low (10-40 K), in contrast T_{rot} for CH_3OH, C_2H_3CN, C_2H_5CN, and $(CH_3)_2O$ are high (70-250 K), and T_{rot} for $HCOOCH_3$ and C_2H_5OH are intermediate (35-80 K). The relation between the rotation temperature versus molecular abundance are shown in Figure 11 of each molecule.

The difference of $T_{rot}(CH_3OH)$ for southern sources (70-82 K) and those of northern sources (150-210 K) may be due to difference of transitions used in our study. Although several transitions of CH_3OH were detected toward southern sources, only two transitions were detected toward northern sources. It is known that excitation of CH_3OH in hot molecular cloud is complicated (Turner 1991; Sutton et al. 1991). The difference of

$T_{rot}(C_2H_5OH)$ for southern sources (70-103 K) and those of northern sources (130-175 K) may also be due to difference of transitions used in the observations. Toward southern sources both of *gauche* and *trans* transitions were detected, however, toward northern sources only *gauche* transitions were detected. According to Pearson et al.(1997), the rotation temperature derived from *gauche* transitions is higher than that from *trans* transitions.

Rotation temperatures of molecules trend to become higher and approach to the gas kinetic temperature with decreasing electric dipole moment. However, all molecular dipole moments we observed are larger than that of CO (0.11 debye) which is one of the probe of gas kinetic temperature. The dipole moment of our observed molecules are μ_a = 1.88 debye for c-C_2H_4O, μ_a = 2.423 debye for CH_3CHO, μ_b = 1.44 debye for CH_3OH, μ_b = 1.438 debye (*trans* - *trans*), μ_a = 1.264 debye ($gauche^+_-$ - $gauche^+_-$), μ_c = 1.101 debye ($gauche^+_-$ - $gauche^-_+$) for C_2H_5OH, μ_b = 1.302 debye for $(CH_3)_2O$, μ_a = 1.63 debye for $HCOOCH_3$, μ_a = 3.815 debye for C_2H_3CN, μ_a = 3.85 debye for C_2H_5CN, and μ_a = 1.396 debye for HCOOH. Therefore, the variety of rotation temperatures can not be attributed to the difference of dipole moments, but seems to indicate that the molecular line emission arises in regions with different physical conditions.

4.5. Star Formation Rate vs Molecular Abundances

From comparison of molecular abundances with the dust temperatures, we concluded that the abundances of organic molecules evaporated from grain mantle increase with the dust temperature. If the dust temperature increase with the evolution of molecular cloud, the abundances of molecules closely related to the grain-chemistry increase with the evolution of molecular cloud.

Lis et al. (1991) pointed out that, if the far-infrared luminosity is produced through reprocessing of the stellar radiation from stars, the luminosity-to-mass ratio provides a measure of star-formation rate per unit mass. Gordon (1988) estimated the luminosity-to-mass ratio in several molecular clouds. The author found L_{IR}/M to be 5.9 $L_\odot M_\odot^{-1}$ for SgrB2(N), 140 $L_\odot M_\odot^{-1}$ for W51A and 1500 $L_\odot M_\odot^{-1}$ for OMC-1. Since W51A includes our observed regions W51e1/e2 and our Orion results is an average of Hot Core and Compact Ridge, it is valuable to compare these L_{IR}/M ratios with our results. If the L_{IR}/M provide a measure of star-formation rate per unit mass, star-formation rates are high in sources where the abundances of large organic molecules, such as the O-bearing

and CN-bearing molecules, are high.

Therefore the abundances of these large organic molecules can be used as a monitor of chemical evolution of the hot core regions.

5. Conclusions

We have detected a new cyclic interstellar molecule, ethylene oxide (c-C_2H_4O), toward SgrB2(N). Then that we surveyed this molecule and its isomer, acetaldehyde (CH_3CHO), in several star-forming regions, and have detected these molecules in hot molecular clouds, DR21(OH), NGC 7538, G34.3+0.2, W3(H_2O), W51e1/e2, Orion Hot Core, Orion Compact Ridge, NGC 6334F, G327.3−0.6, and G31.41+0.31. Acetaldehyde was also detected in Orion-S, Orion Compact Ridge, G10.47+0.03, G322.2+0.6, G75.78+0.34, and Orion 3'N. We also detected CH_3OH, C_2H_5OH, $HCOOCH_3$, $(CH_3)_2O$, C_2H_3CN, C_2H_3CN, and HCOOH toward these sources. For each of these molecular species, rotation temperatures, column densities and fractional abundances were deduced using the rotation diagram analysis. Our main conclusions from these observations are:

- The rotation temperature and column density of ethylene oxide toward SgrB2(N) are $T_{\rm rot}$ = 18 K, and N(c-C_2H_4O) = 3 × 10^{14} cm $^{-2}$, respectively. Fractional abundance relative to H_2 is X(c-C_2H_4O) = 6 × 10^{-11}. This is a factor of more than 200 higher than the abundance predicted by pure gas-phase reaction models.

- The rotation temperatures of observed molecules can be divided into three groups : low temperatures (10-40 K) for c-C_2H_4O, CH_3CHO and HCOOH, high temperatures (70-250 K) for CH_3OH, $(CH_3)_2O$, C_2H_3CN and C_2H_5CN, and intermediate temperatures (35-80 K) for $HCOOCH_3$ and C_2H_5OH. This results indicate that these molecular line emissions may arise in regions with different physical conditions.

- The fractional abundances are 1 × 10^{-11} - 6 × 10^{-10} for ethylene oxide and 7 × 10^{-12} - 3 × 10^{-9} for acetaldehyde. These values are higher than the abundance predicted from pure gas-phase reaction models by a factor of 10-600. The ratio [CH_3CHO]/[c-C_2H_4O] varies from 1.2-13.2.

- The abundances of CH_3OH, C_2H_5OH, $HCOOCH_3$, C_2H_3CN, and C_2H_3CN vary in different molecular clouds by 1-4 orders of magnitude and increase with increasing

dust temperature. This results may indicate the chemical evolution of observed molecular cloud. However, there seems no correlation between the abundances of ethylene oxide or acetaldehyde and the dust temperature, suggesting that these species may be formed in the gas-phase.

- We compared our observational results with some chemical reaction model including grain-surface reactions and considering physical condition of hot molecular cloud. These models reproduce a part of our observational results, however, there are no current chemical models which can sufficiently explain all of the abundances of large organic molecules, especially, C_2H_5OH. More development of detail model calculations are necessary.

- The formation reactions to c-C_2H_4O and CH_3CHO in hot cores are found to start from C_2H_5OH, which is evaporated from grain mantles.

Table 1. Molecular transition data and characteristics of telescopes for detection observations

Transition Transition	Rest freq. [MHz]	Telescope Telescope	E_u[a] [K]	θ_{mb}[a] [″]
$1_{1,1}$-$0_{0,0}$	39 581.60	Haystack	2	57
$4_{2,2}$-$4_{1,3}$	41 579.43	NRO	21	40
$4_{4,1}$-$4_{3,2}$	47 094.97	NRO	23	35
$5_{5,0}$-$5_{4,1}$	47 556.90	NRO	35	35
$3_{1,2}$-$2_{2,1}$	104 688.62	NRO	12	16
$6_{3,4}$-$5_{2,3}$	219 512.82	SEST	40	23
$8_{0,8}$-$7_{1,7}$	235 106.08	SEST	52	21
$8_{1,8}$-$7_{0,7}$	235 106.11	...	...	...
$5_{4,1}$-$4_{3,2}$	249 161.64	SEST	32	20
$5_{5,0}$-$4_{4,1}$	249 623.57	SEST	35	20
$8_{1,7}$-$7_{2,6}$	254 231.79	SEST	59	20
$8_{2,7}$-$7_{1,6}$	254 235.72	...	...	...

[a] E_u is the upper level energy above the ground state

[b] θ_{mb} is the beam size

Table 2. Molecular transition data and characteristics of the SEST observations.

Rest freq. [MHz]	Transition	E_u[a] [K]	A_{ul}[b] [10^{-4} s^{-1}]	θ_{mb}[c] ["]	η_{mb}[d] [%]
c-C_2H_4O:					
94 664.6	$3_{1,3} - 2_{0,2}$	10	0.12	53	75
225 468.0	$5_{4,2} - 4_{3,1}$	33	1.06	22	60
226 043.1	$7_{1,6} - 6_{2,5}$	47	1.66	22	60
226 072.0	$7_{2,6} - 6_{1,5}$	47	1.66	22	60
249 623.6	$5_{5,0} - 4_{4,1}$	35	2.30	20	60
254 231.8	$8_{1,7} - 7_{2,6}$	59	2.48	20	60
254 235.7	$8_{2,7} - 7_{1,6}$	59	2.48	20	60
CH_3CHO:					
112 248.7	$6_{1,6} - 5_{1,5}$ A	21	0.47	45	75
112 254.5	$6_{1,6} - 5_{1,5}$ E	21	0.47	45	75
223 650.1	$12_{1,12} - 11_{1,11}$ E	72	3.92	23	60
223 660.6	$12_{1,12} - 11_{1,11}$ A	72	3.92	23	60
249 323.9	$13_{2,12} - 12_{2,11}$ A	93	5.36	20	60
249 326.6	$13_{2,12} - 12_{2,11}$ E	93	5.36	20	60

[a] E_u is the upper level energy above the ground state

[b] A_{ul} is the Einstein's A coefficiency

[c] θ_{mb} is the beam size

[d] η_{mb} is the main beam efficiency

Table 3. Molecular transition data and characteristics of the NRO/NRAO observations

Rest freq. [MHz]	Transition	E_u[a] [K]	A_{ul}[b] [10^{-4} s^{-1}]	θ_{mb}[c] ["]	η_{mb}[d] [%]
c-C_2H_4O:					
94 664.6	$3_{1,3} - 2_{0,2}$	10	0.12	17	47
226 043.1	$7_{1,6} - 6_{2,5}$	47	1.66	27	45
226 072.0	$7_{2,6} - 6_{1,5}$	47	1.66	27	45
235 106.1	$8_{0,8} - 7_{1,7}$	52	2.33	26	45
235 106.1	$8_{1,8} - 7_{0,7}$	52	2.33	26	45
249 623.6	$5_{5,0} - 4_{4,1}$	35	2.30	24	45
CH_3CHO:					
98 863.3	$5_{1,4} - 4_{1,3}$ A	17	0.31	16	49
98 900.9	$5_{1,4} - 4_{1,3}$ E	17	0.31	16	49
223 650.1	$12_{1,12} - 11_{1,11}$ E	72	3.92	26	45
223 660.6	$12_{1,12} - 11_{1,11}$ A	72	3.92	26	45
249 323.9	$13_{2,12} - 12_{2,11}$ A	93	5.36	24	45
249 326.6	$13_{2,12} - 12_{2,11}$ E	93	5.36	24	45

[a] E_u is the upper level energy above the ground state

[b] A_{ul} is the Einstein's A coefficiency

[c] θ_{mb} is the beam size

[d] η_{mb} is the main beam efficiency

Table 4. Source coordinates and radial velocities with respect to the local standard of rest, V_{LSR}.

Source	α(1950.0)	δ(1950.0)	V_{LSR} [km s^{-1}]	Telescope
W3(H_2O)	$02^h23^m17.^s3$	$+61°38'58.0''$	−47	NRO,NRAO
TMC-1(NH_3)	$04^h38^m17.^s0$	$+25°42'23.3''$	+5.8	NRO
TMC-1	$04^h38^m38.^s6$	$+25°35'45.0''$	+5.9	NRO
Orion-S	$05^h32^m45.^s4$	$-05°26'05.0''$	+6.6	NRO,NRAO
Orion Compact Ridge	$05^h32^m46.^s5$	$-05°24'30.0''$	+8	NRO
Orion Hot Core	$05^h32^m47.^s0$	$-05°24'23.0''$	+8	NRO,NRAO
Orion 3'N	$05^h32^m51.^s0$	$-05°20'50.0''$	+9	SEST
G322.2+0.6	$15^h14^m50.^s0$	$-56°28'00.0''$	−56	SEST
G327.3−0.6	$15^h49^m15.^s6$	$-54°28'07.0''$	−45	SEST
G333.13−0.43	$16^h17^m16.^s8$	$-50°28'17.0''$	−52	SEST
G339.88−1.26	$16^h48^m24.^s8$	$-46°03'33.9''$	−39	SEST
NGC 6334F[a]	$17^h17^m32.^s3$	$-35°44'02.5''$	−7	SEST
G351.6−1.3	$17^h25^m56.^s0$	$-36°37'54.0''$	−12	SEST
M8[b]	$18^h00^m36.^s3$	$-24°22'53.0''$	+10	SEST
G10.47+0.03[c]	$18^h05^m40.^s3$	$-19°52'21.0''$	+68	SEST
G29.96−0.02	$18^h43^m27.^s1$	$-02°42'36.0''$	+97.4	NRO
G31.41+0.31	$18^h44^m59.^s2$	$-01°16'07.0''$	+97	SEST
G34.3+0.2	$18^h50^m46.^s2$	$+01°11'13.0''$	+58	SEST,NRO, NRAO
W51e1/e2	$19^h21^m26.^s3$	$+14°24'36.0''$	+57	NRO,NRAO
G75.78+0.34	$20^h19^m52.^s0$	$+37°17'02.0''$	−0.1	NRO,NRAO
DR21(OH)	$20^h37^m14.^s2$	$+42°12'10.0''$	−3	NRO,NRAO
NGC 7538	$23^h11^m36.^s5$	$+61°11'49.0''$	−57	NRO,NRAO

[a]NGC 6334I, G351.41+0.64

[b]NGC 6523

[c]W31(1)

Table 5. Rotation temperatures, column densities, and fractional abundances relative to H_2

Source	Molecule	T_{rot} [K]	N^a[cm^{-2}]	X
NGC 6334F	c-C_2H_4O	36±10	$(1.1 \pm 0.6) \times 10^{14}$	6×10^{-10}
	CH_3CHO	22±1	$(2.8 \pm 0.6) \times 10^{14}$	1×10^{-9}
	CH_3OH	88±16	$(3.4 \pm 2.1) \times 10^{16}$	2×10^{-7}
	C_2H_5OH	83±57	$(1.7 \pm 2.8) \times 10^{15}$	9×10^{-9}
	CH_3OCH_3	145±54	$(7.5 \pm 5.6) \times 10^{15}$	4×10^{-8}
	HCOOH	38±14	$(1.9 \pm 1.7) \times 10^{14}$	9×10^{-10}
G327.3−0.6	c-C_2H_4O	29±7	$(6.4 \pm 3.2) \times 10^{13}$	3×10^{-10}
	CH_3CHO	21±1	$(5.0 \pm 0.8) \times 10^{14}$	3×10^{-9}
	CH_3OH	80±13	$(2.0 \pm 1.2) \times 10^{16}$	1×10^{-7}
	C_2H_5OH	97±49	$(1.9 \pm 2.2) \times 10^{15}$	1×10^{-8}
	CH_3OCH_3	170±90	$(6.3 \pm 6.3) \times 10^{15}$	3×10^{-8}
	HCOOH	27±15	$(1.7 \pm 2.8) \times 10^{14}$	9×10^{-10}
G31.41+0.31	c-C_2H_4O	35±6	$(6.7 \pm 2.2) \times 10^{13}$	4×10^{-10}
	CH_3CHO	31±2	$(1.8 \pm 0.4) \times 10^{14}$	1×10^{-9}
	CH_3OH	95±16	$(1.4 \pm 0.7) \times 10^{16}$	9×10^{-8}
	C_2H_5OH	94±23	$(2.7 \pm 1.5) \times 10^{15}$	2×10^{-8}
	CH_3OCH_3	147±37	$(3.7 \pm 1.9) \times 10^{15}$	2×10^{-8}
	HCOOH	44±20	$(1.6 \pm 1.6) \times 10^{14}$	1×10^{-9}
G34.3+0.2	c-C_2H_4O	17±7	$(6.6 \pm 8.3) \times 10^{13}$	2×10^{-10}
	CH_3CHO	22±1	$(2.4 \pm 0.2) \times 10^{14}$	8×10^{-10}
	CH_3OH	96±17	$(2.6 \pm 1.4) \times 10^{16}$	9×10^{-8}
	C_2H_5OH	75±37	$(1.7 \pm 2.1) \times 10^{15}$	6×10^{-9}
	CH_3OCH_3	137±32	$(3.7 \pm 1.8) \times 10^{15}$	1×10^{-8}
	C_2H_3CN	[150]	3.2×10^{13}	1×10^{-10}
	C_2H_5CN	[150]	8.1×10^{14}	3×10^{-9}
	$HCOOCH_3$	35±13	$(1.4 \pm 1.0) \times 10^{15}$	5×10^{-9}
G10.47+0.03	c-C_2H_4O	[30]	$<3.9 \times 10^{13}$	$< 3 \times 10^{-10}$
	CH_3CHO	33±4	$(2.1 \pm 0.7) \times 10^{14}$	2×10^{-9}
	CH_3OH	96±16	$(2.7 \pm 1.4) \times 10^{16}$	2×10^{-7}
	C_2H_5OH	[100]	1.3×10^{15}	1×10^{-8}
	CH_3OCH_3	139±23	$(4.4 \pm 1.5) \times 10^{15}$	3×10^{-8}
	HCOOH	23	1.5×10^{14}	1×10^{-9}

Table 5--Continued

Source	Molecule	T_{rot} [K]	N^a[cm^{-2}]	X
SgrB2(N)	c-C_2H_4O	18±3	$(3.3 \pm 0.9) \times 10^{14}$	6×10^{-11}
	CH_3CHO^b	8±1	$(4.0 \pm 2.0) \times 10^{14}$	8×10^{-11}
	CH_3OH^b	148±26	$(8.3 \pm 3.2) \times 10^{16}$	2×10^{-8}
	$C_2H_5OH^b$	72±9	$(7.5 \pm 3.1) \times 10^{15}$	2×10^{-9}
	$CH_3OCH_3{}^b$	55±5	$(2.7 \pm 0.4) \times 10^{15}$	7×10^{-10}
	$HCOOCH_3{}^b$	74±45	$(2.6 \pm 2.5) \times 10^{15}$	5×10^{-10}
	$C_2H_3CN^b$	157±39	$(1.7 \pm 1.2) \times 10^{15}$	3×10^{-10}
	$C_2H_5CN^b$	180±89	$(1.1 \pm 0.8) \times 10^{16}$	2×10^{-9}
	$HCOOH^b$	[30]	7.1×10^{13}	1×10^{-11}
DR21(OH)	c-C_2H_4O	11±0	$(2.5 \pm 0.0) \times 10^{13}$	1×10^{-10}
	CH_3CHO	18±1	$(7.3 \pm 0.7) \times 10^{13}$	4×10^{-10}
	CH_3OH	[150]	2.5×10^{16}	1×10^{-8}
	C_2H_5OH	[150]	$< 1.3 \times 10^{14}$	$< 7 \times 10^{-10}$
	$HCOOCH_3$	[70]	$< 1.0 \times 10^{14}$	$< 5 \times 10^{-10}$
	C_2H_3CN	[150]	$< 4.3 \times 10^{12}$	$< 2 \times 10^{-11}$
	C_2H_5CN	[150]	$< 4.2 \times 10^{13}$	$< 2 \times 10^{-10}$
NGC 7538	c-C_2H_4O	[20]	1.6×10^{13}	2×10^{-11}
	CH_3CHO	18±3	$(4.2 \pm 3.1) \times 10^{13}$	5×10^{-11}
	CH_3OH	[150]	$< 2.6 \times 10^{14}$	$< 3 \times 10^{-10}$
	C_2H_5OH	[150]	$< 8.3 \times 10^{13}$	$< 1 \times 10^{-10}$
	$HCOOCH_3$	[70]	$< 6.3 \times 10^{13}$	$< 8 \times 10^{-11}$
	C_2H_3CN	[150]	$< 2.7 \times 10^{12}$	$< 3 \times 10^{-12}$
	C_2H_5CN	[150]	$< 2.5 \times 10^{13}$	$< 3 \times 10^{-11}$
W3(H_2O)	c-C_2H_4O	[20]	1.3×10^{13}	1×10^{-11}
	CH_3CHO	[20]	2.1×10^{13}	2×10^{-11}
	CH_3OH	[150]	3.9×10^{15}	4×10^{-9}
	C_2H_5OH	[150]	$< 1.1 \times 10^{14}$	$< 1 \times 10^{-10}$
	$HCOOCH_3$	[70]	$< 9.3 \times 10^{13}$	$< 1 \times 10^{-10}$
	C_2H_3CN	[150]	$< 5.7 \times 10^{12}$	$< 6 \times 10^{-12}$
	C_2H_5CN	[150]	$< 3.7 \times 10^{14}$	$< 4 \times 10^{-11}$

Table 5--Continued

Source	Molecule	T_{rot} [K]	N[a][cm^{-2}]	X
W51e1/e2	c-C_2H_4O	12±2	$(1.9 \pm 1.0) \times 10^{13}$	4×10^{-11}
	CH_3CHO	14±1	$(2.5 \pm 0.7) \times 10^{14}$	5×10^{-10}
	CH_3OH	208	1.0×10^{17}	2×10^{-7}
	C_2H_5OH	169±28	$(3.1 \pm 1.1) \times 10^{15}$	6×10^{-9}
	$HCOOCH_3$	80±43	$(1.2 \pm 1.0) \times 10^{16}$	2×10^{-8}
	C_2H_3CN	236±99	$(1.6 \pm 1.0) \times 10^{14}$	3×10^{-10}
	C_2H_5CN	[150]	1.4×10^{15}	3×10^{-9}
Orion-S	c-C_2H_4O	[20]	$< 1.3 \times 10^{13}$	$< 2 \times 10^{-12}$
	CH_3CHO	[20]	5.9×10^{13}	7×10^{-12}
	CH_3OH	[150]	$< 7.7 \times 10^{14}$	$< 1 \times 10^{-10}$
	C_2H_5OH	[150]	$< 3.0 \times 10^{14}$	$< 4 \times 10^{-11}$
	$HCOOCH_3$	[70]	$< 2.4 \times 10^{14}$	$< 3 \times 10^{-11}$
	C_2H_3CN	[150]	$< 1.1 \times 10^{13}$	$< 1 \times 10^{-12}$
	C_2H_5CN	[150]	$< 9.7 \times 10^{13}$	$< 1 \times 10^{-11}$
Orion Compact Ridge	c-C_2H_4O	[20]	1.2×10^{13}	4×10^{-11}
	CH_3CHO	[20]	2.5×10^{13}	8×10^{-11}
	CH_3OH	152	4.9×10^{16}	2×10^{-7}
	C_2H_5OH	[150]	$< 2.8 \times 10^{14}$	$< 9 \times 10^{-10}$
	$HCOOCH_3$	[70]	3.4×10^{15}	1×10^{-8}
	C_2H_3CN	[150]	7.7×10^{13}	3×10^{-10}
	C_2H_5CN	[150]	1.8×10^{15}	6×10^{-9}
Orion Hot Core	c-C_2H_4O	25±9	$(2.4 \pm 1.7) \times 10^{13}$	2×10^{-10}
	CH_3CHO	36±2	$(5.7 \pm 0.8) \times 10^{13}$	6×10^{-10}
	CH_3OH	152	1.4×10^{17}	1×10^{-6}
	C_2H_5OH	[150]	1.5×10^{15}	2×10^{-8}
	$HCOOCH_3$	63±14	$(9.4 \pm 3.3) \times 10^{15}$	9×10^{-8}
	C_2H_3CN	93±7	$(2.1 \pm 0.3) \times 10^{14}$	2×10^{-9}
	C_2H_5CN	[150]	3.1×10^{15}	3×10^{-8}

[a]The column densities and the abundances of southern sources (NGC 6334F, G327.3-0.6, G31.41+0.31, G34.3+0.2, and G10.47+0.03) listed were assumed a 20″ source size

[b]The column densities and abundances listed were obtained from the line survey data (Ohishi et al. 1998)

Brackets indicate fixed T_{rot}

Table 6. Fractional abundances of the observed molecules and predicted abundances from chemical models

		CHH[a]		CTM[b]		MMG[c]	
		C.R[d]	H.C[e]	C.R[f]	H.C[g]	UCC[h]	CC[i]
Molecule	X	$10^{4.5}$ yr	10^{5} yr	$10^{4.6}$ yr	$10^{4.8}$ yr	10^{4} yr	10^{4} yr
C_2H_4O[j]	9(-12)−3(-9)	2.0(-8)	1.2(-12)	1.4(-10)	3.5(-11)	1.4(-9)	1.9(-9)
CH_3OH	4(-9)−1(-6)	2.0(-5)	9.2(-12)	7.2(-7)	1.7(-10)	6.1(-7)	9.3(-7)
C_2H_5OH	2(-9)−2(-8)	8.5(-12)	2.9(-13)	9.2(-12)	4.2(-14)	1.1(-14)	1.2(-13)
$(CH_3)_2O$	7(-10)−4(-8)	1.3(-8)	1.8(-14)	1.5(-8)	1.3(-15)	1.7(-9)	1.5(-9)
$HCOOCH_3$	5(-10)−9(-8)	3.7(-8)	1.9(-14)	7.7(-9)	4.4(-12)	8.7(-10)	1.5(-9)
C_2H_3CN	1(-10)−2(-9)	1.8(-10)	1.8(-9)	...	...	...	...
C_2H_5CN	2(-9)−3(-8)	1.0(-9)	2.4(-8)	...	...	...	...
$HCOOH$	1(-11)−1(-9)	1.3(-10)	1.4(-9)	...	...	...	...

[a]Caselli, Hasegawa, and Herbst (1993)

[b]Charnley, Tielens, and Millar (1992)

[c]Millar, Macdonald, and Gibb (1997)

[d]Model for Orion Compact Ridge; $T_{dust}=T_{gas}=100$ K, $n_H=10^6$ cm^{-3}

[e]Model for Orion Hot Core; $T_{dust}=T_{gas}=200$ K, $n_{H_2}=1.3\times10^7$ cm^{-3}

[f]Model for Orion Compact Ridge; $T_{kin}=100$ K, $n_H=2\times 10^6$ cm^{-3}

[g]Model for Orion Hot Core; $T_{kin}=200$ K, $n_H=2\times 10^7$ cm^{-3}

[h]Model for Ultra Compact Core of G34.3+0.2; $T_{kin}=300$ K, $n_{H_2}=2\times 10^7$ cm^{-3}

[i]Model for Compact Core of G34.3+0.2 ; $T_{kin}=75$-190 K, $n_{H_2}=10^6$ cm^{-3}

[j]C_2H_4O indicates c-C_2H_4O + CH_3CHO

a(b) means a $\times$ 10^b.

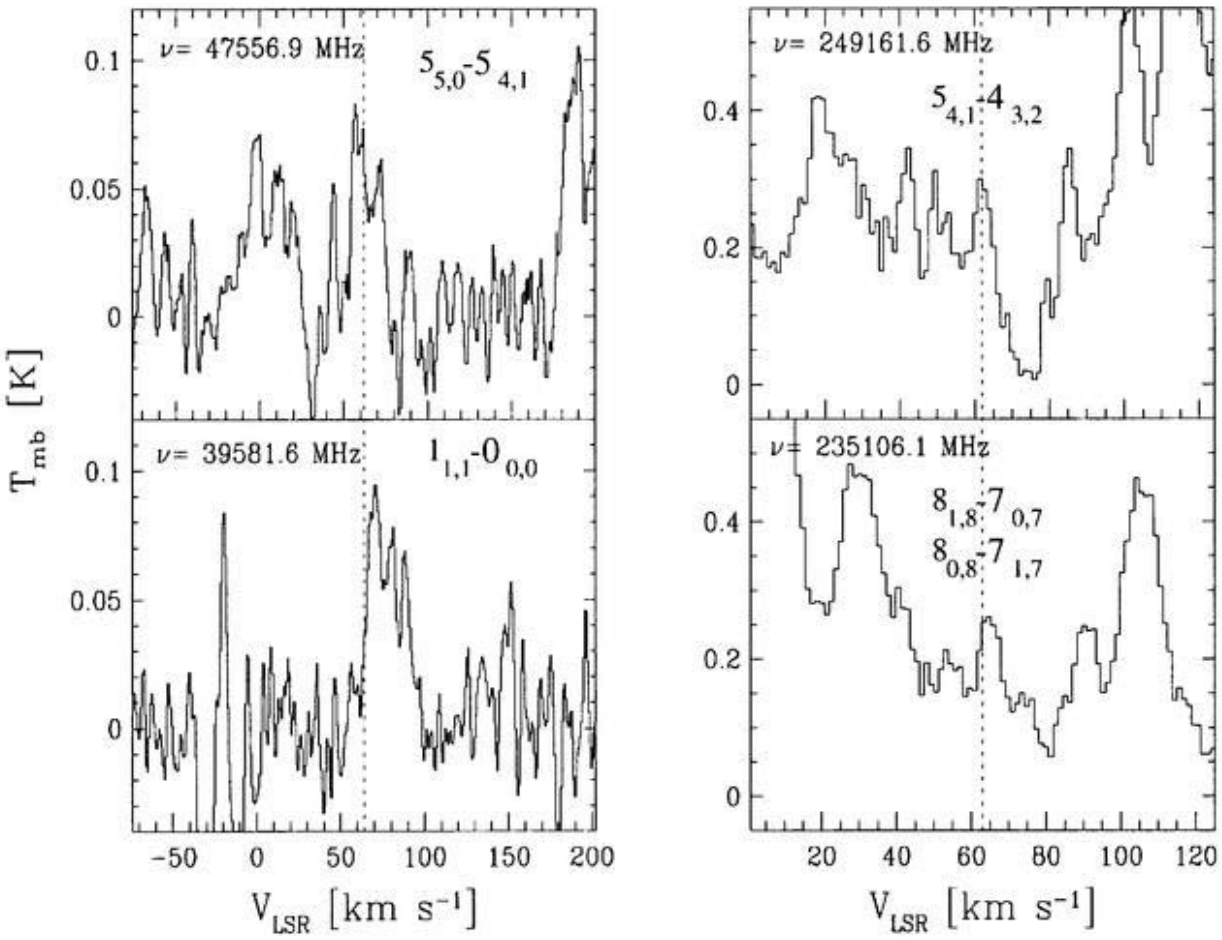

Fig. 1.— Spectra of c-C_2H_4O toward SgrB2(N) [RA(1950.0) = $17^h44^m10.^s1$, DEC(1950.0) = -28°21'17"]. The rest frequency of the transition is shown in the upper left corner, and the dashed line mark the velocity V_{LSR} = 62.0 km s^{-1}.

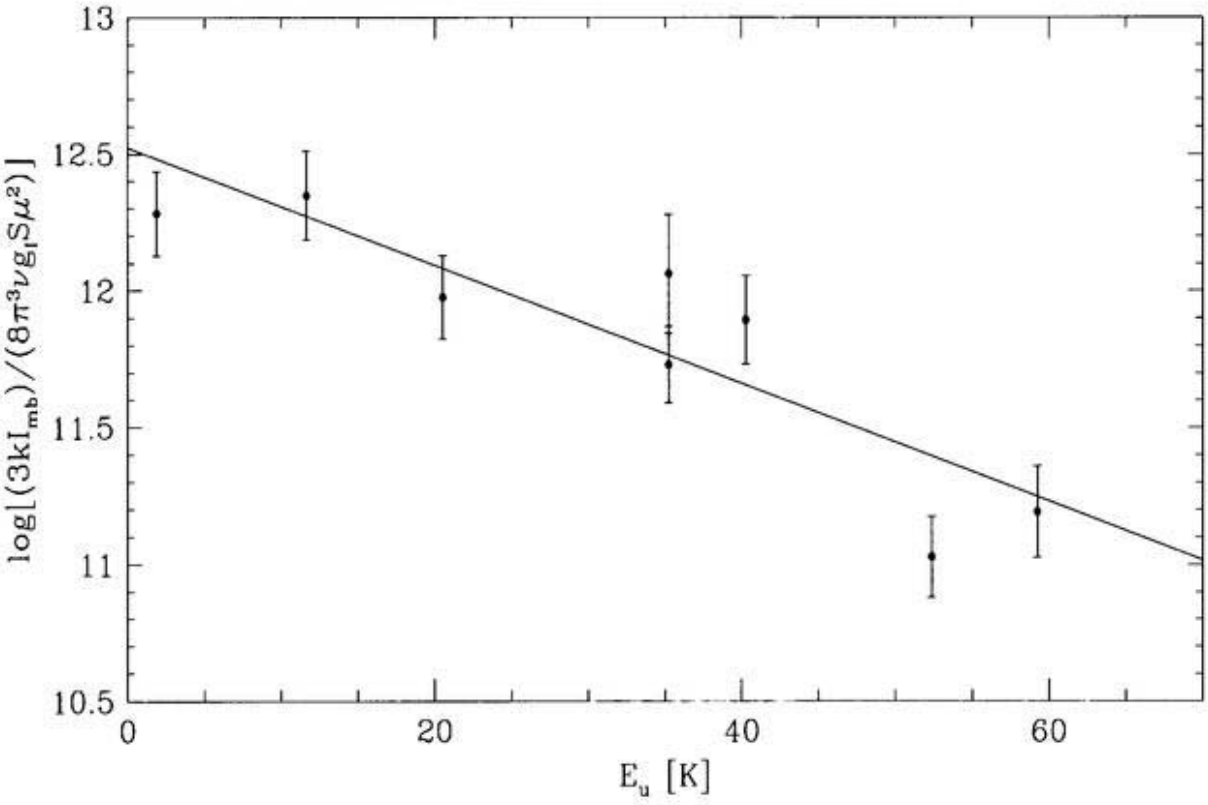

Fig. 2.— A rotation diagram of c-C_2H_4O for SgrB2(N). The 8 points plotted are those given in Table 1. In the level for the y-axis, $I_{\rm mb}$ is the main beam integrated intensity, expressed in units of K km s^{-1}. The slope of the line indicates the $T_{\rm rot}$, and the y-intercept is related to the total column density.

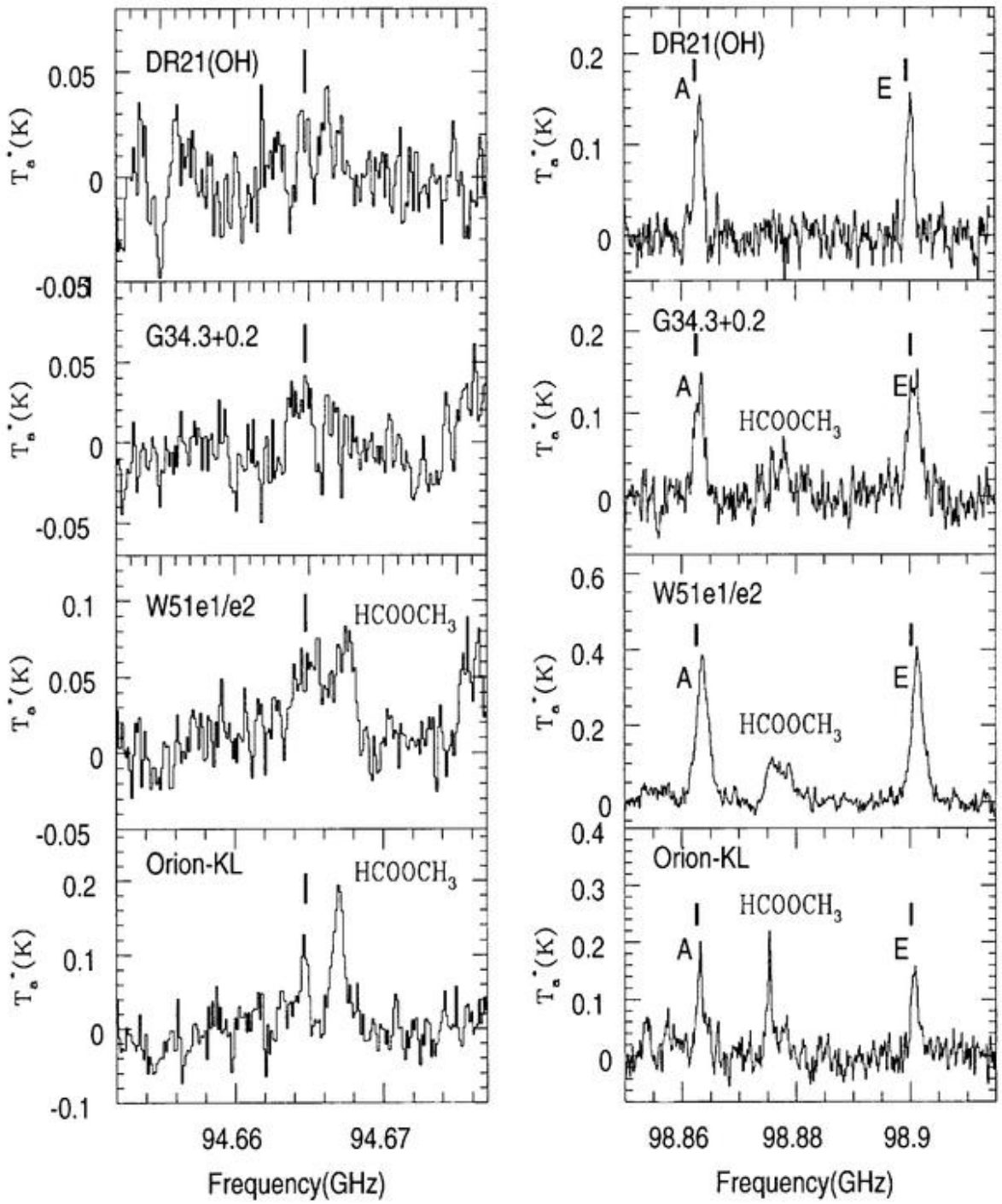

Fig. 3.— Spectra of the 3_{13}-2_{02} transition at 94664.6 MHz of c-C_2H_4O (*left panel*), and spectrum of the 5_{14}-4_{13} A transition at 98863.3 MHz and E transition at 98900.9 MHz of CH_3CHO. Vertical lines indicate the rest frequencies of these transitions.

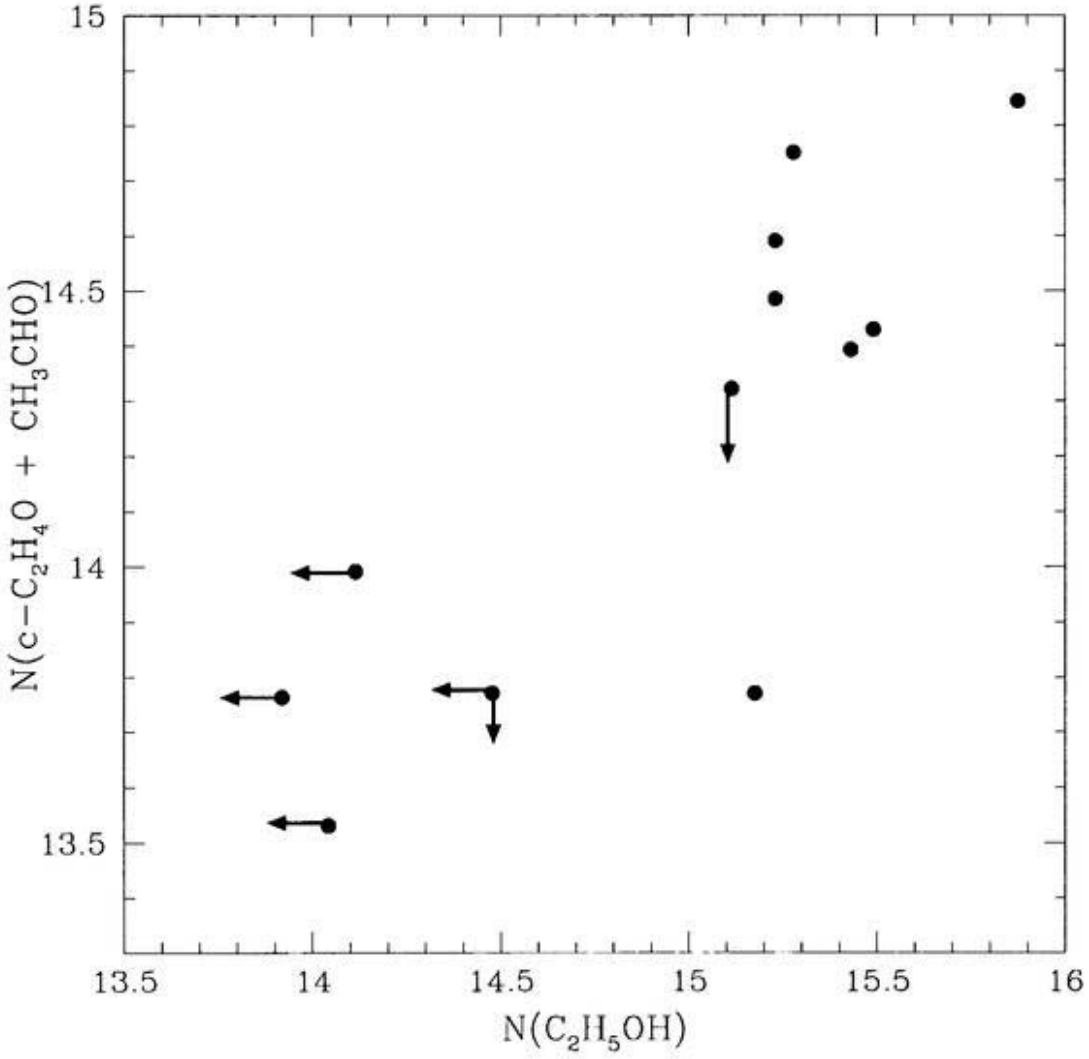

Fig. 4.— Plot of the column density of C_2H_5OH versus that of C_2H_4O group, in the logarithmic scale. Leftarrows indicate upper limit of $N(C_2H_5OH)$ and downarrows indicate upper limit of $N(C_2H_4O$ group).

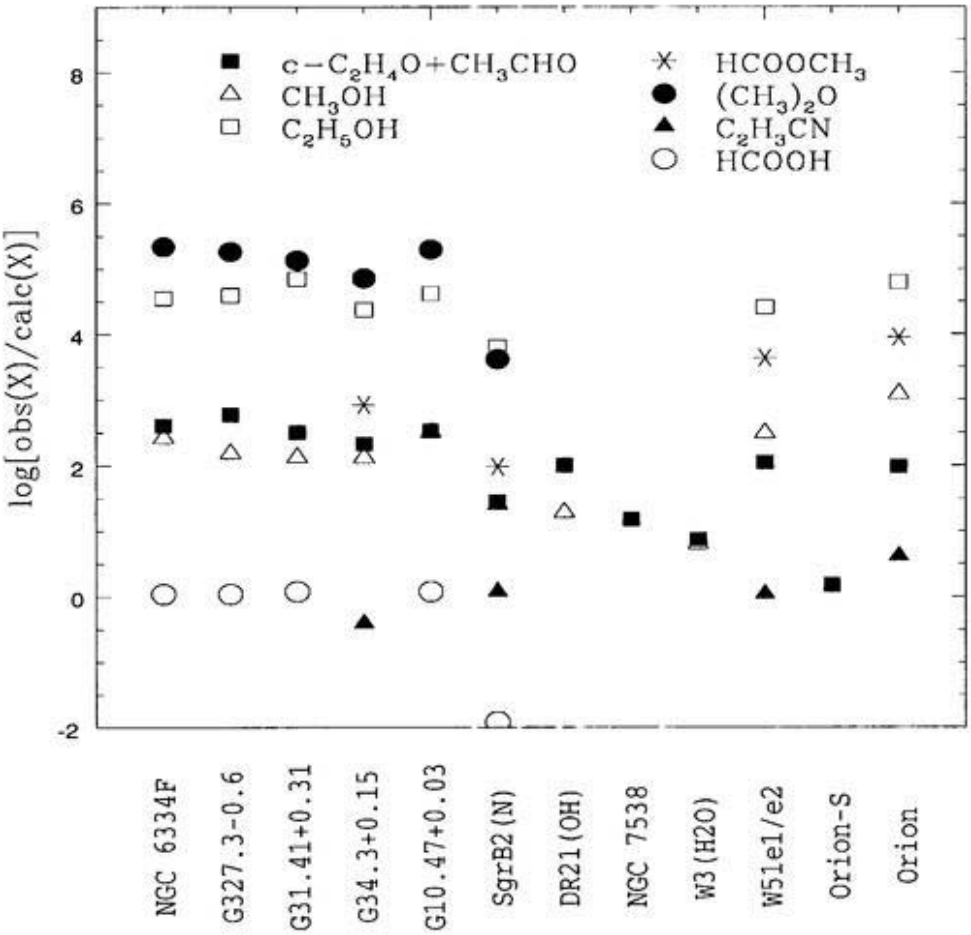

Fig. 5.— Plot of ratios of observed fractional abundances of molecules relative to calculated abundances from the pure gas-phase reaction model (Lee et al. 1996). In this gas-phase model the gas temperature and the hydrogen density are assumed to be T_k = 50 k, and $n_{H_2} = 10^5$ cm^{-3}.

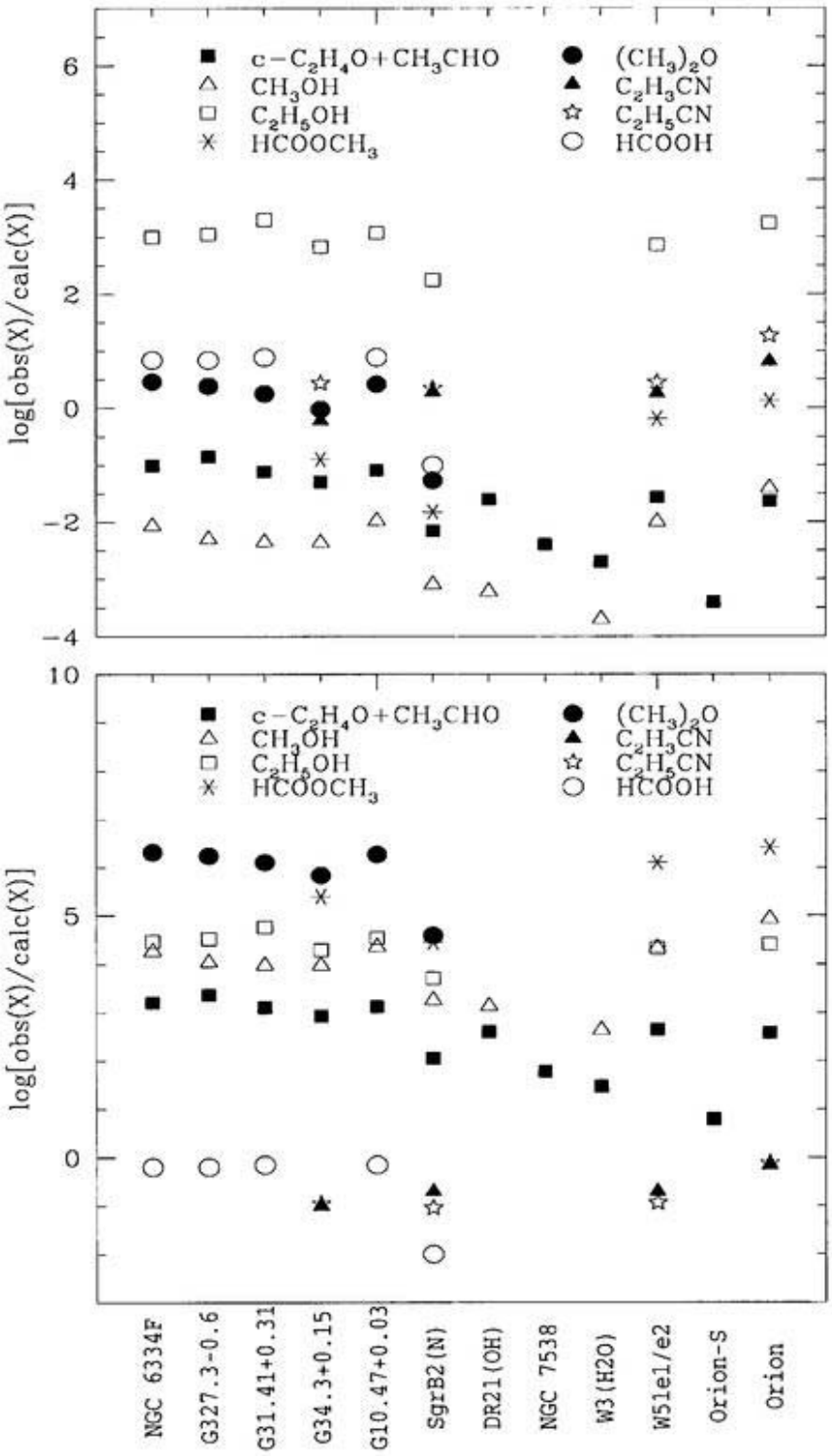

Fig. 6.— Plot of ratios of observed fractional abundances of molecules relative to calculated abundances from CHH model (Caselli, Hasegawa, and Herbst 1993). *upper panel*: Model for Orion Compact Ridge; $T_{dust}=T_{gas}=100$ K, $n_H=10^6$ cm^{-3}. *lower panel*: Model for Hot Core; $T_{dust}=T_{gas}=200$ K, $n_{H_2}=1.3\times10^7$ cm^{-3}

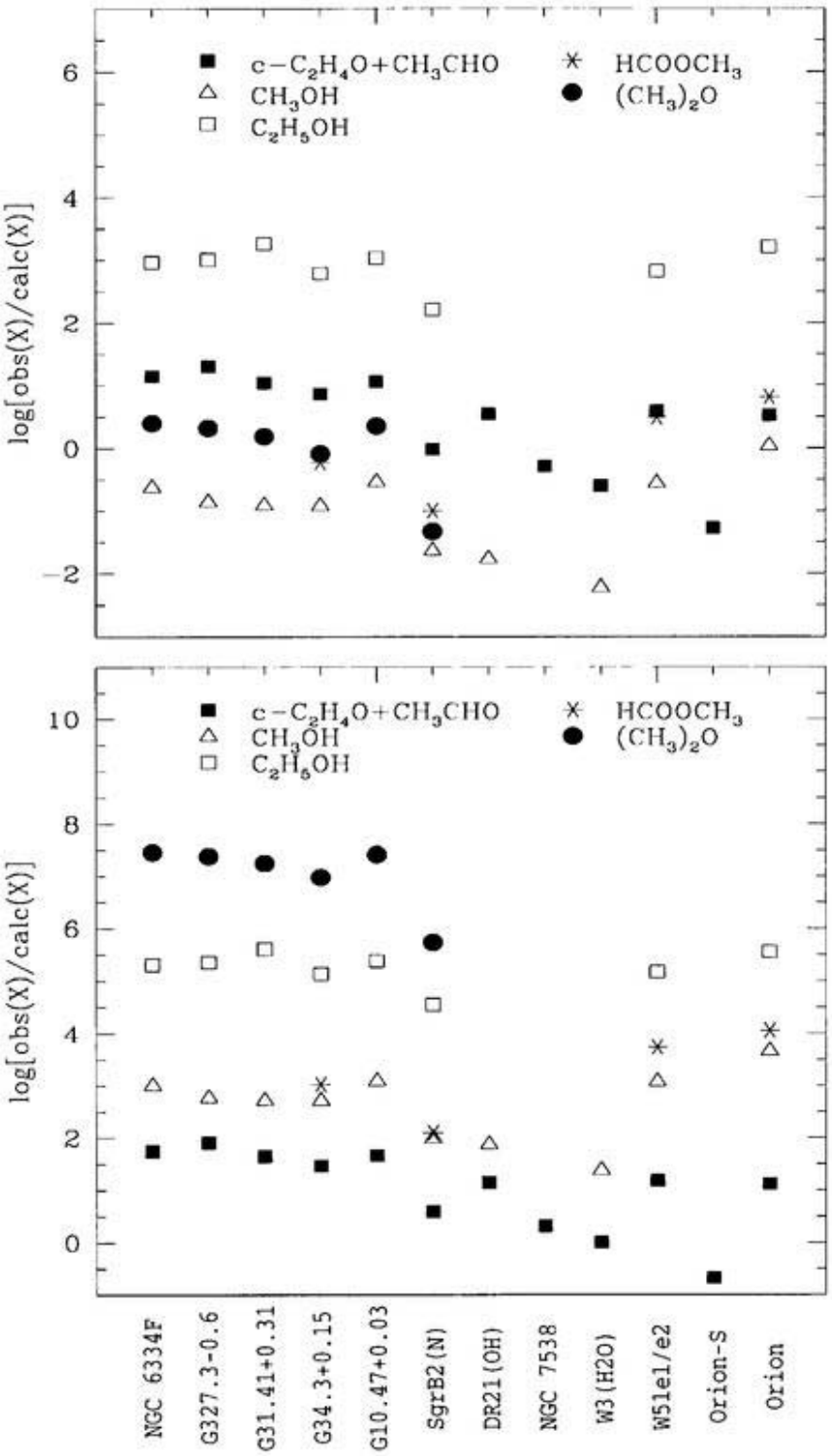

Fig. 7.— Plot of ratios of observed fractional abundances of molecules relative to calculated abundances from CTM model (Charnley, Tielens, and Millar 1992). *upper panel* : Model for Orion Compact Ridge; $T_{\rm kin}$=100 K, $n_{\rm H}$=2× 10^6 cm^{-3}. *lower panel* : Model for Hot Core; $T_{\rm kin}$=200 K, $n_{\rm H}$=2× 10^7 cm^{-3}.

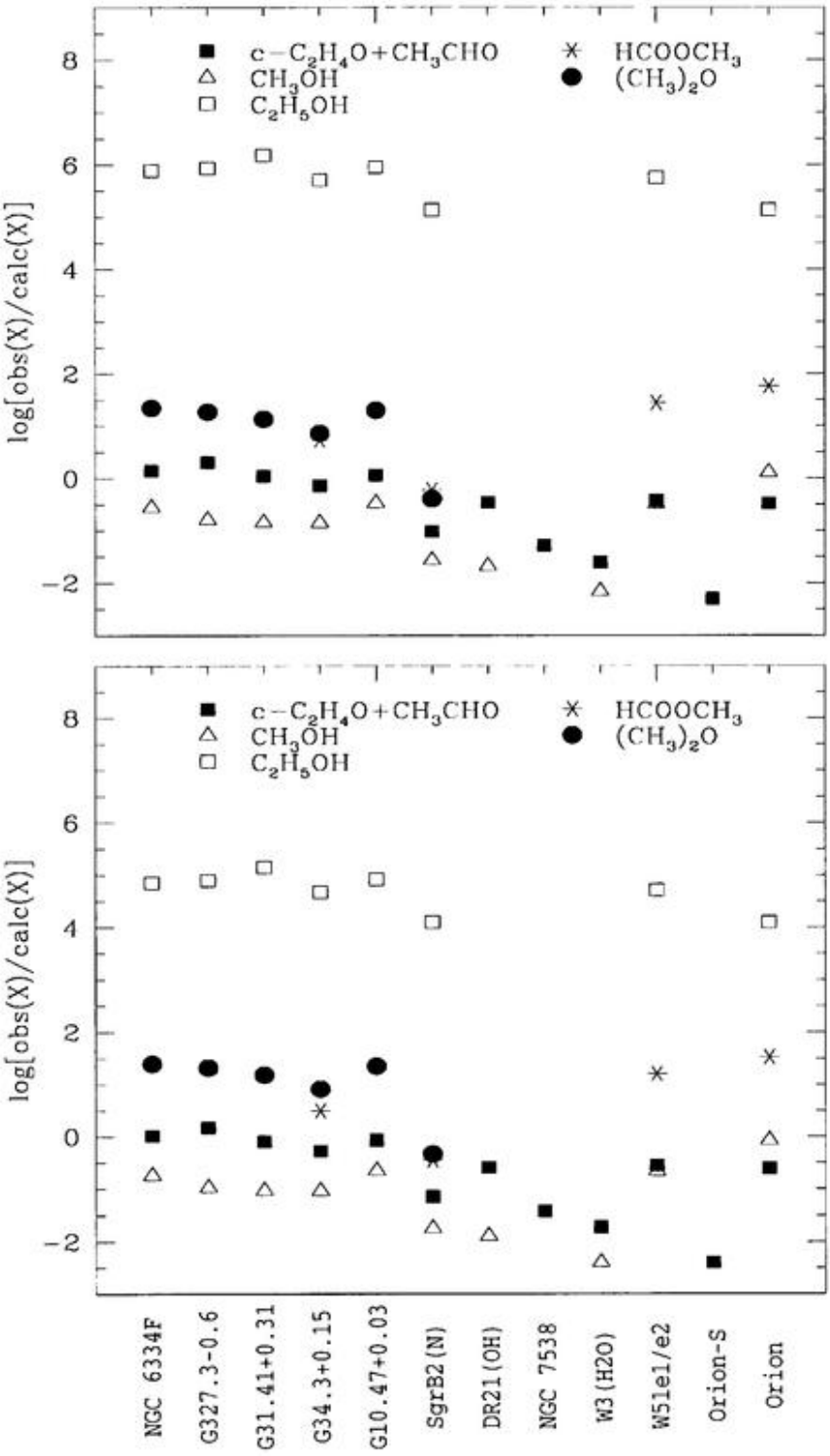

Fig. 8.— Plot of ratios of observed fractional abundances of molecules relative to calculated abundances from MMG model (Millar, Macdonald, and Gibb 1997). *upper panel* : Model for Ultra Compact Core of G34.3+0.2; $T_{\rm kin}$=300 K, $n_{\rm H_2}$=2× 10^7 cm^{-3}. *lower panel* : Model for Compact Core of G34.3+0.2 ; $T_{\rm kin}$=75-190 K, $n_{\rm H_2}$=10^6 cm^{-3}

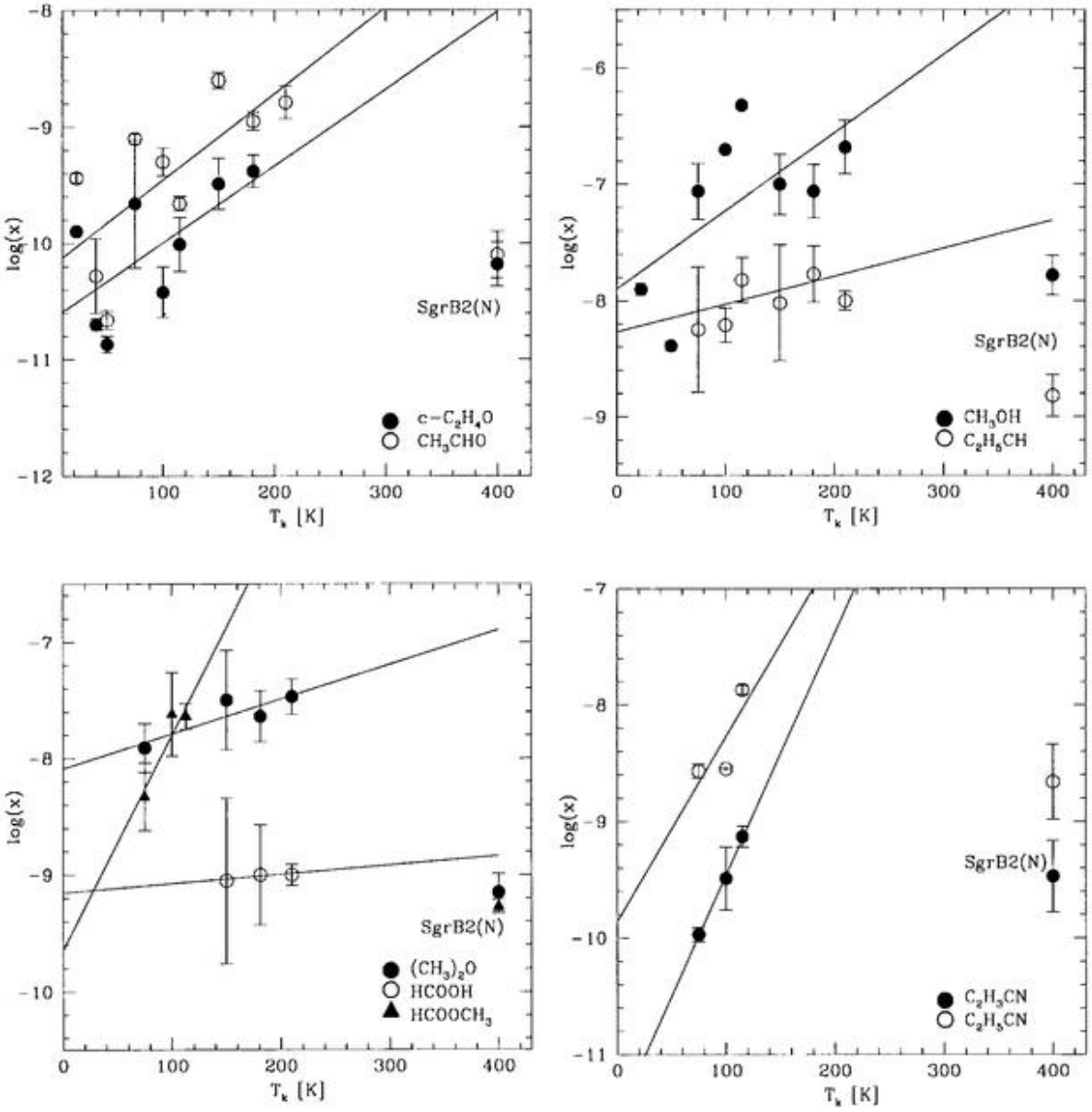

Fig. 9.— Plot of fractional abundances of molecules. The abscissa indicates the gas kinetic temperatures in observed molecular clouds, and the ordinate indicates the fractional abundances, X(molecules), in the logarithmic scale. Gas kinetic temperatures were adopted from literatures; SgrB2(N)–de Vicente et al. (1997), DR21(OH)–Askne et al.(1984), NGC7538, G34.3+0.2, W51e1/e2–Bergman et al. (1989), W3(H_2O)–Turner & Welch (1984), Orion–Andersson et al. (1984), G327.3-0.6–Bergman et al. (1992), G31.41+0.31, G10.47+0.03–Olmi et al. (1996).

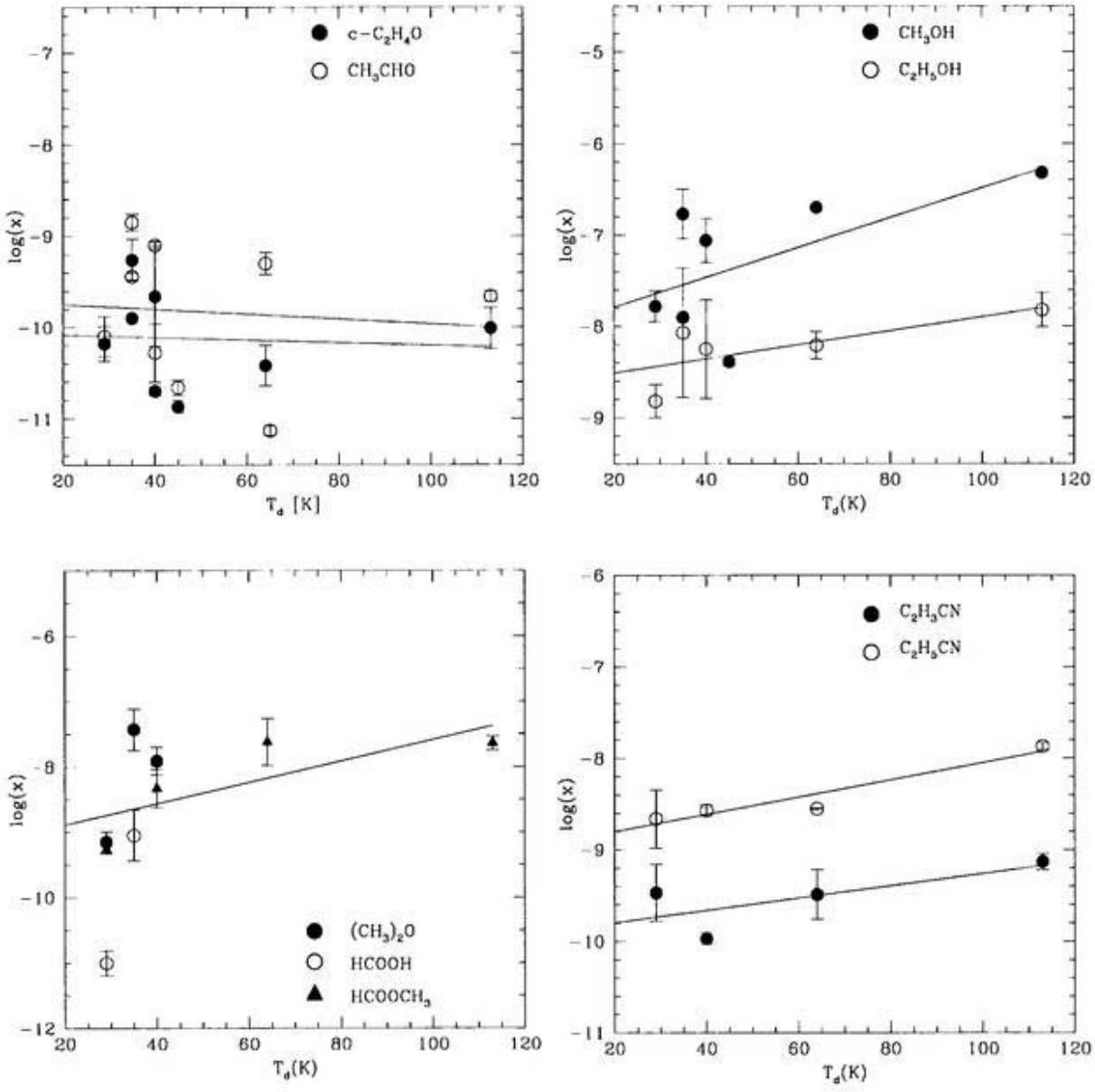

Fig. 10.— Plot of fractional abundances of molecules. The abscissa indicates the dust temperatures in observed molecular clouds, and the ordinate indicates the fractional abundances, X(molecules), in the logarithmic scale. Dust temperatures were adopted from literatures; SgrB2(N), W51e1/e2–Gordon et al. (1988), DR21(OH)–Harvey et al. (1977), NGC6334F–Cheung et al. (1978) ; Loughran et al. (1986) , NGC7538, W3(H_2O)–Thronson & Harper (1979), G34.3+0.2–Hunter et al. (1996), Orion-S–McMullin et al. (1993), Orion–Lee et al. (1983).

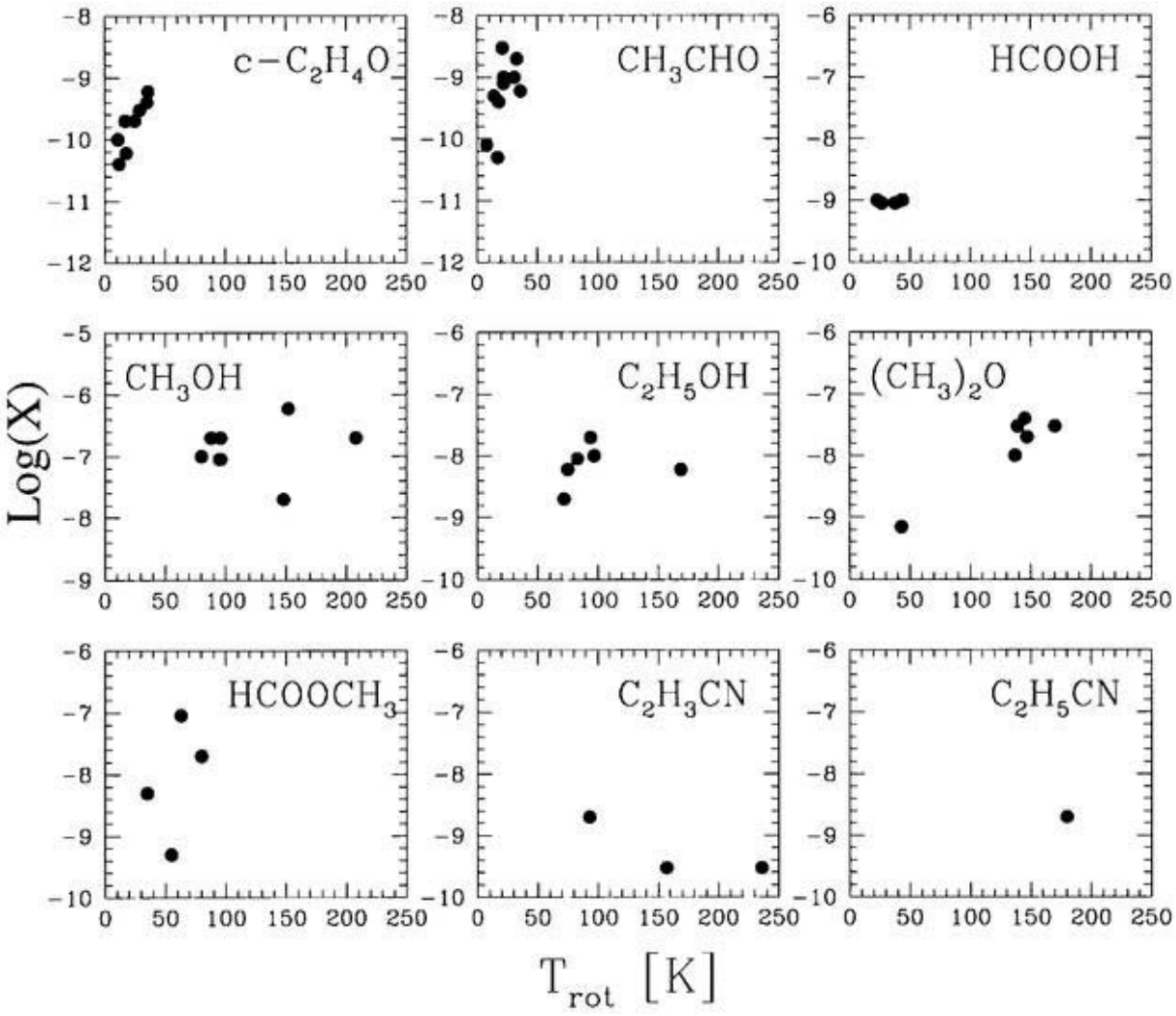

Fig. 11.— Plot of molecular abundances versus rotation temperatures of each molecule. The abscissa indicates the rotation temperatures [K], and the ordinate indicates the fractional abundances, X(molecules), in the logarithmic scale.

Chapter 5

Summary

The motivation of this thesis is to clarify the production mechanism of large organic molecules which are related to the grain-surface chemistry and to understand the relation between the chemical composition and the physical condition in massive star-forming regions.

Firstly, I have made mapping observations of the O-, NH-, and NH_2-bearing molecules toward the SgrB2 molecular cloud to clarify the production mechanism of these molecules. Secondly, based on the detection of new interstellar molecule, ethylene oxide (c-C_2H_4O), toward SgrB2(N), I have made the survey observations of c-C_2H_4O and its structural isomer acetaldehyde (CH_3CHO) toward several massive star-forming regions. The main results obtained with the present study are described below.

1. Formation Mechanism of Large Organic Molecules

It has been believed that a large organic molecule is closely related to dust grains up to now, because the observed abundances of some large organic molecules are higher than predicted values from pure gas-phase reaction models by a few orders of magnitude. If this hypothesis is correct, the distributions of these molecules are limited toward around the H II regions, because there are young stars in H II regions and UV radiation from these stars can heat dust grains. Therefore I expected that the emission of molecules we observed in present study would be limited toward H II regions: for example, SgrB2(N) in the SgrB2 molecular cloud. However, our mapping observations of these large organic molecules toward the SgrB2 molecular cloud have provided different results from my expectation. The emission of CH_3OH and $(CH_3)_2O$ are limited to around the H II region SgrB2(N) because of higher upper level energies, however, the emission of the other large organic molecules are extended. C_2H_5OH and $HCOOCH_3$ have emission not only toward SgrB2(N), but also toward regions where there are no stars, and the NH- and NH_2-bearing molecules show emission peak toward region where there are no stars (See Chap 2,3).

And we compared observed molecular abundances with several chemical models. The fractional abundances of CH_3OH, $(CH_3)_2O$ and $HCOOCH_3$ can be explained by models which include both of the gas-phase reactions and the grain-surface reactions, however, those of CH_3NH_2 and CH_2NH are close to both of the pure gas-phase reaction

model and above-mentioned reaction models. These results indicate that not of all of large organic molecules are produced on grain surface, but in the gas-phase.

Moreover, I found several excitation condition of these large organic molecules from the survey observations of c-C_2H_4O and CH_3CHO toward several massive star-forming regions. The deduced rotation temperatures can be divided into three temperature groups: 10-40 K for c-C_2H_4O, CH_3CHO and HCOOH, 35-80 K for $HCOOCH_3$ and C_2H_5OH, and 70-250 K for CH_3OH, $(CH_3)_2O$, C_2H_3CN and C_2H_5CN (See Chap. 4). It is interpreted that the variety of the rotation temperature indicates that the molecular line emission arises in regions with different physical conditions. Of course, we cannot vanish a possibility that the excitation of these species can be significantly subthermal.

The distributions of CH_3OH and $(CH_3)_2O$ which show high rotation temperature are limited toward H II regions. The distribution of C_2H_3CN is also limited toward H II regions (See Chap 2). According to Miao & Snyder (1997), C_2H_5CN shows compact distribution toward SgrB2(N) and fractional abundance of C_2H_5CN is found to be $\sim 10^{-8}$. This fractional abundance is higher than our result by an order of magnitude. This is interpreted because of difference of beam sizes $6.''7 \times 2.''7$ for interferometric observations of Miao & Snyder (1997) and $15''$ for our single dish observations, indicating that the distribution of C_2H_5CN is very compact. Miao et al. (1995) also found that the emitting regions of C_2H_3CN and C_2H_5CN are limited toward SgrB2(N) and two velocity components ($\sim$ 63 km s^{-1} and 74 km s^{-1}). In our observations, CH_3OH profile also has two velocity components ($\sim$ 64 km s^{-1} and 73 km s^{-1}). This indicates that these molecules coexist in the same volume.

On the other hand, the distributions of C_2H_5OH and $HCOOCH_3$ which show intermediate rotation temperatures are extended. $HCOOCH_3$ is believed to be produced from $CH_3OH_2^+$ and H_2CO in the gas-phase. Therefore the distribution of $HCOOCH_3$ would reflects those of CH_3OH and H_2CO. Although CH_3OH and H_2CO are believed to be important elements which are included in the dust mantle, they can also be produced in the gas-phase reaction. Therefore the distribution of H_2CO may be extended and those of $HCOOCH_3$ will be extend. In fact, low energy transition of CH_3OH at 36 GHz shows extended distribution. On the other hand, the extended distribution of C_2H_5OH cannot be interpreted through gas-phase reactions, so that heating source except for SgrB2(N) is necessary. In SgrB2, it is well known that SiO emission is extended. SiO could be produced in the gas-phase through the sputtering of grains. Since it is known that SiO emission shows very wide velocity width up to 100 km s^{-1}, there may be a

violent motion which induces sputtering in SgrB2, and C_2H_5OH may also be evaporated during the sputtering process. CH_3OH and H_2CO can be evaporated as well.

I also found that production mechanism of c-C_2H_4O and CH_3CHO would be different from other organic molecules. When I compare the abundances of large organic molecules with gas kinetic temperatures and dust temperatures of each source, the abundances of CH_3OH, C_2H_5OH and $HCOOCH_3$ increase with the increase of the gas kinetic temperature and the dust temperature, and those of C_2H_3CN and C_2H_5CN increase with the increase of the dust temperature. In contrast, the abundances of c-C_2H_4O and CH_3CHO increase with the increase of the gas kinetic temperature, but do not increase with the increase of the dust temperature. This indicates that the contribution of gas-phase formation from C_2H_5OH is much larger than that of grain-surface formation with respect to c-C_2H_4O and CH_3CHO. On the other hand, in the case of the CH_3OH, C_2H_5OH, C_2H_3CN and C_2H_5CN, since the contribution of grain-surface formation is large, these molecules are evaporated along with increase of the dust temperature, making their abundances higher.

Thus I found that the contributions of the grain-surface reactions and the gas-phase reactions are different for different large organic molecules. I summarized the production mechanisms and the excitation conditions of large organic molecules in Table 1, and show general idea of their spatial distributions and the contribution of grain-surface reactions in Figure 1. However, it should be mentioned that this idea is a working idea. In order to confirm this hypothesis, it is necessary to map in these molecules toward several massive star-forming regions.

2. Chemical Evolution and Star-Formation

In the SgrB2 molecular cloud, there are two continuum sources whose evolutional stage are different: SgrB2(N) and SgrB2(M). SgrB2(N) is believed to be younger than SgrB2(M) and most large organic molecules are detected toward SgrB2(N). On the other hand, SgrB2(M) is more evolved and UV radiation from many early-type stars probably has destroyed the large organic molecules previously formed from gas/grain chemistry. Moreover, I found variation of abundances of large organic molecules in several massive star-forming regions and positive correlation between the molecular abundances and the gas kinetic temperature or the dust temperature (See Chap 4). The increase of the abundances of CH_3OH, C_2H_5OH, C_2H_3CN and C_2H_5CN with the increase of the dust

temperature indicates that dust grains are heated and abundances of molecules, that were evaporated from dust grains or produced from evaporated molecules, have increased along with the physical evolution of molecular cloud.

According to Charnley et al. (1992), abundances of $(CH_3)_2O$ and $HCOOCH_3$ increase with evolution after evaporation of dust grains up to about $10^{4.5}$ year and decrease dramatically after that. Caselli et al. (1993) also found that the abundances of C_2H_3CN and C_2H_5CN increase up to about 10^5 year after evaporation from dust grains for Orion Compact Ridge model. Our observational results would show chemical evolution up to abundance peak ($10^{4.5}$-10^5 year) after evaporation from dust grains. Lis et al. (1991) pointed out L_{IR}/M provides a measure of star-formation rate. In the source which L_{IR}/M is high (1500 $L_\odot M_\odot^{-1}$ for OMC-1) abundances of large organic dust related molecules are high, and in the source which L_{IR}/M is low (5.9 $L_\odot M_\odot^{-1}$ for SgrB2(N)) they are low. This support above-mentioned hypothesis.

Therefore I conclude that the abundances of molecules which are closely related to grain-surface reactions can be used as diagnostics of the evolution of hot-core regions of molecular cloud.

Table 1. Formation mechanism and excitation condition of large organic molecules

Molecule	Formation mechanism	Reactant	Excitation temperature
C_2H_3CN, C_2H_5CN	dust	HCN	high
CH_3OH	**dust**[b], gas	CO,H	high
$(CH_3)_2O$	gas	$CH_3OH_2^+$,CH_3OH	high
C_2H_5OH	dust	C_2H_2	intermediate
$HCOOCH_3$	gas	$CH_3OH_2^+$,H_2CO	intermediate
NH- and NH_2-bearing molecule	gas	NH_2,NH_3	intermediate
C_2H_4O[a], HCOOH	gas	C_2H_5OH	low

[a]C_2H_4O indicates c-C_2H_4O + CH_3CHO

[b]Boldface indicates most important reaction

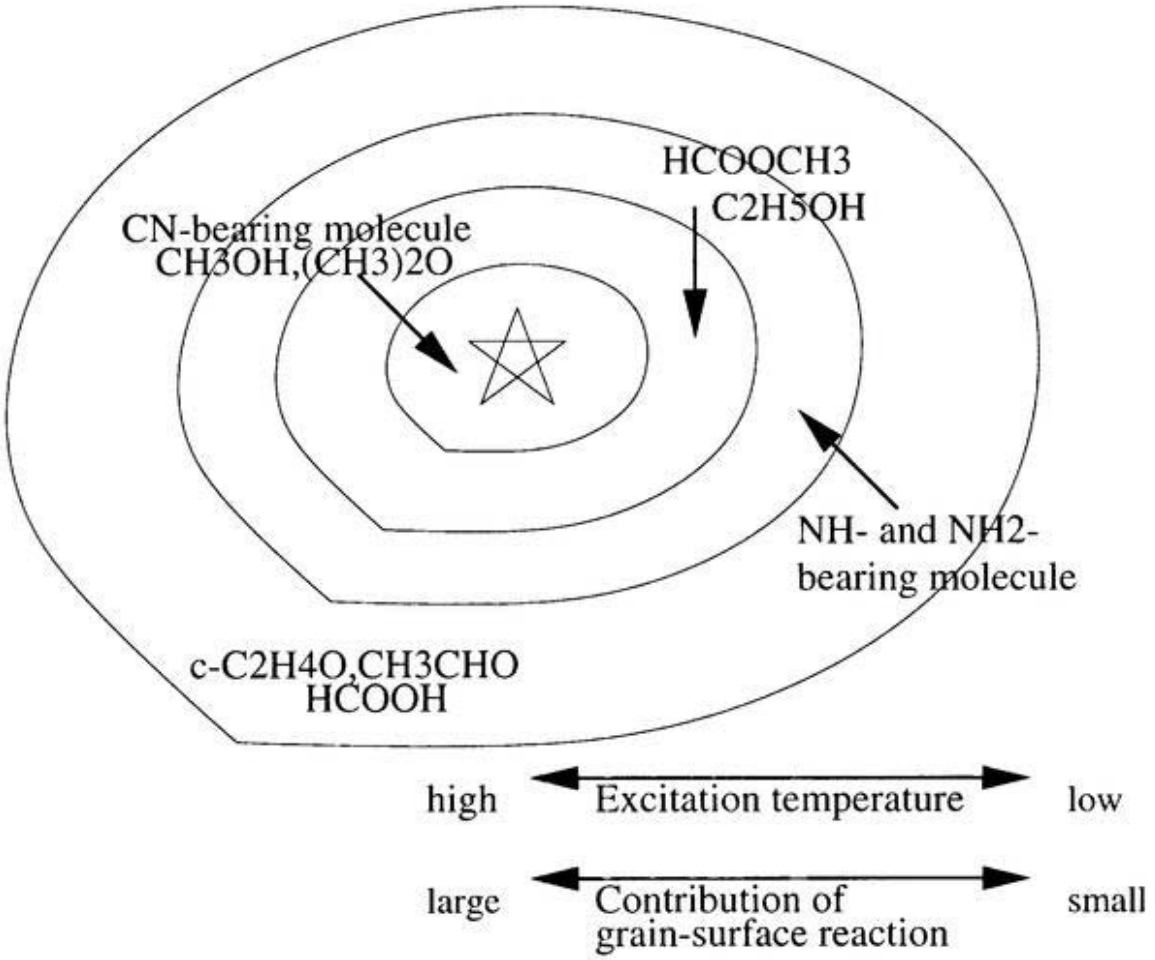

Fig. 1.— General idea of spatial distributions, excitation temperature, and contribution of grain-surface reaction to form large organic molecule

Acknowledgements

First of all, I would like to express my hearty thanks to Associate Professor Masatoshi Ohishi for his advice, encouragement and suggesting the importance of astrochemistry in massive star-forming regions. I also thank Associate Professor Nobuharu Ukita and Professor Takenori Nakano for their helpful suggestions and encouragement.

I have also learned a lot about interstellar chemistry from discussions with many astronomers, particularly Prof. W.M.Irvine, E.Herbst, Å.Hjalmarson, P.Bergman, S.Saito, S.Yamamoto, K.Takagi, N.Nakai, K.Kawaguchi, K.Tatematsu, and Drs. A.Nummelin, J.Dickens, S.Liu, H.Matsuo, K.Sunada, S.Takano, B.Vila-Vilaro, S.Sakamoto, M.Saito, J.Takahashi, Y.Aikawa, N.Kuno, K.Nishiyama, K.Sorai, M.Momose, K.Kotaro, T.Oike, S.Takakuwa, H.Shinnaga, and S.Shiki.

I am very grateful to the NRO staffs, Pof. K.Miyazawa and Drs. S.K.Okumura, K.Sunada, H.Mikoshiba, S.Ishikawa, K.Miyazawa, A.Sakamoto, C.Yamaguchi and Y.Iiduka for the developments of devices and their help during the observations with the Nobeyama 45 m telescope.

I thank A.Nummelin for providing me with his SEST data. I also thank J.Dickens and S.Liu for providing me with their NRAO data.

Finally, I would like to thank my friends and family for their hearty encouragement. I could never complete this dissertation without their supports.

References

Allen, M., & Robinson, G. W. 1977, ApJ, 212, 396

Andersson, M., Askne, J., & Hjalmarson, Å, 1984, A&A, 136, 243

Askne, J., Hoglund, B., Hjalmarson, Å., & Irvine, W.M. 1984, A&A, 130, 311

Benson, J.M., & Johnston, K.J. 1984, ApJ, 277, 181

Bergman, P., & Hjalmarson, Å. The physics and chemistry of interstellar molecular clouds - mm and sub-mm observations in astrophysics: Proceedings of the Symposium, Zermatt, Switzerland, Sept. 22-25, 1988 (A90-33833 14-90). Berlin and New York, Springer-Verlag, 1989, p.124-126.

Bergman, P. 1992, Modelling of Molecular Clouds, Technical Report #227, Chalmers University of Technology, Göteborg

Bernstein, M.P., Sandford, S.A., Allamandola, L.J., Chang, S., & Scharberg, M.A. 1995, ApJ, 454, 327

Blake, G.A., Sutton, E.C., Masson, C.R., & Phillips, T.G. 1986, ApJS, 60, 357

Blake, G.A., Sutton, E.C., Masson, C.R., & Phillips, T.G. 1987, ApJ, 315, 621

Caselli, P., Hasegawa, T.I., & Herbst, E. 1993, ApJ, 408, 548

Cesaroni, R., Walmsley, C.M., Kömpe, C., & Churchwell, E. 1991, A&A, 252, 278

Charnley, S.B., Tielens, A.G.G.M., & Millar, T.J. 1992, ApJ, 399, L71

Charnley, S.B., Kress, M.E., Tielens., A.G.G.M, & Millar, T.J. 1995, ApJ, 448, 232

Cheung, A.C., Rank, D.M., Towmes, C.H., Thronto, D.D., & Welch, W.J. 1968, Phys. Rev. Lett. 21, 1701

Cheung, A.C., Rank, D.M., Towmes, C.H., Thronto, D.D., & Welch, W.J. 1969, Nature, 221, 626

Cheung, L., Frogel, J.A., Hauser, M.G., & Gezari, D.Y., 1978, ApJ, 226, 149

De Pree, C.G., Gaume, R.A., Goss, W.M., & Claussen, M.J. 1995, ApJ, 451, 284

De Pree, C.G., Gaume, R.A., Goss, W.M., & Claussen, M.J. 1996, ApJ, 464, 788

de Vicente, P., Martín-pintado, J., & Willson, T.M., 1997, A&A, 320, 957

Dickens, J.E., Irvine, W.M., DeVries, C.H., & Ohishi, M. 1997, ApJ, 479, 307

Douglas, A.E., & Herzberg, G. 1941, ApJ, 94, 381

Dunham., Jr.T, & Adams, N.G. 1937, Pub. Astron. Soc. Pacific, 49, 26

Flower, D.R., Pineau des Forets, G., & Walmsley, C.M. 1995, A&A, 294, 815

Fourikis, N., Takagi, K., & Morimoto, M. 1974, ApJ, 191, L135

Frerking, M.A., Langer, W.D., & Wilson, R.W. 1982, ApJ, 262, 590

Gaume, R.A., Claussen, M.J., De Pree, C.G., Goss, W.M., & Mehringer, D.M. 1995, ApJ, 449, 663

Genzel, R., & Downes, D. 1979, A&A72, 234

Gilmore, w., Morris, M., Johnston, D.R., Lovas, F.J., Zukerman, B., Turner, B.E., & Palmer, P. 1976, ApJ, 204, 43

Godfrey, P. D., Brown, R. D., Robinson, B. J., & Sinclair, M. W. 1973, ApJ, 13, 119

Goldsmith, P.F., Lis, D.C., Hills, R., & Lasenby, L. 1990, ApJ, 350, 186

Gordon, M.A. 1988, ApJ, 331, 509

Gordon, M. A., Berkermann, U., Mezger, P. G., Zylka, R., Haslam, C. G. T., Kreysa, E., Sievers, A. & Lemke, R. 1993, A&A, 280, 208

Harvey, P.M., Campbell, M.F., & Hoffmaum, W.F. 1977, ApJ, 211, 786

Hasegawa, T.I., & Herbst, E. 1993, Mon. Not., R. astr. Soc., 263, 589

Hawkins, M., & Andrews, L. 1983, *J.Am.Chem.Soc*, 105, 2523

Herbst, E., & Leung, C.M. 1989, ApJS, 69, 271

Herbst, E. 1998, private communication

Herbst, E. 1997, private communication

Hunter, T.R. 1996, American Astronomical Society Meeting, 189, #21.03

Hüttemeister, S., Wilson, T.L., Henkel, C., & Mauersberger, R. 1993, A&A, 276, 445

Hüttemeister, S., Wilson, T.L., Mauersberger, R., Lemme, C., Dahmen, G., & Henkel, C. 1995, A&A, 300, 636

Irvine, W.M., Goldsmith, P.F., & Hjalmarson, Å. 1987, in *Interstellar Processes*, ed. D.J.hollenbach and H.A.Thronson, Jr.(Dordrecht:Reidel), p.561

Irvine, W.M., Friberg, P., Kaifu, N., Kawaguchi, K., Kitamura, Y., Matthews, H.E., Minh, Y., Saito, S., Ukita, N., & Yamamoto, S. 1989, ApJ, 342, 871

Kaifu, N., Morimoto, M., Nagane, K., Akabane, K., Iguchi, T., & Takagi, K. 1974, ApJ, 198, L85

Kuan, Y.-J., & Snyder, L.E. 1996, ApJ, 470, 981

Lee, T.J., Beattie, D.H., Geballe, T.R., & Pickup, D.A. 1983, A&A, 127, 417

Lee, H.-H., Bettens, R.P.A., & Herbst, E. 1996, A&A, 119, 111

Liechti, S., & Wilson, T.L. 1996, A&A, 314, 615

Lis, D.C., Carlstrom, J.E., & Keene, J. 1991, ApJ, 380, 429

Lis, D.C., Goldsmith, P.F., Carlstrom, J.E., & Scoville, N.Z., 1993, ApJ, 411, 773

Loughran, L., Mcbreen, B., Fazio, G.G., Rengarajan, T.N., Maxson, C.W., Serio, S., Sciortino, S., & Ray, T.P. 1986, ApJ, 303, 629

Nakagawa, N. 1980, in IAU Symp.87, Interstellar Molecules ed. B.H.Andrew (Dordrecht:Reidel), 365

Martín-Pintado, J., de Vicente, P., Wilson, T.L., & Johnston, K.J. 1990, A&A, 236, 193

Martín-Pintado, J., Bachiller, R., & Fuente, A. 1992, A&A, 254, 315

Martín-Pintado, J., de Vicente, P., Fuente, A., & Planesas, P. 1997, ApJ, 482, 45

Matthews, H.E., Friberg, P., & Irvine, W.M. 1985, ApJ, 290, 609

McMullin, J.P., Mundy, L.G., & Blake, G.A. 1993, ApJ, 405, 599

Mehringer, D.M., & Snyder, L.E. 1996, ApJ, 471, 897

Miao, Y., Mehringer, D.M., Kuan, Y-.J., & Snyder, L.E. 1995, ApJ, 445, L59

Miao, Y., & Snyder, L.E., 1997, ApJ, 480, L67

Millar, T.J., Rawlings, J.M.C., Bennett, A., Brown, P.D., & Charnley, S.B. 1991, A&A, 87, 585

Millar, T.J., Macdonald, G.H., & Gibb, A.G. 1997, A&A, 325, 1163

Minh, Y.C., Ohishi, M., Rho, D.G., Ishiguro, M., & Irvine, W.M. 1993, ApJ, 411, 773

Minh, Y.C., Haikala, L., Hjalmarson, Å., & Irvine, W.M. 1998, ApJ, 498, 261

Nummelin, A., Bergman, P., Hjalmarson, Å., Friberg, P., Irvine, W.M., Millar, T.J., Ohishi, M., & Saito, S. 1998, ApJS, 117, 427

Ohishi, M., Ishikawa, S., Yamamoto, S., Saito, S., & Amano, T. 1995, ApJ, 446, L43

Ohishi, M., Ishikawa, S., & Kaifu, N. 1998, in preparation

Olmi, L., Cesaroni, R., & Walmsley, C.M. 1996, A&A, 307, 599

Palmer, P., Zuckerman, B., Buhl, D., & Snyder, L.E. 1969, ApJ, 156, L147

Pearson, J.C., Sastry, K.V.L.N., Herbst, E., & De Lucia, F.C. 1997, ApJ, 480, 420

Penzias, A.A. 1981, ApJ, 249, 518

Peng, Y., Vogel, S.N., & Carlstrom, J.E. 1993, ApJ, 418, 255

Reid, M.J., Schneps, M.H., Moran, J.M., Gwinn, C.R., Genzel, R., Downes, D., & Rö nnä ng, B. 1988, ApJ, 330, 809

Rubin, R.H., Swenson, G.W.Jr., Benson, R.C., Tigelaar, H., Flygare, W.H. 1971, ApJ, 169, L39

Schilke, P., Walmsley, C.M., Pineau des Forê ts, G., & Flower, D.R. 1997, A&A, 321, 293

Sutton, E.C., Jaminet, P.A., Danchi, W.C., & Blake, G.A., 1991, ApJS, 77, 255

Suzuki, H. 1979, Prog. Thor. Phys. 62, 18

Swings, P., & Rosefeld, L. 1937, ApJ, 86, 483

Thronson, H.A., JR., & Harper, P.A. 1979, ApJ, 230, 133

Turner, B.E. 1975, ApJ, 201, L149

Turner, J.L., & Welch, W.J. 1984, ApJ, 287, L81

Turner, B.E. 1989, ApJS, 70, 539

Turner, B.E. 1991, ApJS, 76, 617

van Dishoeck, E.F., Jansen, D.J., Schilke, P., & Phillips, T.G. 1993, ApJ, 416, L83

Weinreb, S., Barret, A.H., Meeks, M. L., & Henry, J.C. 1963, Nature, 200, 829

Wilson, T.L., Snyder, L.E., Comoretto, G., Jewell, P.R., & Henkel, C. 1996, A&A, 314, 909